# Ena/VASP Proteins Regulate Vertebrate Nervous System Development

A thesis presented by

**Annabelle Sheila Menzies**

Submitted to the Biology Department
in Partial Fulfillment of the Requirements for the Degree of

Doctor of Philosophy in Biology

at the

Massachusetts Institute of Technology
Cambridge, MA
[September 2004]
August 2004



Signature of Author .....
Department of Biology
August 11, 2004

Certified by .....
Frank B. Gertler
Associate Professor of Biology
Thesis Supervisor

Accepted by .....
Stephen Bell
Chair, Committee on Graduate Students
Department of Biology

Ena/VASP Proteins Regulate Vertebrate Nervous System Development

by

Annabelle Sheila Menzies

Submitted to the Biology Department on August 11, 2004
in Partial Fulfillment of the Requirements for the Degree of
Doctor of Philosophy in Biology

## ABSTRACT

Nervous system development is a complex morphogenetic process. Cell migration, axon guidance and many other regulated cell shape changes build a functional nervous system. These processes depend upon regulation of the actin cytoskeleton. Ena/VASP proteins are able to remodel the actin cytoskeleton in response to extracellular signals and have been shown to regulate the motility and morphology of a variety of cells. I have investigated the *in vivo* requirement for the vertebrate family members, Mena and VASP in nervous system development. I show that Mena and VASP are required for viability and the formation of the neural tube, spinal nerves and several brain commissures. Furthermore, I have investigated Ena/VASP function in neuronal cell migration using an *in vitro* assay and demonstrate that Ena/VASP proteins regulate the migration of cerebellar granule cells.

Thesis Advisor: Frank B. Gertler
Title: Associate Professor of Biology

## ACKNOWLEDGEMENTS

My deepest thanks go to my advisor, Frank Gertler. His support and encouragement helped me learn and grow as a scientist. He is a terrific scientist and I am grateful for everything that I have learned in his lab.

Thanks to all the present and former Gertler lab members for providing a vibrant lab environment. They are a remarkable group of people and I have many good memories of our times in and out of lab.

I am especially grateful to Frank Solomon. I will always remember his "Solomon-like" sayings, his good humor and his generous and honest spirit.

I would like to thank my friends near and far who have enriched my life in innumerable ways. I have been especially fortunate to have the "Bio97" gang nearby to share these graduate school years.

My family has always been and continues to be amazing! I am so lucky to have my parents, Malcolm and Mary, and my sister, Anjali, who have loved and supported me from the very start and mio amore, Marcello, who makes life beautiful.

## TABLE OF CONTENTS

# CHAPTER 1

## Introduction

Nervous system development requires cell migration, axon guidance and other regulated cell shape changes. All these processes depend upon coupling the cytoskeleton to external signals. Ena/VASP proteins transduce cell surface signals into structural changes in the actin cytoskeleton. Cell biological approaches show that Ena/ VASP proteins regulate lamellipodial dynamics and filopodial formation. My work shows the requirement of Ena/VASP for the actin-dependent processes of neurulation, neuronal cell migration and axon guidance. I will begin by describing the general background of these processes and then introduce the Ena/VASP family.

## Actin-Dependent Process Shape the Developing Nervous System

### Neurulation

Neurulation is the process by which the gastrulating embryo forms the neural tube. This rudimentary structure ultimately gives rise to the brain and spinal cord. Neural tube formation consists of a complex series of events by which the midline ectoderm differentiates into neuroepithelia and the relatively flat neuroepithelial layer transforms into a tube-like structure. Regulation of cell shape and polarized cell movements are essential for proper neurulation and these processes are critically dependent upon regulation of the actin cytoskeleton.

Neurulation begins with the induction of the neural plate (Figure 1) (Copp et al., 2003). The notochord induces midline ectoderm to differentiate into neuroepithelial cells that elongate and assume a columnar morphology. Subsequent cell shape changes within

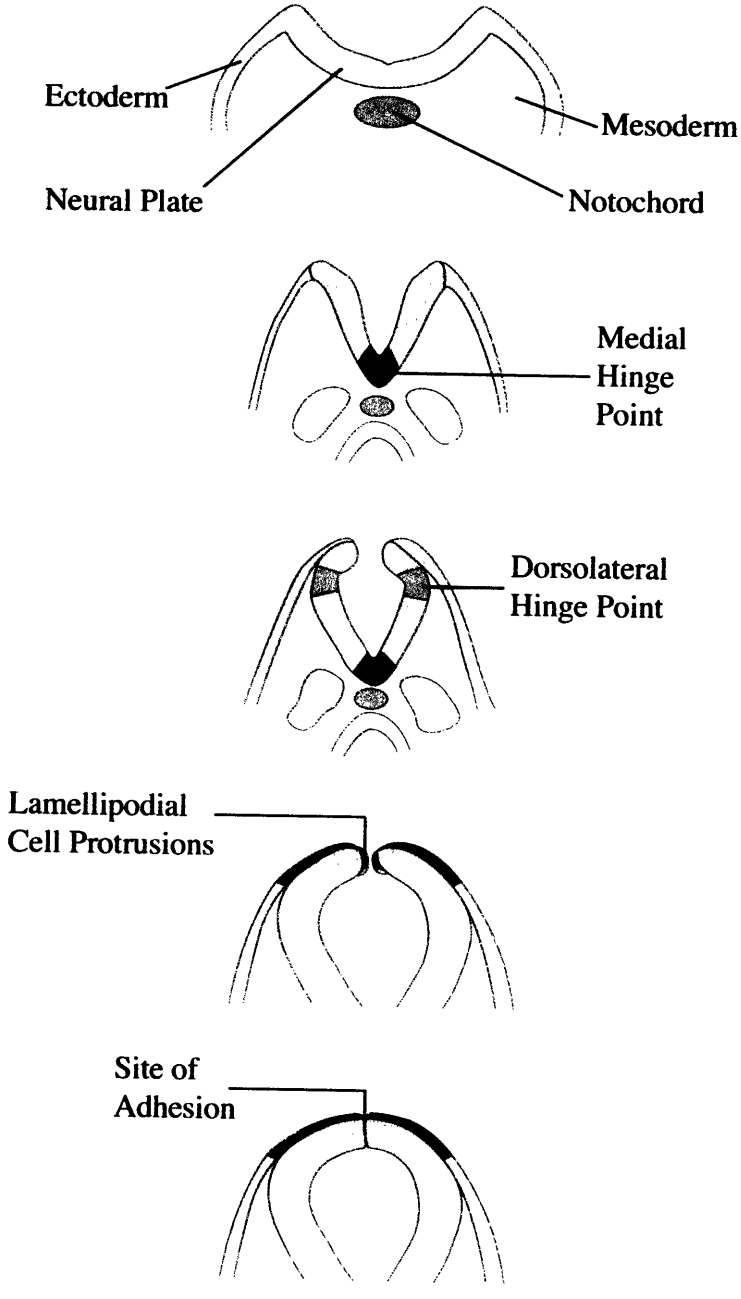
Ectoderm
Mesoderm
Neural Plate
Notochord
Medial
Hinge
Point
Dorsolateral
Hinge Point
Lamellipodial
Cell Protrusions
Site of
Adhesion

**Figure 1**

Figure 1. Neural Tube Formation. Bending of the neural plate at hinge points and convergent extension events (not depicted) bring the neural folds closer together. Lamellipodial protrusions from cells on apposed neural folds facilitate subsequent adhesion and fusion of neural folds. (modified from Copp et. al, 2003)

the neuroepithelium and the surrounding tissue bring about the elevation and fusion of the neural folds. Cells at future hinge point regions become wedge-shaped by apical constriction and basal expansion. The medial hinge point (MHP) forms at the midline while paired dorsal-lateral hinge points (DLHP) form on the sides of the neural plate. These hinge point cells are anchored to the surrounding mesoderm and serve as pivots for bending the neural plate. Intrinsic forces within the neuroepithelium and extrinsic forces in the surrounding tissues elevate the neural folds and bring them in close apposition. Polarized cell movements driving intercalation of neuroepithelial cells cause the neural tube to elongate and narrow all along the body axis and bring the neural folds closer together (Keller, 2002). Similar convergent extension movements within the mesoderm contribute towards elevating the neural folds. In the cephalic region, force generated by apical constriction of neuroepithelial cells all around the lumen of the cephalic neural tube is also thought to contribute to closure (Morriss-Kay and Tuckett, 1985). Neurulation is complete when the neural folds adhere and fuse at the dorsal midline. Cellular protrusions at the apical neural folds reach toward the midline and interdigitate, thereby assisting neural fold fusion (Copp et al., 2003). Failure of cephalic neural tube closure disrupts normal brain development and leads to exencephaly. Spinal neural tube defects result in spina bifida whereas failure of neural tube closure all along the anterior-posterior axis of the embryo results in craniorachischisis.

While a mechanistic understanding of neurulation is not clear, regulated cell shape changes are at the core of neurulation and this involves regulation of the actin cytoskeleton. Apical constriction of cells in hinge points and elsewhere in the

neuroepithelium occurs by the constriction of a ring of actin filaments localized to the apical surface. During convergent extension, cells extend lamellipodia and filopodia that cells use to attach and crawl between cells (Keller, 2002). Moreover, neural fold fusion is though to involve interdigitation of protrusive structures along apical side of the neural folds (Copp et al., 2003). Cell shape changes and formation of protrusive structures such as lamellipodia and filopodia, in other cell types have been shown to be regulated by the actin cytoskeleton. The importance of the actin cytoskeleton is indicated by neural tube defects in mice with targeted mutations of actin-associated genes, such as vinculin, Arg/Abl, shroom and p190RhoGAP (Juriloff and Harris, 2000). Perturbation of actin dynamics by cytochalasin also results in neural tube defects (Morriss-Kay and Tuckett, 1985).

**Neuronal Cell Migration**

In the developing vertebrate central nervous system, neurons are generated in proliferative zones and migrate to their final destination in the brain and spinal cord. Proper placement of neurons with the nervous system is essential for the later stage of synaptogenesis when neurons must form appropriate connections with synaptic partners. Because recent advances have shown that neurogenesis occurs in the adult brain, neuronal cell migration is a process that begins early in vertebrate development and, for some neurons such as the olfactory interneurons, continues throughout life (Doetsch and Alvarez-Buylla, 1996; Lois and Alvarez-Buylla, 1994).

Migrating neurons have been observed in many regions of the brain and their movement characterized as being either radial or tangential (Marin and Rubenstein, 2003). Radially migrating neurons travel along radial glial processes that are oriented perpendicular to the brain surface. In the embryonic cortex, cortical pyramidal neurons are generated in a deep layer and migrate along radial glia to settle in a superficial cortical layer (Gupta et al., 2002). Radial migration also occurs in the cerebellum where granule cells travel from the superficial external granule cell layer (EGL) to their destination in the deeper internal granule cell layer (IGL) (Komuro and Rakic, 1995; Komuro and Rakic, 1998). This form of migration requires close adhesive interactions between neurons and glia, which are mediated by factors such as the cell adhesion molecule, astrotacin (Fishell and Hatten, 1991). Tangentially migrating neurons do not migrate along radial glia and travel in a direction that is relatively parallel to the brain surface. Several types of neurons have been shown to tangentially migrate, such as cerebellar granule cells traveling within the EGL (Komuro et al., 2001). In the cortex, GABA interneurons tangentially migrate from the medial ganglionic eminance, the primitive striatum, to arrive in the cortex while olfactory interneuron precursors travel from the subventricular zone in the anterior lateral ventricle to the olfactory bulb along the rostral migratory stream (Marin and Rubenstein, 2003).

Neurons are guided to target regions by extracellular signals in the environment. Neuronal guidance mechanisms share many of the same receptor-ligand interactions used to guide axons. The repulsive molecules, slit and semaphorin repel olfactory and GABA interneurons, respectively (Tamamaki et al., 2003; Wu et al., 1999). Netrin has been

shown to both repel postnatal granule cells and attract precerebellar neurons (Alcantara et al., 2000). The mechanisms that instruct the cell body to migrate along with the axon or maintain position while allowing the axon to extend are not known, but potentially involve differential adhesion of the cell body to its local environment.

Lamination of the cerebral cortex has been an extensively studied model of neuronal cell migration (Figure 2) (Gupta et al., 2002). The mature cortex is composed of six layers formed by the migration of cortical pyramidal neurons. During embryogenesis, these neurons are generated in the ventricular zone (VZ) and migrate along radial glia to occupy more superficial layers in the cortex. Recently it has been shown that radial glia and cortical neurons are descendants of the same precursor cell in the VZ and that cortical neurons migrate along their "sibling" radial glia (Malatesta et al., 2003). The order in which neurons are generated determines their ultimate position in the laminated cortex, such that later generated neurons crawl past earlier generated neurons to occupy a more superficial layer. The signal to stop migrating is mediated by reelin, a large extracellular matrix molecule secreted by Cajal-Retzius (CR) cells that are located in the most superficial layer of the brain. Reelin binds to the VLDLR and ApoER2 receptors expressed by migrating neurons and the bi-directional adhesion molecule, integrin (Dulabon et al., 2000; Hiesberger et al., 1999). This receptor-ligand interaction has been shown to induce the tyrosine phosphorylation of mDab, an intracellular adaptor protein (Hiesberger et al., 1999; Howell et al., 1999). Reelin has recently been proposed to cause detachment of the neuron from the radial glia (Dulabon et al., 2000). In such a scenario, later generated neurons crawl past earlier generated neurons, arrive close to

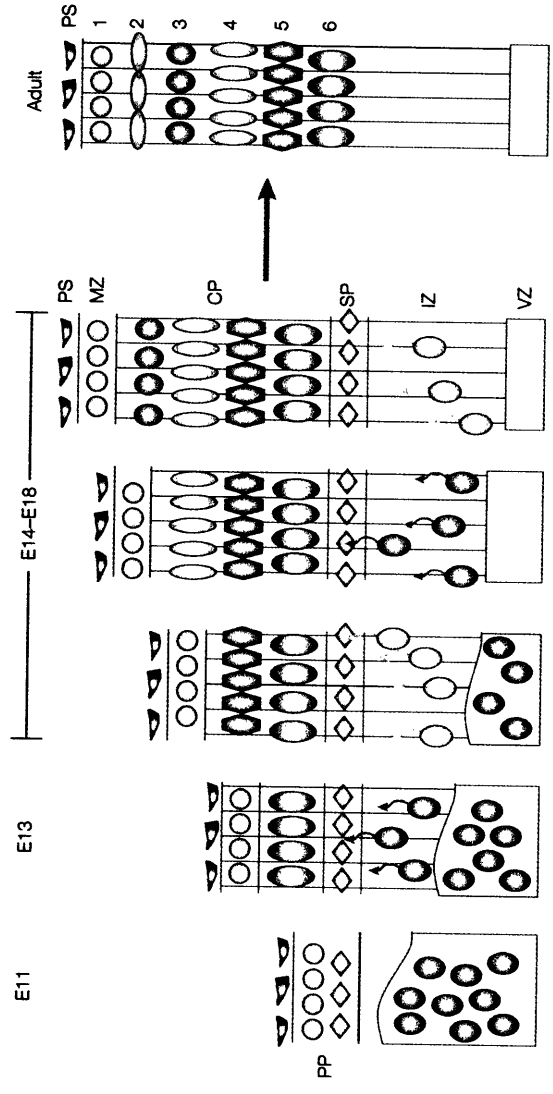


**Figure 2**

Figure 2. Formation of the six distinct cortical layers. At successive embryonic stages (E), postmitotic neurons, originating in the ventricular zone (VZ), migrate along the supportive radial glial processes (depicted as vertical bars). Starting at E11, the first wave of migrating neurons splits the preplate (PP) to generate the marginal zone (MZ) and subplate (SP). Later arriving neurons are progressively added to the cortical plate (CP). Each new cohort migrates past earlier arrived cortical cells and stops just beneath the Cajal-Retzius cells in the marginal zone (MZ). Pial surface (PS). (Gupta et al., 2002)

reelin expressing CR cells, detach from the radial glia and form the new layer by settling in that position.

Advances in live cell imaging and culture techniques have enabled observation of migrating cortical neurons in cultured slice preparations. These experiments demonstrate that migrating neurons extend long cellular process from the cell body that directs cell body movement (Komuro and Rakic, 1995). Furthermore, migrating cortical neurons utilize two modes of migration, namely locomotion and somal translocation (Nadarajah et al., 2001). Glial guided cells locomote by moving their entire cell body and process. The cell body moves in a saltatory manner and the freely motile process maintains a relatively constant length. Somal translocation occurs by moving the nucleus through the process that remains attached near the brain surface. The cell body moves in a continuous fashion while the process shortens as the cell body advances. Some cortical cells appear to only locomote while others start migrating by locomotion and end with somal translocation.

The cytoskeletal elements underlying neuronal cell migration are not well understood. The arrangement of actin and microtubules has been described for cerebellar granule cells (Hatten, 2002). Microtubules form a cage around the nucleus and ring of cortical actin surrounds the cell body. Actin filaments are also enriched at adhesion sites at the base of the cell body and in filopodial projections along the process. The elongated leading process is mainly composed of microtubules that are anchored at centrosomes located within the cell body. While the regulation of cytoskeletal events underlying

neuronal migration are unclear, its importance is indicated by neuronal cell migration defects in mice with mutations in actin and microtubule regulatory genes. Mutations in genes encoding the microtubule associated proteins, DCX, LIS1 and NUDEL indicate an important role for regulation of the microtubule cytoskeleton in migrating neurons (Gupta et al., 2002). The role for actin dynamics is indicated by neuronal migration defects exhibited in humans with mutation in Filamin 1, a gene encoding an actin-binding protein (Fox et al., 1998). It has been proposed that a microtubule based mechanisms pulls the nucleus forward while actin dynamics are important for mediating substrate adhesion and formation of protrusive structures (Hatten, 2002).

**Axon Guidance**

Neuronal cell bodies extend axons that travel great distances to reach synaptic targets. Axons are guided to intermediate targets en route to their final destination (Stoeckli and Landmesser, 1998). At these intermediate targets, or choice points, axons must decide whether to continue straight ahead or change direction. Axons utilize growth cones, specialized structures at the distal tip of developing axons, to dynamically explore the environment and integrate guidance signals into a directional response (Huber et al., 2003). Growth cones grow toward attractive cues and away from repulsive cues thereby steering axonal extension along the proper path. Growth cone motility and hence the ability to explore and respond to guidance cues depends upon rearrangement of the growth cone cytoskeleton. I will begin by discussing the cytoskeletal elements important for growth cone motility and guidance and then discuss some of the major guidance pathways known to regulate axon guidance. Then I will discuss axon guidance of

callosal neurons in the vertebrate brain because a major phenotype exhibited by Ena/VASP mutant mice is a defect in callosal axon guidance.

Coordinate regulation of the growth cone actin and microtubule cytoskeletons is critical for growth cone motility and guidance (Dent and Gertler, 2003). The growth cone peripheral domain is enriched in actin filaments that are organized into lamellipodial and filopodial protrusions (Figure 3). Microtubules are primarily localized in the growth cone central domain and along the axonal shaft but are able to transiently and randomly explore the peripheral domain. Growth cones dynamically regulate their actin cytoskeleton to protrude filopodia and lamellipodia, which is thought to enable growth cones to search out and respond to guidance cues. The direction chosen by the actin-rich protrusion is thought to be stabilized by the preferential capture and invasion of microtubules into this region of the growth cone. Cultured neurons treated with the actin depolymerizing drug, cytochalasin, are able to extend axons but do not form filopodia and are unable to respond to the appropriate guidance cues resulting in pathfinding defects (Bentley and Toroian-Raymond, 1986). Treatment with microtubule depolymerizing drugs causes defects in axon extension and pathfinding presumably by interfering with the stabilizing function of microtubules in the axonal shaft and growth cone (Yamada et al., 1971).

Growth cone turning is thought to occur through the asymmetric protrusion of the growth cone surface towards an attractant and away from a repellant (Figure 3) (Dent and Gertler, 2003). Attractive cues are proposed to promote and/or stabilizes filopodial and

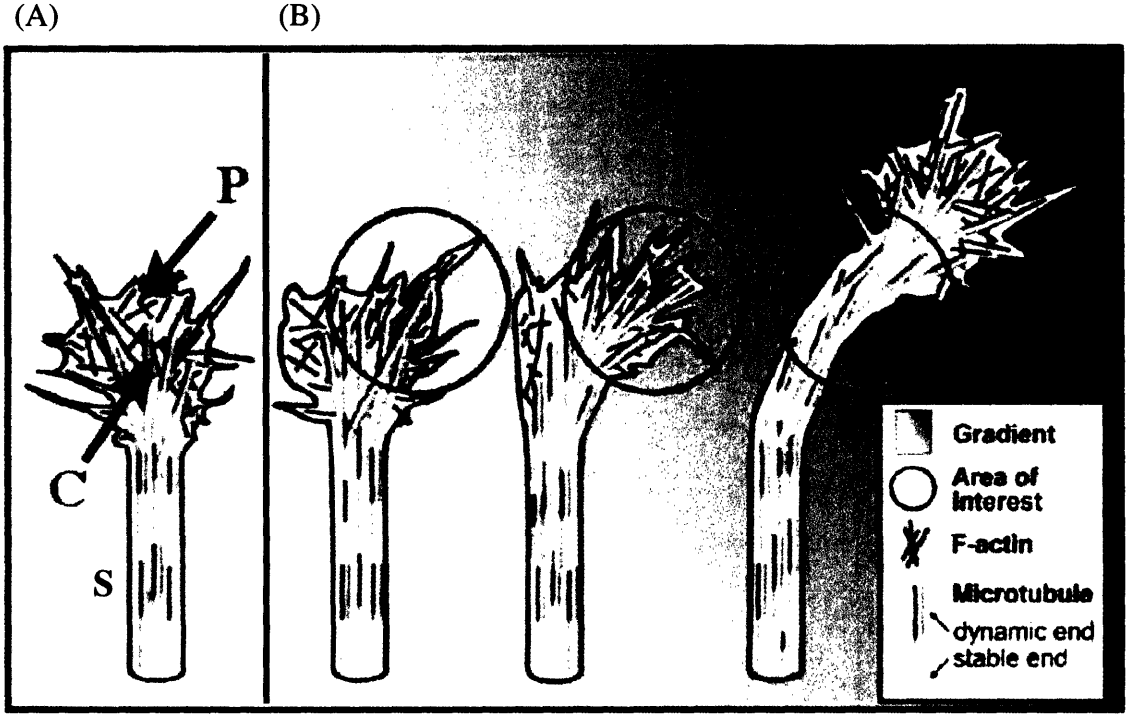
(A)
(B)
P
C
S
Gradient
Area of interest
F-actin
Microtubule
dynamic end
stable end

**Figure 3**

Figure 3. Proposed model for actin and microtubule cytoskeletal remodeling underlying the growth cone turning. (A) Within the growth cone, F-actin is concentrated in the peripheral domain (P) while microtubules are mainly found in the central domain (C) and axonal shaft (S). (B) Sequence of cytoskeletal changes as the growth cone turns towards a chemoattractant gradient (depicted as increasing shades of pink in the background). (modified from Dent and Gertler, 2003)

lamellipodial formation thereby promoting protrusion towards the attractant. This is supported by observations that application of the chemoattractant, netrin-1 induces the formation of filopodia and lamellipodia in cultured neurons (Lebrand et al., 2004; Shekarabi and Kennedy, 2002). Repellants could function in two ways. Repulsive cues may promote protrusion in the growth cone on the side opposite the repellant (Dent and Gertler, 2003). Alternatively, a repulsive cue could inhibit or destabilize filopodial and lamellipodial formation thereby preventing protrusion towards the repellant. Treatment of neurons with the chemorepellent, semaphorin, causes collapse of growth cones, supporting the idea that repellants work by negatively regulating protrusive structures (Jin and Strittmatter, 1997). The net response of attractive and repulsive cues surrounding a growth cone is integrated into an overall response.

Axons are guided by a variety of secreted and membrane bound guidance factors (Huber et al., 2003). A molecular understanding of axon guidance has begun to emerge through the identification of guidance molecules and their cognate receptors. Netrin, slit, semaphorin and ephrins represent the four major families of axon guidance molecules (Chisholm and Tessier-Lavigne, 1999). Semaphorins comprise a large family of secreted and transmembrane bound ligands that mediate growth cone repulsion/collapse through Neuropilin/Plexin receptors. Ephrins are membrane bound ligands for Eph receptor tyrosine kinases and mediate contact-dependent repulsion/collapse of growth cones. The transmembrane forms of semaphorins and ephrin ligands have also been shown to mediate reverse signaling. Slit and netrin are both secreted factors. Slit binds the Robo

receptor and mediates repulsive guidance. Netrin binds the receptors, DCC and Unc-5 through which it mediates attraction and repulsion, respectively.

The response of an individual neuronal growth cone to a given set of guidance signals depends on the repertoire of guidance receptors expressed. Age dependent and experience dependent regulation of guidance receptor expression further determines growth cone responsiveness (Shewan et al., 2002). Growth cone response to a given guidance cue can also be modulated by the secondary messengers, cyclic nucleotides (cAMP and cGMP) and calcium (Song and Poo, 1999). A variety of factors, such as the cell adhesion molecule, laminin, and the neurotransmitter, acetylcholine, influence growth cone guidance to a chemotactic molecule by altering levels of intracellular cAMP and calcium, respectively. For example, the attractive response to netrin-1 by *Xenopus* spinal neurons is reversed to repulsion by lowering the intracellular cAMP concentrations (Hopker et al., 1999; Ming et al., 1997). This "growth cone switching" phenomenon is proposed to act by altering the activity of the cyclic nucleotide dependent kinases, PKA and PKG, and the calcium dependent kinases, calmodulin and CaM kinase. Phospho-regulation of target proteins that regulate the growth cone cytoskeleton would result in the observed reversal in growth cone turning response. Interestingly, phospho-regulation of vertebrate Ena/VASP proteins at a conserved PKA/PKG phosphorylation site is critical for Ena/VASP function in random fibroblast motility (Loureiro et al., 2002). Furthermore, treatment of hippocampal neurons with netrin-1 induces the phosphorylation of Ena/VASP proteins at this site (Lebrand et al., 2004). Phospho-

regulation of Ena/VASP proteins in the growth cone may also be involved in the switching response.

The mechanism by which guidance signals are transduced into remodeling of the actin cytoskeleton remains largely unknown. Most of the known guidance receptors lack obvious intracellular domains or motifs; the kinase domain of the Eph receptor is a notable exception (Chisholm and Tessier-Lavigne, 1999). Moreover, no guidance receptor has been shown to directly interact with the cytoskeleton. Therefore, receptors must signal to proteins that can either directly bind and regulate the growth cone cytoskeleton (ie: Ena/VASP) or relay the signal to downstream targets that eventually result in cytoskeletal rearrangements (ie: Rac, Rho, Cdc42) (Song and Poo, 1999). Several actin-regulatory proteins have been reported to be localized in the growth cone, including Ena/VASP proteins, which are enriched at the tips of growth cone lamellipodia and filopodia (Dent and Gertler, 2003).

Callosal Axon Guidance

The midline is a major choice point in the developing nervous systems of bilateral organisms. In the mammalian brain, the corpus callosum has been used as a model to study the mechanisms governing axon guidance at the midline choice point. Cortical pyramidal neurons, primarily from cortical layers 2,3 and 5, project commissural axons across the midline through the corpus callosum and form synaptic connections in the contralateral cortex. A critical step during callosal development occurs near the midline

between the cerebral hemispheres where callosal axons must choose whether to continue growing in a ventral direction or turn medially and cross.

Recent advances in the anatomical characterization of midline structures and the molecular identification of midline guidance cues have improved our understanding of callosal axon guidance at the midline decision point (Figure 4). The spatial expression of slit by the glial wedge and IG glia serve to channel callosal axons via a surround repulsion mechanism towards the midline (Shu and Richards, 2001). Callosal axons travel medially through this region flanked by slit expression to arrive closer to the midline where netrin expression by cells at the midline is thought to further attract callosal axons across the midline. Disruption of the glial wedge or interference of slit expression by glial wedge cells causes callosal axons to grow further ventrally into the septum, rather than turning medially (Shu and Richards, 2001; Shu et al., 2003b). In addition to these midline signals, fusion of the cerebral hemispheres is required for callosal axon crossing (Ozaki and Wahlsten, 1993). Hemisphere fusion provides a continuous physical substrate between the hemispheres upon which callosal axons travel. Callosal fibers travel underneath the hemisphere fusion point, guided by both repulsive (slit) and attractive (netrin) guidance factors, to arrive in the contralateral hemisphere. The glial sling, a row of cells cradling the corpus callosum, was proposed to be required for callosal axons to cross (Silver and Ogawa, 1983). However, recent investigation has shown that the glial sling is composed of neurons and forms after callosal axons have begun crossing the corpus callosum (Shu et al., 2003a). Therefore, the glial sling is not required for initial callosal guidance across the midline.

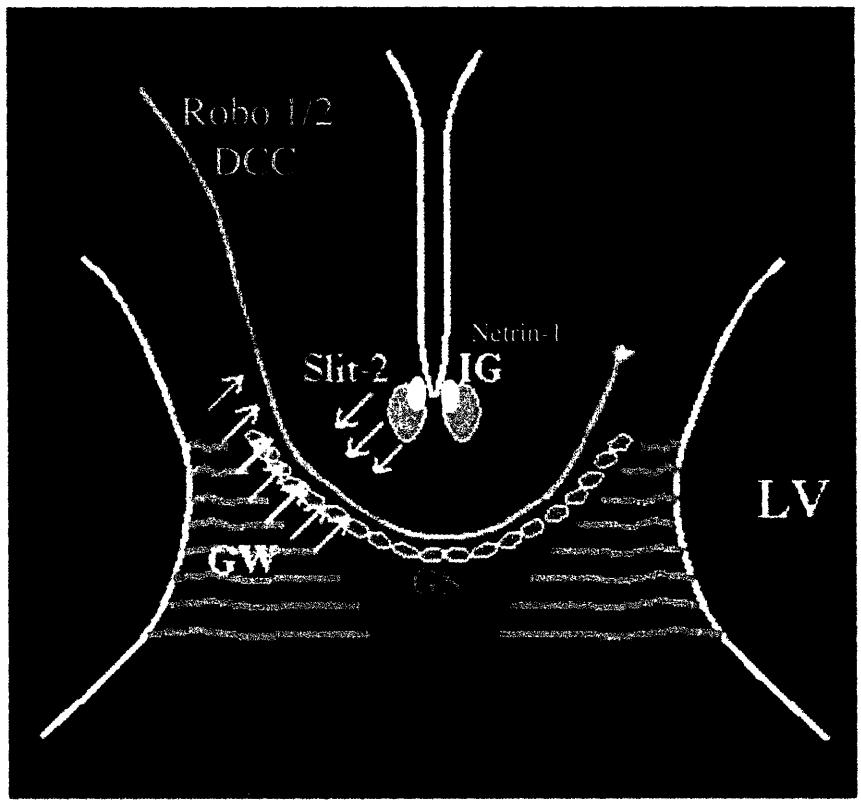


**Figure 4**

Figure 4. Model of Callosal Guidance at the Midline. Callosal axons (red) express Robo1/2 and DCC, receptors for slit and netrin, respectively. Callosal axons are channeled through a region surrounded by the repellant, slit (green), which is expressed by glial wedge cells (GW) and indusium griseum (IG). Netrin (yellow) expressed by midline cells attract callosal axons, which subsequently cross the midline. Glial sling (GS; blue) lateral ventricle (LV) (modified from Shu and Richards, 2003)

## Ena/VASP Family of Actin Regulatory Proteins

Ena/VASP is an evolutionally conserved family of proteins found in vertebrates, invertebrates and the mold *Dictyostelium.* Vertebrates posses three highly related family members, Mena (Mammalian Enabled), VASP (Vasodilator-stimulated phosphoprotein) and EVL (Ena-VASP-like). In contrast, *Drosophila* Ena, *C. elegans* Unc-34 and *Dictyostelium* DdVASP are the singular Ena/VASP orthologs present in invertebrates and slime mold.

### Ena/VASP Protein Features

Ena/VASP proteins share a conserved modular domain structure consisting of a central pro-rich domain flanked by an amino terminal EVH1 domain (Ena-VASP-Homology domain 1) and a carboxy terminal EVH2 domain (Figure 5) (Kwiatkowski et al., 2003). The EVH1 domain interacts with the consensus motif (D/E)FPPPX[D/E][D/E] found in the focal adhesion proteins, zyxin and vinculin, and the axon guidance receptor, Robo/Sax-3. The central Proline rich domain binds profilin, an actin monomer binding protein, and the SH3 domains of Abl, a non-receptor tyrosine kinase. The EVH2 domain contains binding sites for F-actin and G-actin and a coiled-coil region, which mediates oligomerization of Ena/VASP proteins. While the EVH1 has been shown to be important for subcellular localization of Ena/VASP proteins, the Pro-Rich and EVH2 domains are important for Ena/VASP function in actin dynamics.

Ena/VASP orthologs also possess some unique protein features (Figure 5) (Kwiatkowski et al., 2003). Vertebrate Mena contains a stretch of highly charged amino

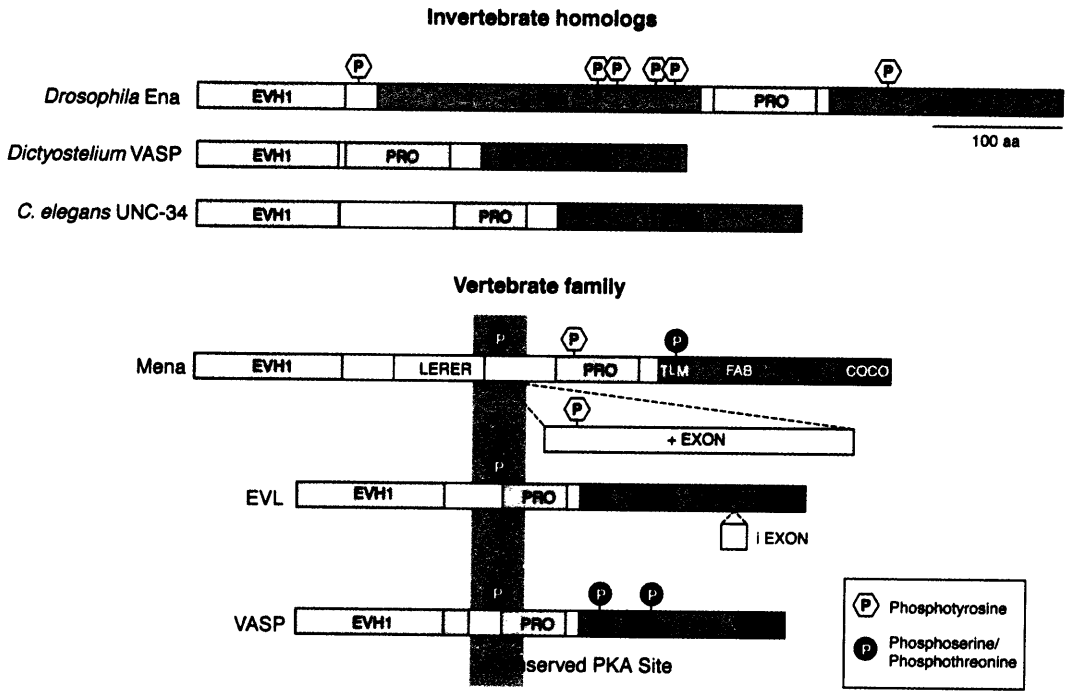
Invertebrate homologs
Drosophila Ena
EVH1
PRO
100 aa
Dictyostelium VASP
EVH1
PRO
C. elegans UNC-34
EVH1
PRO
Vertebrate family
Mena
EVH1
LERER
PRO
TLM
FAB
COCO
+ EXON
EVL
EVH1
PRO
i EXON
VASP
EVH1
PRO
served PKA Site
Phosphotyrosine
Phosphoserine/
Phosphothreonine

# Figure 5

Figure 5. Ena/VASP Family Members and Molecular Architecture. Ena/VASP family members share a conserved domain structure consisting of a central proline-rich domain (PRO) and amino and carboxy terminal Ena-VASP-Homology domain 1 and 2 (EVH1 and EVH2) domains, respectively. Family members also contain unique features as indicated. (Kwiatkowski, et al., 2003)

acid repeats (LERER region) inserted between the EVH1 and Pro-rich domains. *Drosophila* Ena contains a glutamine rich insertion in a similar position. No functional properties have been ascribed to either the LERER or glutamine-rich regions in Mena and Ena, respectively. Mena also contains a neural specific alternatively spliced exon (+ exon) located between the LERER and Pro-Rich domains. EVL contains an alternatively spliced exon located within the EVH2 domain.

Vertebrate Ena/VASP proteins share a conserved PKA/PKG phosphorylation site near the EVH1 domain that has been shown to be essential for Ena/VASP function in fibroblast motility (Loureiro et al., 2002). However, Mena and VASP possess additional PKA/PKG phosphorylation sites within the EVH2 domain that are not conserved among all vertebrate proteins. While Mena and Ena are the only orthologs known to be tyrosine kinase substrates, the functional significance of tyrosine phosphorylation remains unclear (Comer et al., 1998; Tani et al., 2003).

Despite structural differences between family members, Ena/VASP proteins function interchangeably in a variety of assays. Motility defects in fibroblasts lacking Ena/VASP function can be rescued by re-expression of any vertebrate homolog as well as *Drosophila* Ena (Loureiro et al., 2002). Furthermore, expression of VASP has been demonstrated to rescues *Ena* null mutant phenotypes (Ahern-Djamali et al., 1998). Additionally all vertebrate proteins support the motility of the intracellular pathogen, *Listeria monocytogenes,* which has been employed as a model to study proteins that regulate actin-based motility (Laurent et al., 1999).

Subcellular localization and cellular functions of Ena/VASP proteins

Ena/VASP proteins are enriched at cell-cell and cell-matrix contacts (Krause et al., 2003). Ena/VASP proteins are also enriched in protrusive cellular structures where dynamic actin assembly occurs such as the tips of lamellipodia and filopodia. The ability of Ena/VASP proteins to interact directly with actin and other actin-regulatory proteins and the subcellular localization of Ena/VASP proteins to sites of actin polymerization, indicates that Ena/VASP proteins may regulate the actin cytoskeleton. Direct evidence came from studies in cultured fibroblasts and neurons where altering the function of Ena/VASP proteins resulted in differences in the ultrastructural organization of the actin cytoskeleton (Bear et al., 2002; Lebrand et al., 2004). These studies showed that Ena/VASP promotes the formation of long actin filaments.

Ena/VASP proteins regulate the formation of lamellipodia and filopodia, actin-rich protrusive structures found in a variety of cell types. Lamellipodia are composed of actin arranged in a dendritic array whereas in filopodia parallel actin filaments are tightly bundled. In fibroblasts lacking Ena/VASP function, the actin network underlying the lamellipodia is composed of short and highly branched actin filaments whereas actin filaments are long and sparsely branched in cells with excess Ena/VASP activity (Bear et al., 2002). Fibroblasts lacking Ena/VASP activity protrude a lamellipodia in a slow but persistent manner (Bear et al., 2000). Lamellipodial protrusion in cells with excess Ena/VASP activity is rapid and transient with unstable protrusions that often fold back resulting in membrane ruffling. In a whole cell motility assay, cells move faster in the absence of Ena/VASP function (Bear et al., 2000). It has been hypothesized that cells

lacking Ena/VASP function move faster because the actin ultrastructure underlying the lamellipodia provides a stiff force pushing the membrane forward, ultimately resulting in net translocation. In cells with excess Ena/VASP activity, the underlying actin organization does not lead to productive protrusions and is thought to result in slower net translocation (Bear et al., 2002). In neurons, Ena/VASP activity promotes the generation of long actin filaments, which are bundled into filopodia (Lebrand et al., 2004). Moreover, neurons lacking Ena/VASP do not form filopodia. Additional experiments showed that Ena/VASP proteins are required to form filopodial in response to treatment with netrin-1.

Invertebrate Ena/VASP Mutants

Invertebrate mutants of Ena/VASP proteins exhibit defects in several actin-dependent processes including cell migration, axon/dendrite guidance and dorsal closure. The presence of misplaced neurons and misrouted axons and dendrites in *Ena* and *unc-34* mutants indicates that Ena/VASP function is required for proper guidance of cell bodies, axons and dendrites. Genetic and biochemical interaction further implicate Ena/VASP function in specific signaling pathways downstream of the receptors, Dlar, Robo/Sax-3, DCC/Unc-40 and Unc-5.

Guidance Defects in *Drosophila Ena* and *C. elegans Unc-34*

The role of Ena/VASP proteins in nervous system development was first demonstrated in flies. *Drosophila* Enabled (Ena) was originally identified in a screen for dominant mutations that suppressed *abl* dependent phenotypes (Gertler et al., 1990). Abl,

a nonreceptor tyrosine kinase, well known for its oncogenic capabilities, has been shown to be important for proper development of motor and commissural axons in the peripheral and central nervous systems (PNS, CNS), respectively. *Abl*-/- flies are pupal lethal (Gertler et al., 1990) and motor axons of the Intersegmental Nerve b (ISNb) exhibit a "stop short" phenotype in which they halt extension prior to reaching their target muscle (Wills et al., 1999b). In the CNS, Abl function is important for commissural axons to cross the midline (Gertler et al., 1990). Mutations in Ena suppress *abl*-dependent phenotypes. Further characterization revealed that *ena* null flies are embryonic lethal and exhibit nervous system phenotypes independent of the *abl* mutation.

*Drosophila Ena*-/- mutants exhibit several axon guidance defects in the PNS and CNS. In *Ena*-/- mutants, motor axons of the Intersegmental Nerve b (ISNb) exhibit a "bypass" phenotype in which axons fail to branch and instead grow past their target muscle (Wills et al., 1999a). Genetic analysis has shown that Ena functions with Abl and the axon guidance molecule, Dlar, a receptor protein tyrosine phosphatase, for proper guidance of ISNb motor axons (Wills et al., 1999a). While *abl* mutants exhibit an ISNb "stop short" phenotype, *Dlar* and *ena* mutants exhibit an ISNb "bypass" phenotype. Mutations in Ena suppress *abl* and enhance *Dlar* ISNb guidance defects. Ena has also been shown to biochemically interact with Dlar and be tyrosine phosphorylated by Abl (Comer et al., 1998; Wills et al., 1999a).

*Drosophila* Ena function is also required for proper guidance of CNS axons. Axon guidance defects occur at the CNS midline in *ena*-/- mutants where commissural

(crossing) axons inappropriately cross and ipsilateral (non-crossing) axons sometimes ectopically cross the midline (Gertler et al., 1995). Ena mutations suppress *abl*-dependent phenotypes and enhance *robo*-dependent commissural guidance defects suggesting that Ena functions with abl and robo for proper guidance of these axons (Bashaw et al., 2000; Gertler et al., 1990). Furthermore, Ena has been shown to bind the cytoplasmic domain of *Drosophila* Robo, which is proposed to be required for Ena functions downstream of Robo signaling (Bashaw et al., 2000). However, Ena does not mediate all of Robo's repulsive effects since *ena-/-* mutants exhibit weaker phenotypes than *robo-/-* and many axons are repulsed in the absence of Ena.

Ena/VASP function in axon guidance is conserved in *C. elegans* and has been linked to specific guidance pathways involving both attractive and repulsive responses. Mutants in the *C. elegans* Ena/VASP ortholog, Unc-34, exhibit guidance defects in a variety of neurons, including commissural PVQ axons, AVM sensory axons and a subset of interneurons (Yu et al., 2002). Additionally, *unc-34* mutants also exhibit cell migration defects resulting in mispositioned CAN neurons. Several of the axon guidance and cell migration defects in *unc-34* mutants are similar to defects in the *C. elegans* mutant deficient for Sax-3, the worm Robo ortholog. Furthermore, *unc-34* suppresses gain-of function phenotypes in the Sax-3 pathway and biochemically interacts with Sax-3 (Yu et al., 2002). These observations suggest that Ena/VASP proteins function in repulsion downstream of Robo, the slit receptor, in worms as well as flies. Unc-34 has also been shown to influence netrin signaling downstream of the attractive Unc-40, the worm DCC ortholog, and repulsive Unc-5 receptors in worms. Constitutive activation of

Unc-40, the attractive netrin receptor, results in a variety of phenotypes, which include defects in axon guidance, outgrowth and branching and deformed cell body shape (Gitai et al., 2003). Mutations in Unc-34 partially suppress all these phenotypes. Mutations in Unc-34 also suppresses axon guidance defects due to ectopic expression of Unc-5, the repulsive netrin receptor (Colavita and Culotti, 1998). These studies suggest that Ena/VASP proteins are downstream effector targets of slit and netrin signaling pathways.

Ena/VASP proteins are also important for the guidance of dendritic processes (Gao et al., 1999). A genetic screen in *Drosophila* was performed to identify genes important for different aspects of dendritic development including outgrowth, branching and guidance. Mutations in ena specifically disturbed the guidance of dendritic processes. While Ena/VASP proteins are important transducers of guidance information in a variety of contexts, further investigation is required to determine the precise mechanism by which Ena/VASP guides axons, dendrites and cell bodies.

Dorsal Closure Defects in *Drosophila Ena*

Analysis of *ena* mutants reveals that Ena functions in epithelial morphogenesis. *Drosophila ena* mutants exhibit mild defects in dorsal closure (Grevengoed et al., 2001), a process analogous to vertebrate neurulation in which epithelial cell shape changes permit the elongation and closure of the dorsal side of the embryo. Coordinate regulation of epithelial cell shape changes maintains tension across the sheet and enables a smooth epithelial sheet to advance towards the midline. Cells at the leading edge of the epithelial sheet extend filopodia medially and "zipper-up" to fuse the two epithelial sheets. Genetic

analysis showed that Ena functions with abl in the process of dorsal closure (Grevengoed et al., 2001). Mutations in Ena suppress the dorsal closure defects in *abl* mutants. In *abl* mutants, epithelial cells do not change shape in a coordinated way giving the epithelial sheet a jagged appearance and resulting in failed or delayed closure. Moreover, while Ena normally localizes to the apical epithelium, it excessively accumulates in the absence of abl. Ectopic aggregates of F-actin co-localize to regions of the apical epithelium where Ena accumulation is observed (Grevengoed et al., 2001). Excessive and ectopic Ena and F-actin accumulation has also been observed in the apical microvilli in *abl* mutants (Grevengoed et al., 2003). Moreover, mosaic analysis shows a loss of cortical F-actin in *ena* mutant cells in the follicular epithelium (Baum and Perrimon, 2001). Together these data suggest that Abl regulates the localization of ena to discrete locations within the cell where ena promotes actin filament assembly.

In the following chapters, I will describe my work analyzing the requirement of the vertebrate Ena/VASP proteins in nervous system development. This analysis shows that these proteins are required for the development of several neural derived structures.

## References

Ahern-Djamali, S. M., Comer, A. R., Bachmann, C., Kastenmeier, A. S., Reddy, S. K., Beckerle, M. C., Walter, U., and Hoffmann, F. M. (1998). Mutations in Drosophila enabled and rescue by human vasodilator-stimulated phosphoprotein (VASP) indicate important functional roles for Ena/VASP homology domain 1 (EVH1) and EVH2 domains. Mol Biol Cell *9*, 2157-2171.

Alcantara, S., Ruiz, M., De Castro, F., Soriano, E., and Sotelo, C. (2000). Netrin 1 acts as an attractive or as a repulsive cue for distinct migrating neurons during the development of the cerebellar system. Development *127*, 1359-1372.

Bashaw, G. J., Kidd, T., Murray, D., Pawson, T., and Goodman, C. S. (2000). Repulsive axon guidance: Abelson and Enabled play opposing roles downstream of the roundabout receptor. Cell *101*, 703-715.

Baum, B., and Perrimon, N. (2001). Spatial control of the actin cytoskeleton in Drosophila epithelial cells. Nat Cell Biol *3*, 883-890.

Bear, J. E., Loureiro, J. J., Libova, I., Fassler, R., Wehland, J., and Gertler, F. B. (2000). Negative regulation of fibroblast motility by Ena/VASP proteins. Cell *101*, 717-728.

Bear, J. E., Svitkina, T. M., Krause, M., Schafer, D. A., Loureiro, J. J., Strasser, G. A., Maly, I. V., Chaga, O. Y., Cooper, J. A., Borisy, G. G., and Gertler, F. B. (2002). Antagonism between Ena/VASP proteins and actin filament capping regulates fibroblast motility. Cell *109*, 509-521.

Bentley, D., and Toroian-Raymond, A. (1986). Disoriented pathfinding by pioneer neurone growth cones deprived of filopodia by cytochalasin treatment. Nature *323*, 712-715.

Chisholm, A., and Tessier-Lavigne, M. (1999). Conservation and divergence of axon guidance mechanisms. Curr Opin Neurobiol *9*, 603-615.

Colavita, A., and Culotti, J. G. (1998). Suppressors of ectopic UNC-5 growth cone steering identify eight genes involved in axon guidance in Caenorhabditis elegans. Dev Biol *194*, 72-85.

Comer, A. R., Ahern-Djamali, S. M., Juang, J. L., Jackson, P. D., and Hoffmann, F. M. (1998). Phosphorylation of Enabled by the Drosophila Abelson tyrosine kinase regulates the in vivo function and protein-protein interactions of Enabled. Mol Cell Biol *18*, 152-160.

Copp, A. J., Greene, N. D., and Murdoch, J. N. (2003). The genetic basis of mammalian neurulation. Nat Rev Genet *4*, 784-793.
Dent, E. W., and Gertler, F. B. (2003). Cytoskeletal dynamics and transport in growth cone motility and axon guidance. Neuron *40*, 209-227.

Doetsch, F., and Alvarez-Buylla, A. (1996). Network of tangential pathways for neuronal migration in adult mammalian brain. Proc Natl Acad Sci U S A *93*, 14895-14900.

Dulabon, L., Olson, E. C., Taglienti, M. G., Eisenhuth, S., McGrath, B., Walsh, C. A., Kreidberg, J. A., and Anton, E. S. (2000). Reelin binds alpha3beta1 integrin and inhibits neuronal migration. Neuron *27*, 33-44.

Fishell, G., and Hatten, M. E. (1991). Astrotactin provides a receptor system for CNS neuronal migration. Development *113*, 755-765.

Fox, J. W., Lamperti, E. D., Eksioglu, Y. Z., Hong, S. E., Feng, Y., Graham, D. A., Scheffer, I. E., Dobyns, W. B., Hirsch, B. A., Radtke, R. A., *et al.* (1998). Mutations in filamin 1 prevent migration of cerebral cortical neurons in human periventricular heterotopia. Neuron *21*, 1315-1325.

Gao, F. B., Brenman, J. E., Jan, L. Y., and Jan, Y. N. (1999). Genes regulating dendritic outgrowth, branching, and routing in Drosophila. Genes Dev *13*, 2549-2561.

Gertler, F. B., Comer, A. R., Juang, J. L., Ahern, S. M., Clark, M. J., Liebl, E. C., and Hoffmann, F. M. (1995). enabled, a dosage-sensitive suppressor of mutations in the Drosophila Abl tyrosine kinase, encodes an Abl substrate with SH3 domain-binding properties. Genes Dev *9*, 521-533.

Gertler, F. B., Doctor, J. S., and Hoffmann, F. M. (1990). Genetic suppression of mutations in the Drosophila abl proto-oncogene homolog. Science *248*, 857-860.

Gitai, Z., Yu, T. W., Lundquist, E. A., Tessier-Lavigne, M., and Bargmann, C. I. (2003). The netrin receptor UNC-40/DCC stimulates axon attraction and outgrowth through enabled and, in parallel, Rac and UNC-115/AbLIM. Neuron *37*, 53-65.

Grevengoed, E. E., Fox, D. T., Gates, J., and Peifer, M. (2003). Balancing different types of actin polymerization at distinct sites: roles for Abelson kinase and Enabled. J Cell Biol *163*, 1267-1279.

Grevengoed, E. E., Loureiro, J. J., Jesse, T. L., and Peifer, M. (2001). Abelson kinase regulates epithelial morphogenesis in Drosophila. J Cell Biol *155*, 1185-1198.

Gupta, A., Tsai, L. H., and Wynshaw-Boris, A. (2002). Life is a journey: a genetic look at neocortical development. Nat Rev Genet *3*, 342-355.

Hatten, M. E. (2002). New directions in neuronal migration. Science *297*, 1660-1663.
Hiesberger, T., Trommsdorff, M., Howell, B. W., Goffinet, A., Mumby, M. C., Cooper, J. A., and Herz, J. (1999). Direct binding of Reelin to VLDL receptor and ApoE receptor 2 induces tyrosine phosphorylation of disabled-1 and modulates tau phosphorylation. Neuron *24*, 481-489.

Hopker, V. H., Shewan, D., Tessier-Lavigne, M., Poo, M., and Holt, C. (1999). Growth-cone attraction to netrin-1 is converted to repulsion by laminin-1. Nature *401*, 69-73.

Howell, B. W., Herrick, T. M., and Cooper, J. A. (1999). Reelin-induced tryosine phosphorylation of disabled 1 during neuronal positioning. Genes Dev *13*, 643-648.

Huber, A. B., Kolodkin, A. L., Ginty, D. D., and Cloutier, J. F. (2003). Signaling at the growth cone: ligand-receptor complexes and the control of axon growth and guidance. Annu Rev Neurosci *26*, 509-563.

Jin, Z., and Strittmatter, S. M. (1997). Rac1 mediates collapsin-1-induced growth cone collapse. J Neurosci *17*, 6256-6263.

Juriloff, D. M., and Harris, M. J. (2000). Mouse models for neural tube closure defects. Hum Mol Genet *9*, 993-1000.

Keller, R. (2002). Shaping the vertebrate body plan by polarized embryonic cell movements. Science *298*, 1950-1954.

Komuro, H., and Rakic, P. (1995). Dynamics of granule cell migration: a confocal microscopic study in acute cerebellar slice preparations. J Neurosci *15*, 1110-1120.

Komuro, H., and Rakic, P. (1998). Distinct modes of neuronal migration in different domains of developing cerebellar cortex. J Neurosci *18*, 1478-1490.

Komuro, H., Yacubova, E., and Rakic, P. (2001). Mode and tempo of tangential cell migration in the cerebellar external granular layer. J Neurosci *21*, 527-540.

Krause, M., Dent, E. W., Bear, J. E., Loureiro, J. J., and Gertler, F. B. (2003). Ena/VASP proteins: regulators of the actin cytoskeleton and cell migration. Annu Rev Cell Dev Biol *19*, 541-564.

Kwiatkowski, A. V., Gertler, F. B., and Loureiro, J. J. (2003). Function and regulation of Ena/VASP proteins. Trends Cell Biol *13*, 386-392.

Laurent, V., Loisel, T. P., Harbeck, B., Wehman, A., Grobe, L., Jockusch, B. M., Wehland, J., Gertler, F. B., and Carlier, M. F. (1999). Role of proteins of the Ena/VASP family in actin-based motility of Listeria monocytogenes. J Cell Biol *144*, 1245-1258.
Lebrand, C., Dent, E. W., Strasser, G. A., Lanier, L. M., Krause, M., Svitkina, T. M., Borisy, G. G., and Gertler, F. B. (2004). Critical role of Ena/VASP proteins for filopodia formation in neurons and in function downstream of netrin-1. Neuron *42*, 37-49.

Lois, C., and Alvarez-Buylla, A. (1994). Long-distance neuronal migration in the adult mammalian brain. Science *264*, 1145-1148.

Loureiro, J. J., Rubinson, D. A., Bear, J. E., Baltus, G. A., Kwiatkowski, A. V., and Gertler, F. B. (2002). Critical roles of phosphorylation and actin binding motifs, but not

the central proline-rich region, for Ena/vasodilator-stimulated phosphoprotein (VASP) function during cell migration. Mol Biol Cell *13*, 2533-2546.

Malatesta, P., Hack, M. A., Hartfuss, E., Kettenmann, H., Klinkert, W., Kirchhoff, F., and Gotz, M. (2003). Neuronal or glial progeny: regional differences in radial glia fate. Neuron *37*, 751-764.

Marin, O., and Rubenstein, J. L. (2003). Cell migration in the forebrain. Annu Rev Neurosci *26*, 441-483.

Ming, G. L., Song, H. J., Berninger, B., Holt, C. E., Tessier-Lavigne, M., and Poo, M. M. (1997). cAMP-dependent growth cone guidance by netrin-1. Neuron *19*, 1225-1235.

Morriss-Kay, G., and Tuckett, F. (1985). The role of microfilaments in cranial neurulation in rat embryos: effects of short-term exposure to cytochalasin D. J Embryol Exp Morphol *88*, 333-348.

Nadarajah, B., Brunstrom, J. E., Grutzendler, J., Wong, R. O., and Pearlman, A. L. (2001). Two modes of radial migration in early development of the cerebral cortex. Nat Neurosci *4*, 143-150.

Ozaki, H. S., and Wahlsten, D. (1993). Cortical axon trajectories and growth cone morphologies in fetuses of acallosal mouse strains. J Comp Neurol *336*, 595-604.

Shekarabi, M., and Kennedy, T. E. (2002). The netrin-1 receptor DCC promotes filopodia formation and cell spreading by activating Cdc42 and Rac1. Mol Cell Neurosci *19*, 1-17.

Shewan, D., Dwivedy, A., Anderson, R., and Holt, C. E. (2002). Age-related changes underlie switch in netrin-1 responsiveness as growth cones advance along visual pathway. Nat Neurosci *5*, 955-962.

Shu, T., Puche, A. C., and Richards, L. J. (2003a). Development of midline glial populations at the corticoseptal boundary. J Neurobiol *57*, 81-94.

Shu, T., and Richards, L. J. (2001). Cortical axon guidance by the glial wedge during the development of the corpus callosum. J Neurosci *21*, 2749-2758.

Shu, T., Sundaresan, V., McCarthy, M. M., and Richards, L. J. (2003b). Slit2 guides both precrossing and postcrossing callosal axons at the midline in vivo. J Neurosci *23*, 8176-8184.

Silver, J., and Ogawa, M. Y. (1983). Postnatally induced formation of the corpus callosum in acallosal mice on glia-coated cellulose bridges. Science *220*, 1067-1069.

Song, H. J., and Poo, M. M. (1999). Signal transduction underlying growth cone guidance by diffusible factors. Curr Opin Neurobiol *9*, 355-363.

Stoeckli, E. T., and Landmesser, L. T. (1998). Axon guidance at choice points. Curr Opin Neurobiol *8*, 73-79.

Tamamaki, N., Fujimori, K., Nojyo, Y., Kaneko, T., and Takauji, R. (2003). Evidence that Sema3A and Sema3F regulate the migration of GABAergic neurons in the developing neocortex. J Comp Neurol *455*, 238-248.

Tani, K., Sato, S., Sukezane, T., Kojima, H., Hirose, H., Hanafusa, H., and Shishido, T. (2003). Abl interactor 1 promotes tyrosine 296 phosphorylation of mammalian enabled (Mena) by c-Abl kinase. J Biol Chem *278*, 21685-21692.

Wills, Z., Bateman, J., Korey, C. A., Comer, A., and Van Vactor, D. (1999a). The tyrosine kinase Abl and its substrate enabled collaborate with the receptor phosphatase Dlar to control motor axon guidance. Neuron *22*, 301-312.

Wills, Z., Marr, L., Zinn, K., Goodman, C. S., and Van Vactor, D. (1999b). Profilin and the Abl tyrosine kinase are required for motor axon outgrowth in the Drosophila embryo. Neuron *22*, 291-299.

Wu, W., Wong, K., Chen, J., Jiang, Z., Dupuis, S., Wu, J. Y., and Rao, Y. (1999). Directional guidance of neuronal migration in the olfactory system by the protein Slit. Nature *400*, 331-336.

Yamada, K. M., Spooner, B. S., and Wessells, N. K. (1971). Ultrastructure and function of growth cones and axons of cultured nerve cells. J Cell Biol *49*, 614-635.

Yu, T. W., Hao, J. C., Lim, W., Tessier-Lavigne, M., and Bargmann, C. I. (2002). Shared receptors in axon guidance: SAX-3/Robo signals via UNC-34/Enabled and a Netrin-independent UNC-40/DCC function. Nat Neurosci *5*, 1147-1154.

# CHAPTER 2

## Mena Is Required for Neurulation and Commissure Formation

Lorene M. Lanier[1,7], Monte A. Gates[2,7], Walter Witke[3], A. Sheila Menzies[1], Ann M. Wehman[1], Jeffrey D. Macklis[2], David Kwiatkowski[4], Philippe Soriano[5], and Frank B. Gertler[1,5,6]

[1]Department of Biology, Massachusetts Institute of Technology, Cambridge, Massachusetts 02139, USA; [2]Division of Neuroscience, Children's Hospital, Harvard Medical School, Boston, Massachusetts 02115, USA; [3]European Molecular Biology Laboratory, Mouse Biology Programme, Monterotondo, Italy 00016; [4]Genetics Laboratory, Hematology Division, Harvard Medical School, Boston, Massachusetts 02115, USA; [5]Fred Hutchinson Cancer Research Center, Seattle, Washington 98104, USA

[7]These authors contributed equally to this work.

ASM performed the experiments presented in Figure 4A and 4B and together with MAG for experiments in Figures 5 and 7.

Chapter 2 was published in Neuron 22: 313-325 (1999).

**Abstract**

Mammalian enabled (Mena) is a member of a protein family thought to link signal transduction pathways to localized remodeling of the actin cytoskeleton. Mena binds directly to Profilin, an actin-binding protein that modulates actin polymerization. In primary neurons, Mena is concentrated at the tips of growth cone filopodia. Mena-deficient mice are viable; however, axons projecting from interhemispheric cortico-cortical neurons are misrouted in early neonates, and failed decussation of the corpus callosum as well as defects in the hippocampal commissure and the pontocerebellar pathway are evident in the adult. Mena-deficient mice that are heterozygous for a Profilin I deletion die in utero and display defects in neurulation, demonstrating an important functional role for Mena in regulation of the actin cytoskeleton.

## Introduction

In recent years, much has been learned about the signals that guide axons as they navigate toward their targets. It is known that axonal growth cones respond to a variety of attractive and repulsive cues present in the extracellular environment and that response to such cues is often modulated by phosphorylation-dependent signaling (Caroni 1998; Flanagan and Van Vactor 1998). The identities of the downstream targets of these signaling events and how they ultimately transduce signals into effects on growth cone motility remain unclear.

Genetic screens in *Drosophila* and *C. elegans* have identified cell surface receptors that regulate growth cone behavior at particular choice points and/or in response to chemoattractants and repellents. For example, the Robo/Sax3 receptor family controls a repulsive response to midline signals (Kidd et al. 1998; Zallen et al. 1998), while Netrins and their receptors have been implicated in both repulsive and attractive axon guidance signaling along the dorsoventral axis in *C. elegans*, in motor and commissural neurons in *Drosophila*, and in commissural axons in vertebrates (Keynes and Cook 1996).

The Abl nonreceptor tyrosine kinase has also been implicated in axon guidance in *Drosophila*. The requirements for Abl in axon formation are more obvious when combined with mutations in one of a number of loci that act as dose-dependent modifiers of *Abl* (Gertler et al. 1993). The mammalian homolog of one of these modifiers, *Disabled* (*Dab*), is required for proper control of neuronal cell migration in the developing cortex (Howell et al. 1997). Genetic screens for suppressors of Abl-dependent phenotypes identified multiple alleles of only one locus, *Enabled* (*Ena*; Gertler et al. 1990). Heterozygosity for *Ena* alleviates *Abl*-dependent neuronal phenotypes, while homozygosity for *Ena* alone causes highly penetrant defects in axon guidance and fasciculation (Gertler et al. 1995).

Ena is the prototype of a family of proteins that includes Mena, VASP, and EVL (the "Ena/VASP" family). Mena (mammalian enabled) was identified as a mammalian ortholog of *Drosophila* Ena (Gertler et al. 1996). VASP (vasodilator-stimulated

phosphoprotein) was originally characterized in platelets as a stoichiometric substrate of cyclic nucleotide-dependent kinases and is required for the regulation of platelet aggregation, a process that depends upon rapid actin assembly (Halbrügge and Walter 1989; Aszodi et al. 1999). EVL (Ena-VASP-like) was identified as an expressed sequence tag with homology to Ena and VASP (Gertler et al. 1996).

The Ena/VASP family shares a common structural organization composed of highly conserved NH2- and COOH-terminal domains called Ena-VASP homology 1 and 2 (EVH1 and EVH2) that flank a central proline-rich domain. The EVH1 domain mediates subcellular targeting by binding to the motif D/EFPPPP, which is found in the cellular focal adhesion proteins Zyxin and Vinculin and in the ActA protein from the intracellular bacteria Listeria monocytogenes (Niebuhr et al. 1997). The EVH2 domain contains a predicted coiled coil-like sequence and is thought to mediate oligomerization of Ena/VASP proteins (Ahern-Djamali et al. 1998). The central proline-rich domain mediates direct interactions with the actin-binding protein Profilin and with the SH3 domains of the tyrosine kinases Abl, Arg, and Src (Gertler et al. 1996). A higher molecular weight form of Mena is produced by the alternate inclusion of an exon (the "[+]" exon) between the EVH1 domain and the proline-rich core; this Mena(+) isoform is enriched in the developing nervous system and is the only Mena isoform found to be tyrosine phosphorylated during development (Gertler et al. 1996). Mena, VASP, and EVL share a single conserved site for phosphorylation by cyclic nucleotide-dependent protein kinase A (PKA) and are in vivo substrates for PKA (Butt et al. 1994; Gertler et al. 1996; F. B. G., unpublished data). In addition, Mena and VASP share a second consensus

phosphorylation site that, in the case of VASP, has also been shown to be a target for cyclic GMP-dependent kinases (Butt et al. 1994).

Several findings implicate Mena and VASP in the regulation of cytoskeletal dynamics. First, Mena and VASP accumulate at focal adhesions, which are sites of bidirectional signaling between the cytoskeleton and the extracellular matrix, and in regions of dynamic actin remodeling such as the lamellipodia at the leading edge of motile cells (Reinhard et al. 1992; Gertler et al. 1996). Second, at least one member of the Ena/VASP family must be present for rapid, directed, actin-based movement of Listeria (V. Laurent, J. Wehland, F. B. G., and M. Carlier, unpublished data). Profilin has also been implicated in Listeria movement (Theriot et al. 1994), and it has been postulated that one function of Mena and VASP in this context is to bind ActA and link Profilin to the surface of Listeria. Third, expression of the neural specific Mena(+) isoform in fibroblasts leads to the formation of actin-rich cell surface protrusions, suggesting that at least this Mena variant can induce actin remodeling (Gertler et al. 1996). Ectopic expression of the other form of Mena, or of EVL or VASP, does not induce actin protrusion (Gertler et al. 1996; F. B. G., unpublished data).

The fact that Mena(+) is highly expressed in the developing nervous system and can induce actin protrusion led to the hypothesis that, like Ena, Mena(+) could play a role in regulating growth cone motility and axon guidance. In the developing axon, actin polymerization drives formation of growth cone filopodia and is required for axon pathfinding, whereas microtubule polymerization extends and stabilizes the axon shaft

once a direction is chosen (Mitchison and Kirschner 1988). Extension or retraction of filopodia is the first morphological change observed in response to guidance signals, suggesting that proteins that regulate actin polymerization in the filopodia may play a central role in transducing extracellular signals into changes in growth cone motility.

Although many proteins have been reported to be in growth cones, relatively few have been shown to be enriched in filopodia. Among those identified are β1 integrin, a trasmembrane protein that binds extracellular ligands and is physically linked to the actin cytoskeleton, and members of the Ezrin-Radixin-Moesin (ERM) family, intracellular proteins that physically link actin filaments to the plasma membrane (Wu et al. 1996). Under certain conditions, phosphotyrosine is also detected at the distal tips of filopodia, although the identity of the tyrosine-phosphorylation substrate(s) has not been determined (Wu and Goldberg 1993). Localization of these proteins in the filopodia appears to affect growth cone dynamics and may be important in regulating axon guidance (Wu and Goldberg 1993; Wu et al. 1996; Paglini et al. 1998).

In this report, we present data indicating that Mena plays an important role in the regulation of growth cone dynamics and axon guidance. We have generated Mena-deficient mice and analyzed the phenotype of the mutant animals. We show that Mena is expressed in the developing nervous system and is required for the normal formation of several major axonal projection pathways in the brain, including the corpus callosum and hippocampal commissure. Consistent with a role for Mena in axon guidance, we find that Mena is highly concentrated in the distal tips of growth cone filopodia. Finally, we

describe a potent interaction between mutations in *Mena* and *Profilin I* that reveals a role for these molecules in neural tube closure and provides the first genetic evidence linking Mena function to regulation of actin cytoskeletal dynamics.

## Experimental Procedures

**Targeted Disruption of Mena.** A targeting vector was constructed by fusing an 8 kb fragment of genomic DNA from the first intron of Mena to a splice-acceptor β geo cassette with a polyadenylation site (Friedrich and Soriano 1991) followed by a 1.1 kb fragment from the third intron of Mena. A PGK-diphtheria toxin cassette was inserted after the short arm fragment for negative selection. Further details of the construction and the Mena genomic locus are available upon request. The targeting vector was electroporated into AK7 ES cells (Imamoto and Soriano 1993). Correctly targeted clones were identified by PCR and verified by Southern blotting analysis. Four ES clones were used to generate chimeras by blastocyst injection. Germline transmission of the disrupted allele was verified by PCR and Southern blot analysis. ES cell culture and blastocyst injection were performed as described (Friedrich and Soriano 1991).

**Western Blot Analysis.** Organs were dissected and placed in buffer (RIPA; 50 mM Tris [pH 8.0], 150 mM NaCl, 1% triton, 0.5% deoxycholate, 0.1% SDS, 1 μM pepstatin, 1 mM PMSF, 0.3 μM aprotinin, 1 μM Leupeptin, 5 μM E-64, 1 mM EDTA, 1 mM sodium vanadate, 50 mM sodium fluoride, 2 mm levamisole, 30 mM sodium pyrophosphate), the tissues were dissociated using a tissue homogenizer, and extracts were centrifuged for 30

min at 100,000 g. Protein concentrations were determined using the BCA assay (Pierce). SDS-PAGE electrophoresis and Western blotting were done using standard techniques. Antibodies included anti-Mena (polyclonal antiserum 2197), anti-Tubulin (polyclonal T3526, Sigma), anti-EVL (monoclonal 84H1), anti-VASP (polyclonal M4, Alexis Corp.), and horseradish peroxidase-conjugated goat anti-rabbit and anti-mouse (Jackson ImmunoResearch). Signal was developed using the Renaissance chemiluminescence reagent (Dupont-NEN).

**In Situ Hybridization.** In situ hybridization was done following protocol 2 as described (Hogan et al. 1994). Probes were prepared by in vitro transcription of linearized template DNA (either the entire Mena coding sequence or the [+] exon alone) using digoxigenin labeled nucleotides (Boehringer Mannheim). Sense and antisense probes were prepared using the T7 and T3 promoters at opposite ends of the linearized template. Signal was developed using an alkaline phosphatase-conjugated anti-digoxigenin antibody (Boehringer Mannheim) and BCIP/NBT (Vector Labs).

**Tissue Preparation and Histological Analysis.** Animals were anesthetized with Avertin and transcardially perfused with 4% PFA. Brains were dissected and either placed directly in 4% PFA (for silver staining, DiI labeling, and immunocytochemistry) or in 30% sucrose followed by 4% PFA (X-gal histochemistry and subsequent anti-Py, anti-MAP-2, or anti-neurofilament immunocytochemistry; Snyder et al. 1997). Silver staining was done as described (Fink and Heimer 1967).

X-gal histochemistry was developed as described (Hogan et al. 1994). Specimens were either embedded in OCT and cut on a cryostat (Figure 4A and Figure 4B) or were frozen and cut using a freezing microtome (Figure 4C). After X-gal histochemistry, sections were rinsed, blocked, and incubated sequentially with primary antibodies (anti-Py [Woodhams et al. 1989] or anti- neurofilament [Amersham]), biotinylated secondary antibody, Avidin-Biotin complex (Vector Laboratories), and diaminobenzidine substrate (Pierce).

**DiI Labeling.** After perfusion, P0 brain specimens were placed in fresh 4% PFA for 2–3 days. A glass capillary (outside diameter 70 μm), attached to a Nanojector (Drummond Scientific Co.), was filled with 0.5 μl of 10% DiI in 100% ETOH (Honig and Hume 1989) and lowered 100 μm deep into the cortical surface at five sites along the rostral-caudal midline (i.e., cingulate cortex), and 50 nl of the DiI was slowly injected. The specimen was subsequently placed back in fresh 4% PFA and incubated at 37°C for 8–10 weeks, after which 50 μm coronal sections were cut using a vibrating microtome (Vibratome) and mounted with Fluromount G (Electron Microscopy Sciences).

**Cell Culture and Immunocytochemistry.** Primary hippocampal neurons were prepared from E16 mouse as described for E18 rat (Goslin and Banker 1991). After 24 hrs, cells were fixed in 4% PFA/PBS, blocked with 10% BSA/PBS, and permeablized with 0.2% Triton-X100/PBS. Primary antibodies included poly- and monoclonal anti-Mena antibodies, polyclonal anti-(+) exon antibody, and monoclonal antibody 13H9 (Goslin et al. 1989). Secondary antibodies included cy-5-goat anti-rabbit, Texas-red donkey anti-

rabbit, and FITC-donkey anti-mouse (Jackson ImmunoResearch). Coverslips were mounted with DABCO in polyvinyl alcohol and imaged using a Deltavision deconvolution imaging microscope.

Glial cultures were prepared from P0 mouse cortex and plated onto tissue culture dishes in plating medium (MEM, 10% horse serum, 0.6% glucose). Cortical cultures were prepared from E15 mice, plated on poly-L-lysine coated dishes and maintained in serum free medium (1:1 F-12:MEM supplemented as described for serum-free hippocampal culture, except using 25 μg/ml insulin). Under these conditions, the majority of the cells are neuronal, though nondividing glia persist.

**Analysis of *Mena–profilin* Animals.** The construction of the *profilin I* targeting vector will be reported elsewhere (W. W. and D. K., unpublished data). The *profilin I* mutation was generated in J1 ES cells, which were derived from a 129sv strain (Li et al. 1992). *profilin I* heterozygotes were bred with $Mena^{\beta geo}$ heterozygotes. The *profilin I*, $Mena^{\beta geo}$ double heterozygous progeny were intercrossed for the analysis presented. Consistent results from this cross were observed with these animals and with double heterozygous animals that had been backcrossed into a congenic 129sv strain for up to four generations. Although it is formally possible that the defects seen in the $Mena^{\beta geo/\beta geo}$;*profilin I*-/+ animals are associated with a tightly linked locus, it is striking that we analyzed over a hundred animals and never observed neural tube defects segregating independently of the *profilin I* allele. E9.5 embryos from *Mena–profilin* crosses were dissected, tails were removed for genotyping (see above), and embryos were fixed in 4% PFA, then photographed, and stored in PBS. Embryos for scanning electron

microscopy were dehydrated in methanol/PBST, washed in methanol, and allowed to air dry for 5 min prior to mounting with adhesive tape.

## Results

### Generation and Biochemical Characterization of Mena-Deficient Mice

A targeted disruption of the Mena locus was generated through homologous recombination in embryonic stem (ES) cells. Exons 2 and 3 of the *Mena* gene were replaced by a cassette encoding a β-galactosidase (LacZ)–neomycin fusion protein (βgeo; Figure 1A). The resulting locus produced a fusion protein containing the 5' untranslated region of Mena and the initiator methionine fused in frame to βgeo. This strategy resulted in a *Mena* protein null mutant and introduced a *lacZ* reporter gene under the control of the endogenous Mena promoter (creating the $Mena^{\beta geo}$ allele).

Four independent $Mena^{\beta geo/+}$ ES cell lines were used to obtain germline transmission of the mutant allele. Genotypes of the resulting animals were determined by Southern blot analysis (data not shown) and polymerase chain reaction (PCR; Figure 1B). All four ES cell lines gave equivalent results, so one of these lines was selected for further analysis. *Mena* homozygous mutant animals ($Mena^{\beta geo/\beta geo}$) were fully viable and were recovered in the appropriate Mendelian ratios (data not shown). Homozygous mutant animals were smaller than their littermates until adulthood and exhibited abnormal cage behavior, including reduced activity (data not shown). Western blot analysis of extracts from embryonic heads and adult brains was used to verify that the

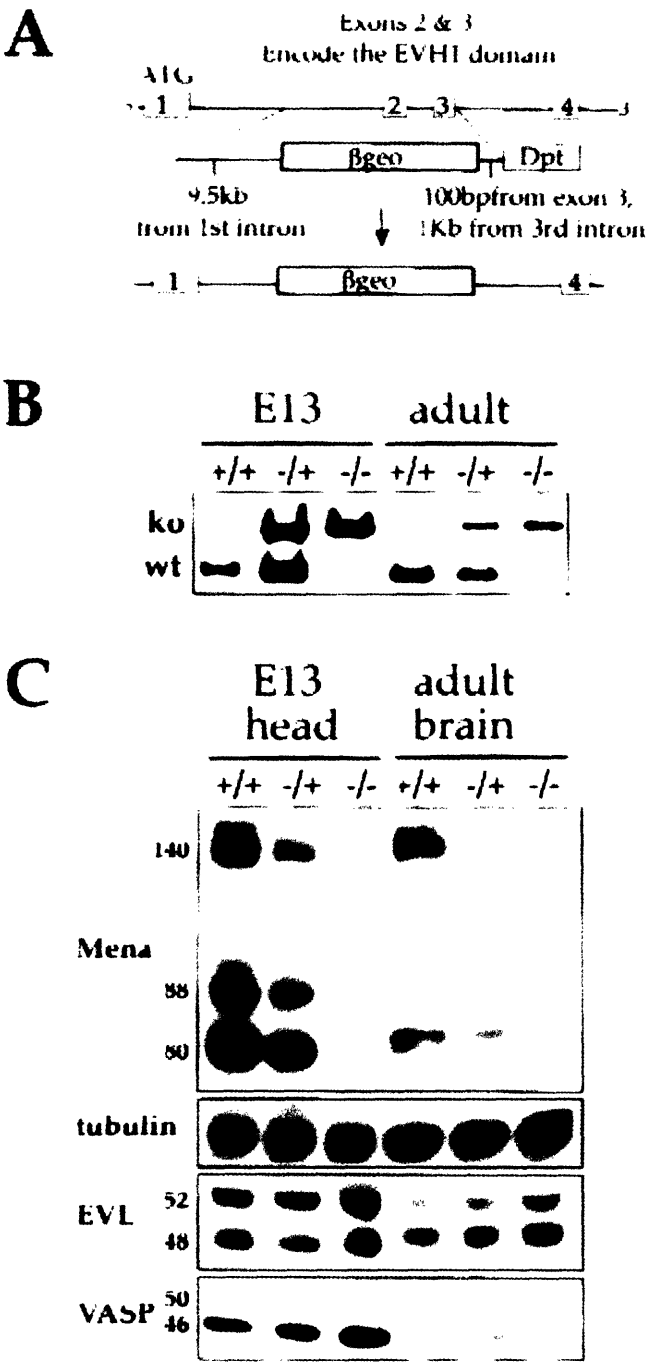
A
Exons 2 & 3
Encode the EVH1 domain
ATG
1
2
3
4
βgeo
Dpt
9.5kb
from 1st intron
100bpfrom exon 3,
1Kb from 3rd intron
1
βgeo
4
B
E13
adult
+/+ -/+ -/- +/+ -/+ -/-
ko
wt
C
E13
head
adult
brain
+/+ -/+ -/- +/+ -/+ -/-
140
Mena
88
80
tubulin
EVL
52
48
VASP
50
46

**Figure 1**

**Figure 1. Generation and Biochemical Characterization of the *Mena*$^{\beta geo}$ Mutation**

(A) The targeting vector contained a β-galactosidase–neomycin (βgeo) fusion cassette flanked by genomic sequence from the first and third introns of the Mena locus. Homologous recombination between the intron sequences deleted exons 2 and 3 of the Mena locus and inserted the *βgeo* gene. Inclusion of both the neomycin and diphtheria toxin (Dpt) genes allowed for both positive selection of recombinants and negative selection against nonhomologous recombination.

(B) PCR analysis was done on E13 and adult animals. Position of the wild-type (wt) and *Mena*$^{\beta geo}$ mutant (ko) bands are indicated.

(C) Extracts from wild-type (+/+), heterozygous (-/+), and homozygous (-/-) E13 heads and adult brains were analyzed by Western blot using antibodies to Mena, Tubulin, EVL, and VASP. Analysis of Tubulin levels confirms that equal amounts of protein were loaded in each lane. Relative molecular weights are indicated.

*Mena*$^{\beta geo}$ allele was a protein null. As previously reported, three forms of Mena (corresponding to bands of 80, 88, and 140 kDa; Gertler et al. 1996) are expressed in embryonic heads, while only the 80 and 140 kDa forms are expressed in adult brains (Figure 1C). Expression of all three forms of Mena was reduced in the heterozygotes and completely eliminated in the homozygotes. Finally, reduction in Mena expression may lead to a slight increase in expression of EVL and VASP (Figure 1C; The 52 and 50 kDa bands of EVL and VASP represent serine/threonine phosphorylated versions of the 48 and 46 kDa bands, respectively; Halbrügge and Walter 1989; A. Lambrechts and F. B. G., unpublished data).

**Mena Protein Expression**

The distribution of Mena in wild-type adult organs was compared to that of EVL and VASP (Figure 2A). The 140 kDa form of Mena was detected only in the brain, while the 80 kDa form of Mena was expressed predominantly in brain, testis, ovaries, and fat. In contrast, EVL and VASP were most highly expressed in thymus and spleen, and the relative intensities of the phospho and dephospho forms varied from tissue to tissue, suggesting that EVL and VASP may be differentially regulated in the brain and organs. Because Mena was expressed at high levels in the brain, while both VASP and EVL were expressed at low levels, the distribution of Mena in adult and developing brain was characterized in greater detail.

The 80 and 140 kDa forms of Mena were detected in all regions of the adult brain, with highest levels in the hippocampus, cortex, and midbrain, and lowest levels in the

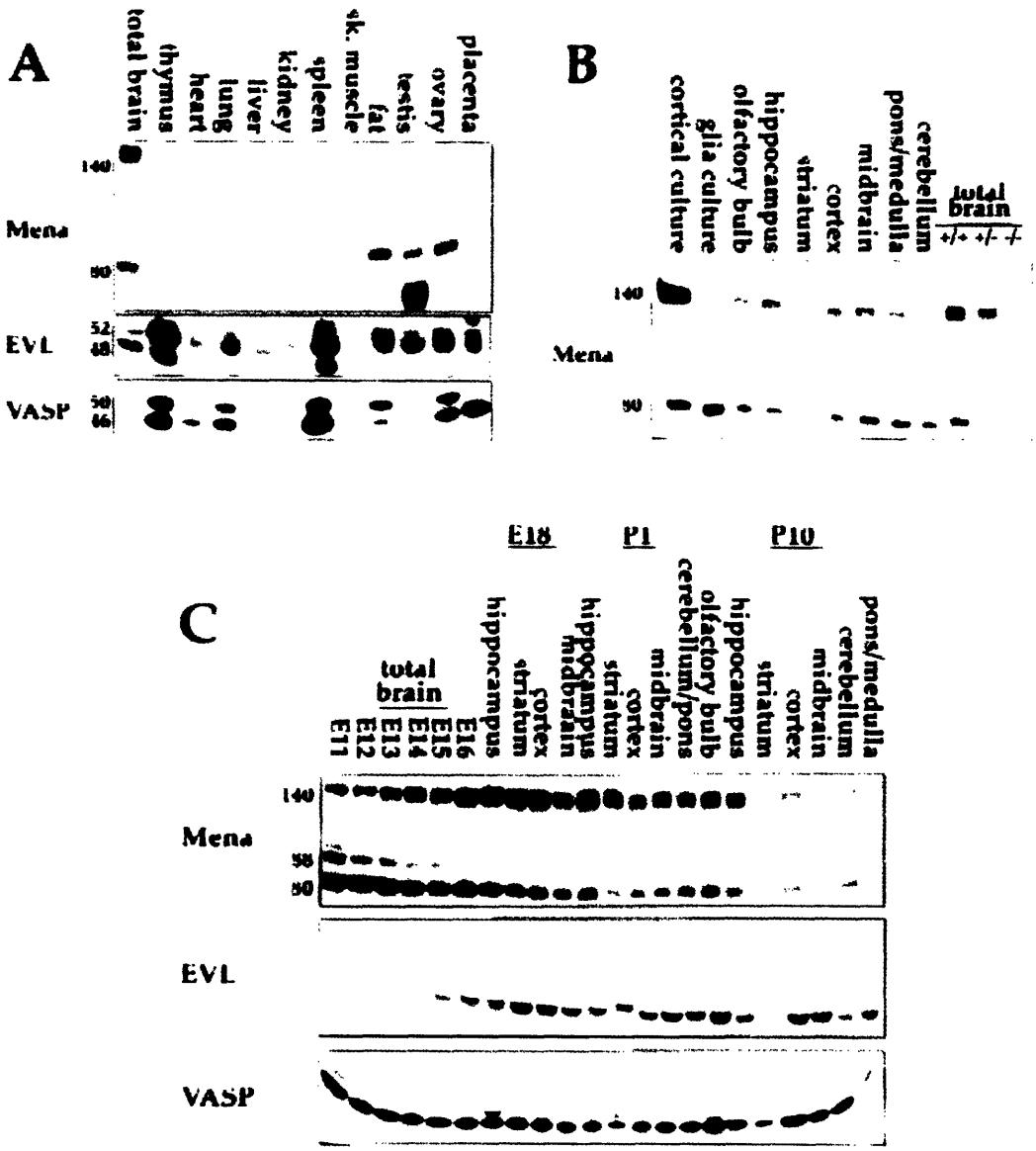
A
total brain
thymus
heart
lung
liver
kidney
spleen
tk. muscle
fat
testis
ovary
placenta
Mena
EVL
VASP
140
80
52
48
30
66
B
cortical culture
glia culture
olfactory bulb
hippocampus
striatum
cortex
midbrain
pons/medulla
cerebellum
total brain
+/+ +/- -
Mena
140
80
C
E18
P1
P10
total brain
E11
E12
E13
E14
E15
E16
hippocampus
cortex
striatum
hippocampus
midbrain
striatum
cortex
midbrain
cerebellum/pons
olfactory bulb
hippocampus
striatum
cortex
midbrain
cerebellum
pons/medulla
Mena
EVL
VASP
140
80
30

# Figure 2

**Figure 2. Western Blot Analysis of Mena Expression Patterns**

(A) Detection of Mena, EVL, and VASP in extracts from adult brain and organs.

(B) Detection of Mena in extracts from adult brain regions. Extracts from glial and cortical cultures are shown to demonstrate that the 140 kDa form of Mena is neuron-specific. Brain regions include: olfactory bulb, hippocampus, striatum (caudate, putamen, and globus pallidus), cortex, midbrain (including thalamus), pons/medulla, and cerebellum. Extracts from total brain of wild-type (+/+), heterozygous (-/+), and homozygous(-/-) adult animals are shown for comparison.

(C) Detection of Mena, EVL, and VASP in the developing brain. Extracts were prepared from either total brain (E11-E16) or from the indicated brain regions (E18, P1, P10). Extracts in (C) were prepared from total E13 heads, while extracts in Figure 2C were prepared from brain only, indicating that at early stages (E13) EVL expression in the head is in regions outside the brain. Analysis of Tubulin levels confirmed that equal amounts of protein were loaded in each lane (data not shown)

striatum and cerebellum (Figure 2B). The 140 kDa form of Mena was expressed at relatively high levels in serum-free cortical cultures (which are enriched for neurons) and was not detected in glial cultures, suggesting the 140 kDa form is indeed neuron-specific and that it may be the predominant form of Mena in neurons. In embryonic brains, all three forms of Mena are detected at embryonic day 11 (E11), the earliest time point examined (Figure 2C). Expression of the 88 kDa form decreased steadily and became almost undetectable by E16, while expression of the 140 kDa form began to increase at E13 and peaked between E16 and E18. In contrast to Mena, EVL expression in the brain was first detected at E15 (Figure 2C). In situ hybridization confirmed that in early stage embryos EVL is highly expressed in the branchial and pharyngeal arches, but not in the brain (data not shown). VASP expression appeared to be fairly constant throughout development of the brain, but then decreased to relatively low levels in the adult brain (Figure 2C).

The pattern of Mena expression in embryonic tissues was determined by in situ hybridization of whole-mount embryos using either a probe that detects all Mena transcripts or a probe specific to the Mena(+) exon. At E8.5, Mena was particularly enriched in the neuroepithelium, the forebrain, and the somites (Figure 3A). A dorsal view of the same embryo shows that Mena was highly expressed in the edges of the neural folds (Figure 3B). By E10.5, Mena expression was detected in the brain, dorsal root ganglia (DRG), somites, and limb buds (Figure 3C and Figure 3D). In addition, Mena was highly expressed in the branchial and pharyngeal arches, neural crest-derived structures that give rise to portions of the face and neck. At E10.5, a probe for the (+)

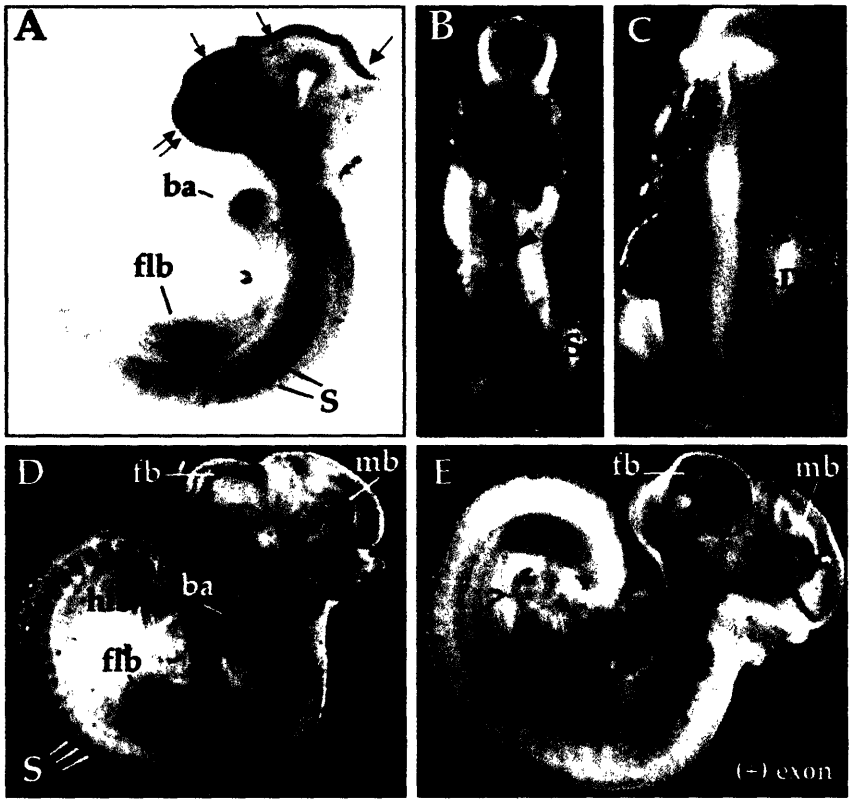


**Figure 3**

**Figure 3. Mena Expression in the Developing Embryo Determined by In Situ Hybridization**

(A) At E8.5, Mena is detected primarily in the somites (S), neuroepithelium (single arrows), and the cephalic neural folds overlying the forebrain region (double arrow). Low level expression is detected in the branchial arch (ba) and the forelimb bud (flb).

(B) Dorsal view of the same E8.5 specimen in (A) shows high level of Mena expression in the dorsal neural crest (arrow head).

(C) E10.5 dorsal view. High level Mena expression is detected in the somites (S) and dorsal root ganglia (DRG).

(D) Side view of the same E10.5 embryo in (C). Mena expression is detected in the forebrain (fb), midbrain (mb), branchial arch (ba), pharyngeal arch (pa), forelimb bud (flb), hindlimb bud (hlb), and somites (S).

(E) A probe specific for the (+) exon detects expression of the neuronal specific 140 kDa form of Mena in the developing central nervous system, including the forebrain (fb) and midbrain (mb), but not in the DRG or limb buds.

exon detected the Mena(+) isoform in regions of the developing central nervous system (CNS), but not in the DRG of the developing peripheral nervous system (Figure 3E).

The *Mena*$^{\beta geo}$ allele provides a convenient and sensitive means to characterize Mena expression at the cellular level. β geo activity is restricted to cell bodies and can be used to identify cell types, but it is not readily detected in axonal projections. High levels of *Mena*$^{\beta geo}$ expression were detected in distinct bands of cells in the developing cortex at E16, a time when neurons are migrating from the ventricular zone to the cortical layers and axons are beginning to project across the corpus callosum (Figure 4A; Macklis 1993; Koester and O'Leary 1994). In the adult brain, *Mena*$^{\beta geo}$ expression was detected in laminae 2/3 and 5 of the cortex and was particularly enriched in the hippocampus and the septum (Figure 4C and Figure 4F). In agreement with anti-Mena Western blot data (Figure 2B and Figure 2C), relatively low level expression was detected in the striatum and globus pallidus. Double labeling of sections with LacZ and antibodies to either neurofilament protein, MAP-2 or Py, an antigen found in a subset of projection neurons (Woodhams et al. 1989), confirmed that in the cortex *Mena*$^{\beta geo}$ was expressed in pyramidal neurons of layers 2/3 and 5 (Figure 4C– MAP2 data not shown).

**Axonal Pathfinding Defects in *Mena*$^{\beta geo/\beta geo}$ Mutant Animals**

Given Mena expression patterns and the axonal defects detected in *Ena* mutant flies (Gertler et al. 1995), we speculated that *Mena*$^{\beta geo/\beta geo}$ homozygous animals would display abnormalities in the brain. Indeed, neurofilament staining of sections through the forebrains of adult *Mena*$^{\beta geo/\beta geo}$ animals revealed striking abnormalities in the corpus

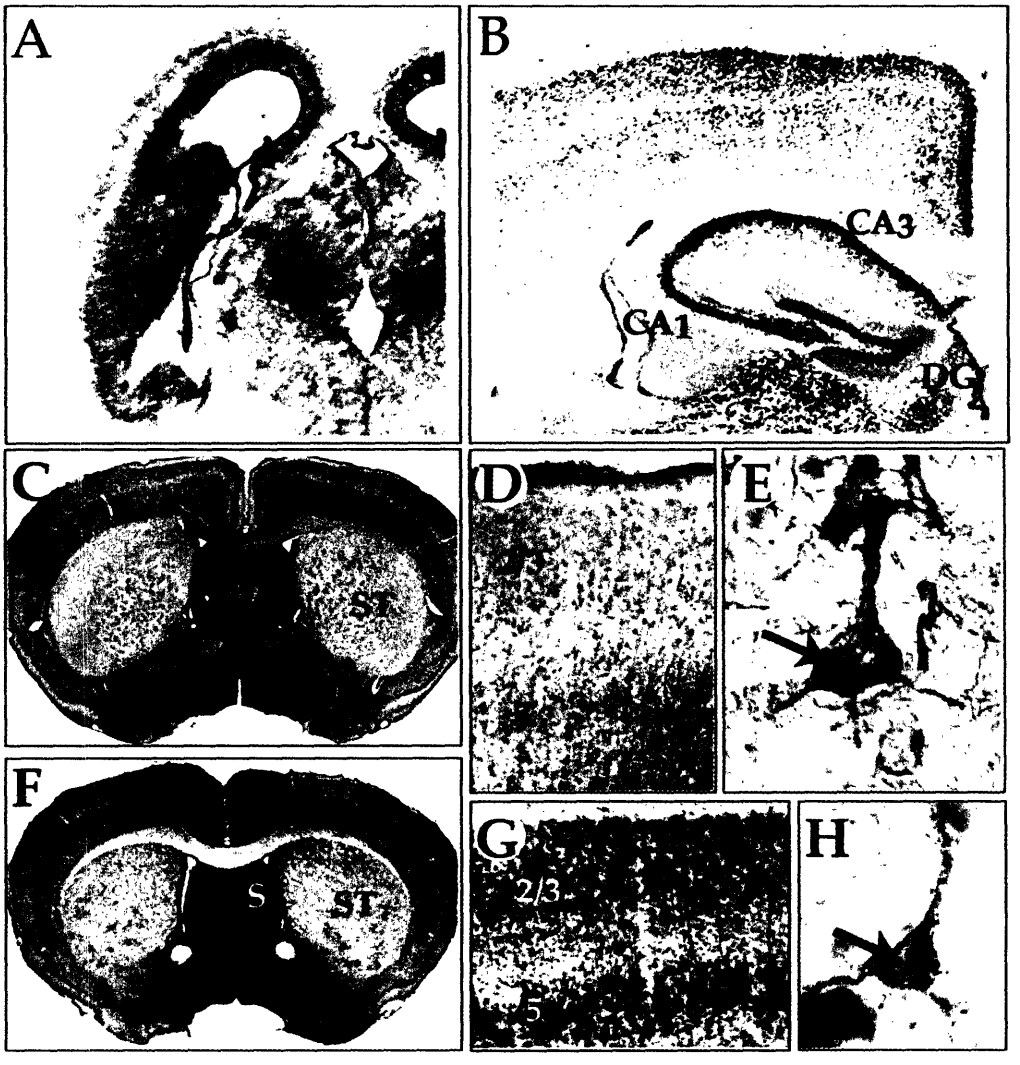


**Figure 4**

**Figure 4. Mena Expression in the Developing and Adult Brain**

*Mena*$^{\beta geo}$ expression in heterozygote (*Mena*$^{\beta geo/+}$) animals was used as a reporter for Mena expression. *Mena*$^{\beta geo/+}$ animals were phenotypically indistinguishable from wild-type animals, except for the LacZ expression (data not shown). LacZ activity is indicated by a purple/blue (A and B) or blue (C–H) precipitate, depending on how the specimen is processed.

(A) At E16, *Mena*$^{\beta geo}$ is highly expressed in a banded pattern in the developing cortex and in midbrain. Specimen is counterstained with EosinY.

(B) In a section through the adult forebrain, *Mena*$^{\beta geo}$ is most highly expressed in cortical laminae 2/3 and 5, and in the hippocampus, including the CA1 and CA3 regions, and the dentate gyrus (DG).

(C–H) More rostral sections through the adult forebrain were double labeled for LacZ (blue) and either neurofilament protein (C–E) or Py antigen (F–H). (C and F) At 2x magnification, highest levels of *Mena*$^{\beta geo}$ expression are detected in the septum (S) and distinct laminae of the cortex. Relatively low expression is detected in the striatum (ST). At 20x (D and G), it is apparent that *Mena*$^{\beta geo}$ is expressed primarily in cortical laminae 2/3 and 5. At 60x magnification (E and H), *Mena*$^{\beta geo}$ expression is localized in the cell bodies of pyramidal neurons in cortical laminae 5 (arrows).

callosum, the major axonal projection pathway connecting the two hemispheres of the brain (Figure 5D). Wild-type littermates showed a morphologically normal corpus callosum, as did *Mena*$^{\beta geo/+}$ heterozygotes (Figure 5A). In *Mena*$^{\beta geo/\beta geo}$ animals, fibers in the corpus callosum appeared to reach a point just medial to the cingulum bundle as normal but then failed to project medially and cross the midline. Instead, most of the fibers formed dense neuromas just dorsomedial to the forebrain lateral ventricles (Probst bundles [P]; Figure 5D; Probst 1901). In contrast, the anterior commissure and the hippocampus, including the dentate gyrus, appeared to develop normally (Figure 5E and Figure 5F). Spontaneous agenesis of the corpus callosum has been observed in several inbred strains of mice, including 129sv (Wahlsten 1982). Therefore, the *Mena* mutation was backcrossed to C57BL6 mice for ten generations, and all mice analyzed in these experiments were the coisogenic F1 progeny of crosses between the 129sv inbred and the C57BL6 backcrossed lines. Agenesis of the corpus callosum was observed in 11 out of 20 *Mena*$^{\beta geo/\beta geo}$ animals but was never observed in 20 littermate control animals, indicating that the defects result from loss of Mena rather than as an effect of genetic background. The penetrance of commissural defects in the *Mena* mutants is similar to that seen in several other genetic models for axon guidance (e.g., Orioli et al. 1996) and may reflect redundancy in the Ena/VASP family (see Discussion). It is also possible that the remaining *Mena*$^{\beta geo/\beta geo}$ mutants have more subtle defects in midline crossing, the identification of which will require further analysis.

Using silver staining to visualize the fiber tracts at higher resolution, it was possible to observe that in the *Mena*$^{\beta geo/\beta geo}$ mutants a few fibers emerged from the Probst


A
cng
cc
B
fo
ac
C
CA1
CA3
DG
D
cng
fp
E
fo
ac
F
CA1
CA3
DG
G
cng
ac
H
cc
fo
hc
ac
I
hc
ac
J
cng
fp
ac
K
fo
ac
L
ac
M
N

**Figure 5**

**Figure 5. Histological Comparison of Wild-Type and Mutant Adult Brains**

Matched section of wild-type and homozygous mutant (*Mena*$^{\beta geo/\beta geo}$) brains were analyzed either by neurofilament immunocytochemistry (A–F) or by silver staining (G–N).

(A–C) Neurofilament staining of rostral to caudal sections through a wild-type brain reveals the properly developed corpus callosum (cc), cingulum bundle (cng), anterior commissure (ac), and hippocampal regions CA1, CA3, and dentate gyrus (DG).

(D–F) Similar sections through a homozygous mutant reveal the presence of Probst bundles (P) and failed midline crossing of axons traversing the corpus callosum.

(G–L) Silver staining of matched sections through wild-type (G–I) and *Mena*$^{\beta geo/\beta geo}$ mutant (J–K) brains at magnification of 2x (G and J), 4x (H and K), and 20x (I and J).

(G–I) In the wild-type brain, it is possible to see the pre- and postcommissural fornix (fopr and fop, respectively) and the hippocampal commissure (hc), in addition to those structures seen by neurofilament staining.

(J–L) In the *Mena*$^{\beta geo/\beta geo}$ mutant, many structures are abnormal or missing.

(K and L) A few fibers from the corpus callosum appear to project ventrally and cross just above the dorsal fornix (arrow head).

(L) Cells are visible in the midline (arrow), but fibers of the hippocampal commissure do not appear to cross as they do in the wild-type control (compare to [I] and [L]).

(M and N) Comparison of matched sections through the pons of wild-type (M) and *Mena*$^{\beta geo/\beta geo}$ mutant (N) brains reveals that a decreased number of axons reach and eventually cross the midline.

bundles and projected medially, crossing the midline just above the dorsal fornix (Figure 5J). Within the fornix, fibers of the hippocampal commissure appeared abnormal; instead of crossing contralaterally, they appeared to reach the midline and project ipsilaterally (compare Figure 5I and Figure 5L). In more caudal sections, hippocampal commissure fibers crossed the midline (data not shown), indicating that the defects in the hippocampal commissure are most likely due to misrouting and/or reduction in the number of fibers. Close examination of the sections revealed the presence of cells at the midline (Figure 5L), indicating that the interhemispheric fissure had fused properly during development. Defects in midline fiber crossing were also observed in the pons, where decreased numbers of pontocerebellar fibers reached and crossed the midline (Figure 5M and Figure 5N). No defects were observed in other commissures, including spinal motor neuron tracts, or in cortical lamination, indicating that there was not a global failure in midline crossing or neuronal cell migration (data not shown). DARPP-32 immunocytochemistry was used to analyze axonal projections in the internal capsule for potential defects in axonal fasciculation and/or pathway formation; however, no obvious disturbances were noted in these axonal pathways (data not shown).

To determine if the corpus callosum failed to form during development or whether it formed and then degenerated, we analyzed the development of this structure by DiI labeling. At P0, the corpus callosum of wild-type animals was well formed and projected contralaterally through the midline (Figure 6A and Figure 6B). In *Mena*$^{\beta geo/\beta geo}$ littermates, fibers of the corpus callosum reached the presumptive cingulum bundle but then appeared to project dorsally and turn away from the midline (Figure 6C and Figure

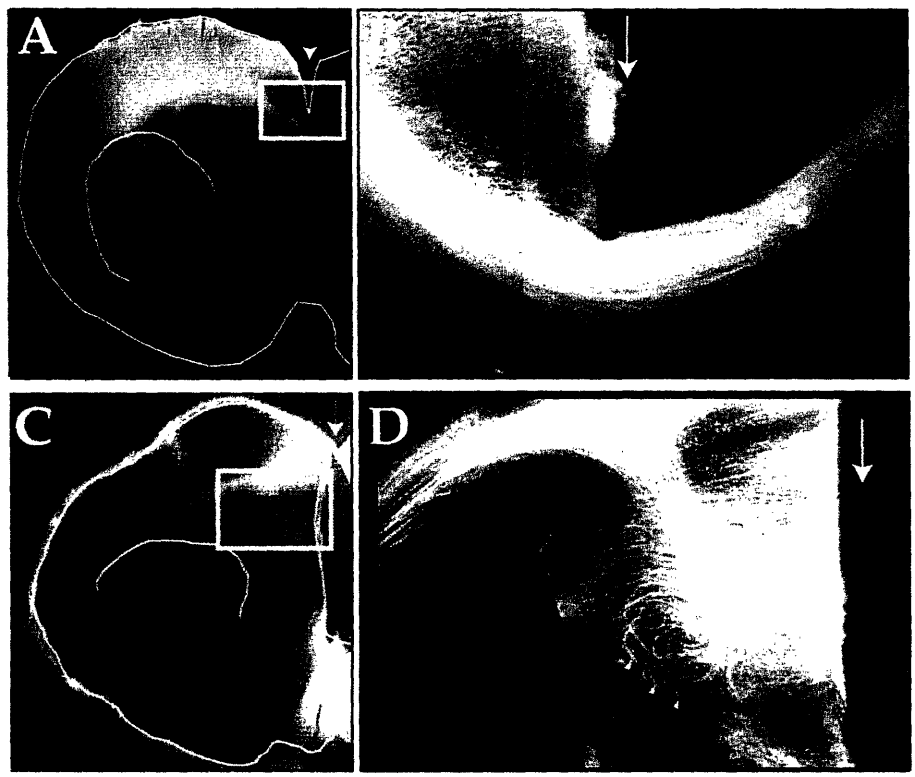


**Figure 6**

**Figure 6. Analysis of Axonal Projections in the Developing Brain**

Axonal projections were viewed by DiI dye tracing in matched sections through the corpus callosum of P0 wild-type (A and B) and *Mena*$^{\beta geo/\beta geo}$ mutant (C and D) brains. (A and C) Low magnification bright field images were traced (shown as a white line) and overlaid on the fluorescence image in order to show orientation. The boxed area is shown at higher magnification (B and D). Arrows indicate the position of the midline. Arrowheads (D) point to misrouted axons.

6D). Therefore, the defects in the corpus callosum associated with the *Mena*$^{\beta geo/\beta geo}$ mutation were due primarily to a failure of the axons to project across the midline during development.

**Mena Localization in Neuronal Growth Cones**

Given the axon guidance defects in the *Mena* mutants, it was important to determine if the subcellular distribution of Mena was consistent with a role for Mena in axon guidance and/or growth cone motility. To do this, we chose to use cultured primary embryonic hippocampal neurons, which elaborate multiple dendrites and a single morphologically and histologically distinguishable axon (Goslin and Banker 1991). Immunocytochemical analysis revealed that Mena was highly enriched in the lamellipodium and at the tips of the axonal growth cones (Figure 7A). Identical results were observed with poly- and monoclonal anti-Mena antibodies; no signal was observed when primary antibodies were omitted (data not shown). Similar Mena localization was seen in dendritic growth cones and at various stages of differentiation (data not shown), suggesting that Mena may function in both types of growth cones throughout development. The pattern of staining was the same when antiserum specific for the (+) exon was used, suggesting that the neuron-specific 140 kDa form of Mena is enriched at the tips of filopodia (data not shown). Whether Mena staining in filopodia is due solely to the presence of the 140 kDa form, or whether both the 80 and 140 kDa forms are present in filopodia, remains to be determined. To put Mena localization in the context of other proteins that have been localized to growth cone filopodia, triple labeling was done to localize Mena, ERM proteins, and filamentous actin (F-actin; Figure 7B). The merged

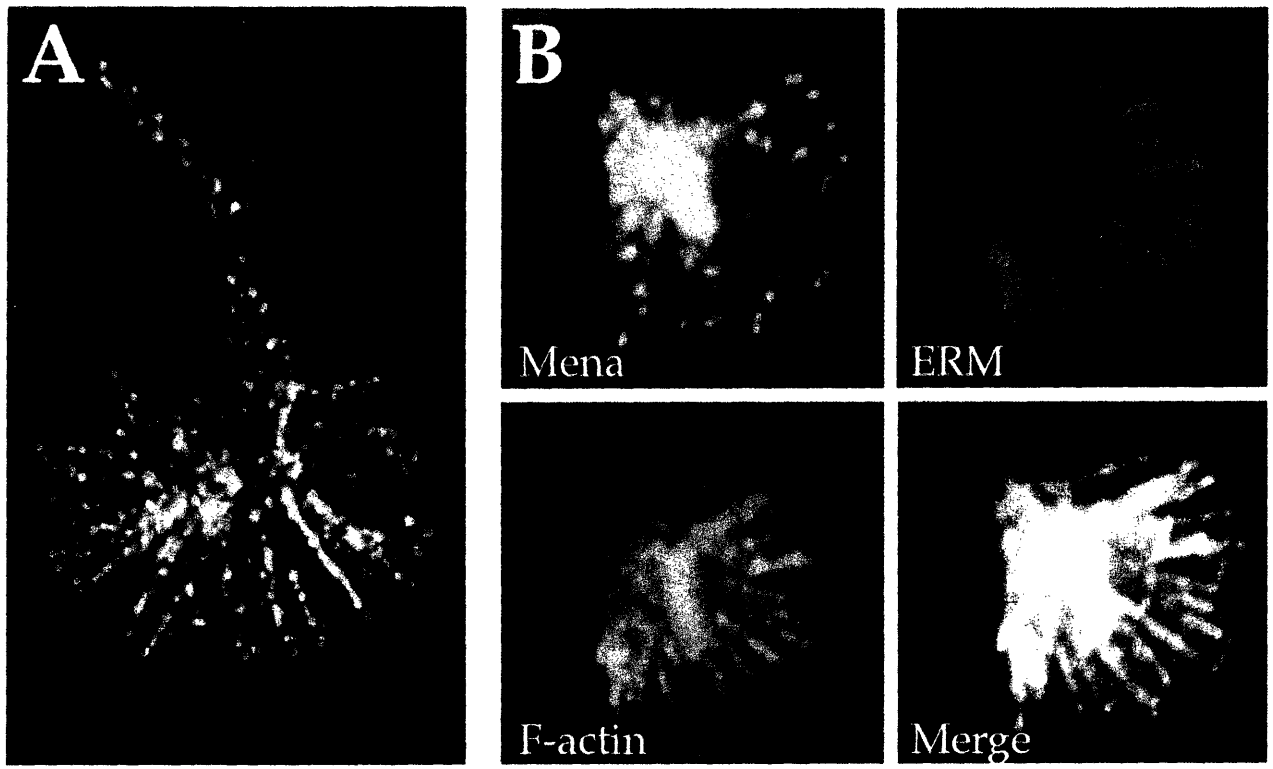


**Figure 7**

**Figure 7. Mena Localization in Growth Cone Filopodia**

Embryonic hippocampal neurons were fixed and labeled with antibodies to detect Mena and ERM proteins and with rhodamine-phalloidin to detect filamentous actin (F-actin). (A) Mena (green) is enriched at the tips of growth cone filopodia, distal to F-actin (red). (B) Triple labeling reveals that Mena (red) is distal to both F-actin (green) and the ERM proteins (blue). This is most clearly seen in the merged image.

image clearly demonstrates that in filopodia, Mena staining is observed distal to both actin and the ERM proteins.

**Genetic Interaction between Mena and Profilin I**

A key to understanding Mena function comes from biochemical studies of Mena ligands and of Mena function in the actin-based motility of Listeria. Mena binds with high affinity to Profilin I (Gertler et al. 1996), an actin-binding protein that plays a role in regulating the rate of actin polymerization (Theriot and Mitchison 1993). Both Ena/VASP proteins and Profilin are required for rapid movement and cell-to-cell spread of the Listeria (Smith et al. 1996; Niebuhr et al. 1997). These observations led to the hypothesis that one function of Mena may involve its ability to bind Profilin, which could in turn modulate actin dynamics. We used a genetic approach to test the significance of the Mena–Profilin I interaction, reasoning that reducing the amount of Profilin I within cells might sensitize animals to loss of Mena and thereby expose requirements for these proteins. In an otherwise wild-type animal, *profilin I* heterozygotes are viable, but produce 50% of the normal amount of Profilin I, while *profilin I* homozygous mutants display preimplantation lethality (W. W. and D. K., unpublished data). Animals doubly heterozygous for *Mena* and *profilin I* mutations were mated, and the genotypes of viable progeny classes were determined (Table 1). Strikingly, no viable *Mena* homozygous/*profilin I* heterozygous (*Mena*$^{\beta geo/\beta geo}$;*profilin I*$^{-/+}$) animals were recovered, while other progeny types, including *Mena*$^{\beta geo/+}$;*profilin I*$^{-/+}$, were recovered at the expected frequency. No significant changes in profilin levels were detected in *Mena*$^{\beta geo/\beta geo}$ animals (data not shown). Genotype analysis at E9.5 and E16 revealed that

Table 1. Genotypes of Progeny from *Mena*$^{+/-}$ *profilin I*$^{+/-}$ × *Mena*$^{+/-}$ *profilin I*$^{+/-}$ Matings[a]

| Genotype | *Mena*$^{+/+}$ *profilin I*$^{+/+}$ | *Mena*$^{+/-}$ *profilin I*$^{+/+}$ | *Mena*$^{-/-}$ *profilin I*$^{+/+}$ | *Mena*$^{+/+}$ *profilin I*$^{+/-}$ | *Mena*$^{+/-}$ *profilin I*$^{+/-}$ | *Mena*$^{-/-}$ *profilin I*$^{+/-}$ |
|---|---|---|---|---|---|---|
| Frequency Expected[b] | 1/12 | 1/6 | 1/12 | 1/6 | 1/3 | 1/6 |
| # Expected | 28 | 56 | 28 | 56 | 112 | 28 |
| # Observed | 38 | 72 | 38 | 67 | 121 | 0 |

[a] Genotypes were determined between postnatal day 8 and 10. *Mena*$^{\beta geo/\beta geo}$ is abbreviated as *Mena*$^{-/-}$; *Mena*$^{\beta geo/+}$ is abbreviated as *Mena*$^{+/-}$.
[b] *profilin I*$^{-/-}$ is preimplantation lethal, therefore progeny classes containing the *profilin*$^{-/-}$ genotype were omitted from the calculation of expected frequency.

*Mena*$^{\beta geo/\beta geo}$*;profilin I*$^{-/+}$ embryos were present in Mendelian frequencies (data not shown), suggesting that these animals die perinatally.

Light microscopy of E9.5 embryos revealed that the *Mena*$^{\beta geo/\beta geo}$*;profilin I*$^{-/+}$ animals were smaller than their *Mena*$^{\beta geo/+}$*;profilin I*$^{-/+}$ littermates and often had abnormally formed heads (Figure 8A and Figure 8B). Analysis at E9.5 indicated that the cephalic neural tube failed to close in half (6 of 13) of the *Mena*$^{\beta geo/\beta geo}$;profilin I$^{-/+}$ embryos, but was closed in all other embryos (n = 104; Figure 8C and Figure 8D). Cephalic neural tube closure is initiated at four distinct points (Copp 1994). Close analysis of the *Mena*$^{\beta geo/\beta geo}$*;profilin I*$^{-/+}$ animals revealed that the defects in neural tube closure occurred at closure points 1, 2, and 4 (3 of 13 embryos) or at points 2 and 4 (3 of 13). At E16.5, failure of neural tube closure sometimes manifested as either exencephaly (4 of 9 embryos) or anencephaly (1 of 9 embryos). Consistent with their apparent role in neural tube closure, Mena and Profilin I are both highly expressed in cephalic neuroectoderm (Figure 3A and Figure 3B; A. Lambrechts and F. B. G., unpublished). These results indicate that a 50% reduction in the concentration of profilin I sensitizes animals to a loss of Mena and suggest a requirement for Mena and Profilin I function in neural tube closure, an actin-dependent process.

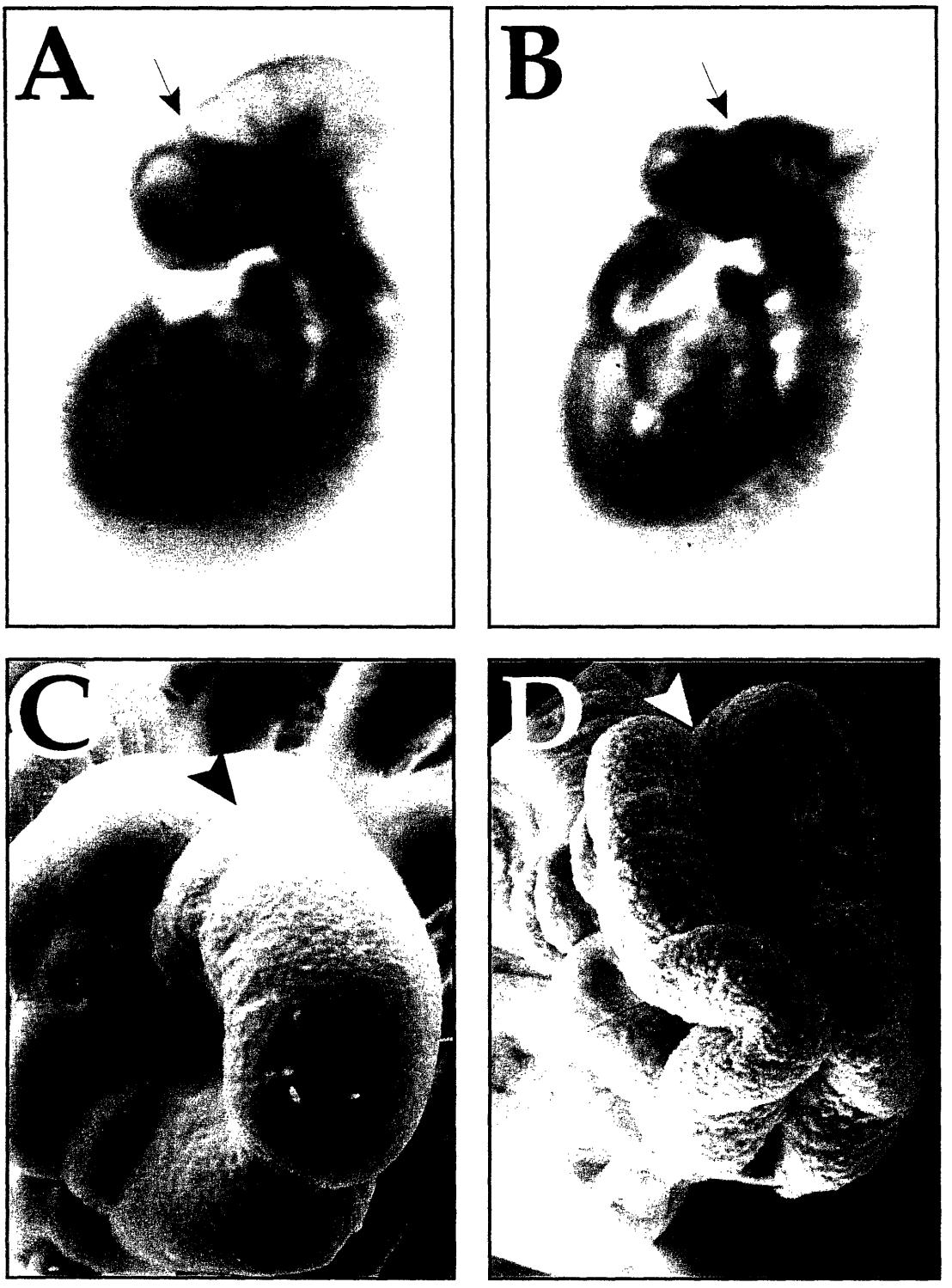


**Figure 8**

**Figure 8. Genetic Interaction between Mena and Profilin I**

The phenotype of E9.5 *Mena*$^{-/+}$;*profilin I*$^{-/+}$ double heterozygous animals (A and C) was compared to that of *Mena*$^{-/-}$;*profilin I*$^{-/+}$ littermates (B and D).

(A and B) Light microscopy reveals that the *Mena*$^{-/-}$;*profilin I*$^{-/+}$ embryo is small compared to its *Mena*$^{-/+}$;*profilin I*$^{-/+}$ littermate, and the structure of its head is abnormal.

(C and D) Environmental scanning electron microscopy of E9.5 littermates reveals that the cephalic neural tube is completely closed in the *Mena*$^{-/+}$;*profilin I*$^{-/+}$ embryo (C) but remains open in the *Mena*$^{-/-}$;*profilin I*$^{-/+}$. Arrowhead shown to mark orientation.

## Discussion

### Mena Is Required for Commissural Axon Guidance

A great deal of interest has focused on elucidating the cytoskeletal basis of axonal growth cone motility and guidance. Our results indicate that Mena, a molecule known to be involved in actin-cytoskeletal dynamics, is required for the formation of several major axonal projection pathways in the brain. Mice lacking Mena are viable but show striking malformation of the corpus callosum, hippocampal commissure, and the pontocerebellar fibers. The morphology of other axonal pathways, including the anterior commissure and spinal motor neurons, appeared normal, indicating that Mena is not required for formation of these pathways. Dye labeling experiments revealed that the callosal axons appear to be misrouted during development. These data, in conjunction with the finding that Mena is highly enriched at the distal tips of growth cone filopodia, suggest that Mena plays a critical role in commissural axon guidance.

Studies of invertebrate Mena homologs also suggest a role for Mena in axon guidance. Ena, the *Drosophila* homolog of Mena, was originally identified as a suppressor of CNS defects in *abl/dab* mutants (Gertler et al. 1990). Ena homozygotes show highly penetrant CNS and motor axon guidance defects, and neural specific expression of Ena greatly attenuates the motor neuron phenotype in *Ena* mutant embryos (Gertler et al., 1995; Wills et al., 1999a [this issue of *Neuron*]). Furthermore, mutations in Ena suppress the CNS axon guidance defects associated with the *abl/fasciclin I* double mutant (Elkins et al. 1990; Gertler et al. 1990). Finally, the *C. elegans* Unc34 locus,

which is required for the guidance of certain axons, was recently identified as a member of the Ena/VASP family (G. Garriga and F. B. G., unpublished data).

While we favor a model in which Mena function is required within the axons for guidance, the present data do not permit us to exclude the possibility that the axonal phenotypes in *Mena* mutants arise as a secondary consequence of other defects, such as failure to form the "glial sling" (a band of glial cells that support axons as they cross the midline [Silver et al. 1982]). Several observations lead us to believe, however, that the defects in commissural axon guidance in *Mena* mutants are cell autonomous. First, dye labeling experiments indicated that in *Mena* mutants axons of the developing corpus callosum appear to turn laterally and project away before contacting the midline. In cases of callosal agenesis associated with glial sling defects, callosal axons are reported to contact the meninges at the midline before turning and projecting ipsilaterally (Ozaki and Wahlsten 1993). Second, in the *Mena* mutants, defects were also observed in the pontocerebellar pathways, the formation of which is not known to be dependent on the glial sling. Third, in some of the mutant animals, a few callosal fibers were able to cross the midline, suggesting that during development there is a substrate within the midline that is capable of supporting fiber crossover. While these observations are not definitive proof of cell autonomy, it is striking that mutations in Mena or its homologs result in apparent axon guidance defects in three different organisms, especially since the issue of glial sling formation does not appear to apply to the invertebrate homologs.

The neural tube closure defects seen in the *Mena*$^{\beta geo/\beta geo}$; *profilin I*$^{-/+}$ animals reveal that Mena plays a critical role in neurulation in addition to its function in axon guidance. Mena function in neurulation involves Profilin and therefore might be linked to regulation of the actin cytoskeleton. Cephalic neural tube closure depends on actin-driven changes in the shape of cells within the dorsal-lateral hinge point (DLHP) of the neuroepithelium (Karfunkel 1971). During the process of convergence, the cells of the DLHP become elongated and wedge shaped, providing the motive force for dorsolateral furrowing (Smith and Schoenwolf 1997). The phenotypes of the *Mena*$^{\beta geo/\beta geo}$;*profilin I*$^{-/+}$ embryos indicate a failure of neural tube closure sometime between convergence and fusion of the neural folds and may result from improper regulation of actin dynamics within the DLHP. Furthermore, it seems likely that Mena and Profilin I may be involved in regulating actin dynamics in many cell types throughout development, but the severe neurulation defects in the *Mena*$^{\beta geo/\beta geo}$;*profilin I*$^{-/+}$ embryos complicate the analysis of these phenotypes. It will be interesting to determine if *Mena*$^{\beta geo/\beta geo}$;*profilin I*$^{-/+}$ embryos that do not have obvious neural tube defects, but nonetheless die perinatally, suffer from other defects in cell migration or axon guidance. Interestingly, mutations in other actin-regulating proteins, such as the related Macmarcks and Marcks, are known to result in neural tube defects and exencephaly (Stumpo et al. 1995; Chen et al. 1996). Furthermore, deletion of both Arg and Abl, tyrosine kinases known to associate with actin (Van Etten et al. 1994), causes a collapse of the neural tube that is accompanied by the presence of ectopic actin-rich aggregates in the neuroepithelium (Koleske et al. 1998). Since Mena associates in vitro with the SH3 domains of Abl and Arg, and given the links between

Abl signaling and Ena function in *Drosophila*, Koleske and colleagues speculate that the neurulation defect in *Abl/Arg* mutants may result from improper regulation of Mena.

**Redundant and Unique Functions of Mena, EVL, and VASP**

The phenotype of the Mena-deficient mice suggests that Mena may have a unique function in guidance of specific axons rather than, or perhaps in addition to, a general role in growth cone motility. This interpretation is supported by the finding that cultured embryonic hippocampal neurons from Mena-deficient mice appear, at least superficially, to develop normally (data not shown). It is therefore possible that, despite its localization at the tips of growth cone filopodia, Mena does not play a role in general growth cone motility. Alternatively, a role for Mena in general growth cone motility may be masked by the presence of the related family members EVL and VASP. Indeed, EVL and VASP are both expressed in portions of the developing nervous system and EVL is localized to the tips of growth cone filopodia (data not shown). The overlapping activities of Ena/VASP family members have been demonstrated by the ability of either Mena or VASP to rescue the viability of *Drosophila Ena* mutants (Ahern-Djamali et al. 1998; F. B. G. et al., unpublished data) and by experiments that show that Mena, EVL, and VASP are interchangeable in their ability to facilitate Listeria movement (F. B. G. et al., unpublished data).

Despite these redundancies, the phenotype of the *Mena* mutants suggests that Mena has a unique function not provided by EVL or VASP. This conclusion is supported by the fact that no CNS defects are detected in VASP-deficient mice (Aszodi et al. 1999).

The unique function of Mena may be provided by the neuronal specific 140 kDa Mena(+) isoform, which is known to have the ability to direct actin remodeling; EVL and VASP do not have neural specific variants and do not induce actin remodeling. The proposal that Mena(+) may play a role in commissural axon guidance is consistent with the finding that expression of Mena(+) peaks between E15 and P1, a time when the majority of the callosal and hippocampal commissure axons are migrating across the midline (Ozaki and Wahlsten 1993).

Interestingly, Mena(+), but neither the 80 kDa form of Mena, nor EVL or VASP, appears to be a substrate for tyrosine phosphorylation (Gertler et al. 1996; F. B. G. et al., unpublished data). In *Drosophila*, Ena is a target of Abl phosphorylation, and Ena function in axon guidance may be regulated by the opposing activities of Abl and the Dlar receptor tyrosine phosphatase (Wills et al. 1999a). How tyrosine phosphorylation affects Mena(+) function and whether Mena(+) is one of the phosphotyrosine substrates detected in the tips of growth cone filopodia remain to be determined. Nonetheless, it is possible that the Mena(+) isoform has a unique, tyrosine phosphorylation–dependent function in axon guidance analogous to that of Ena, while the 80 kDa form of Mena may have a more general function in growth cone and cell motility that can be partially replaced by EVL or VASP.

**How Is Mena Localized in Growth Cone Filopodia?**

The enrichment of Mena and/or Mena(+) at the distal tips of growth cone filopodia positions Mena appropriately to mediate axon guidance cues, but the

mechanism by which Mena is enriched at the tips of filopodia remains unclear. In fibroblasts, Mena localization at focal adhesions is mediated by EVH1 domain interactions with the D/EFPPPP-containing ligands Zyxin and Vinculin (Niebuhr et al. 1997). While Zyxin and Vinculin have been detected in filopodia of chicken sensory neurons (Gomez et al. 1996; Sydor et al. 1996), we have been unable to localize either molecule in filopodia of hippocampal neurons, suggesting that interaction with Vinculin and/or Zyxin is not the primary mechanism for localization of Mena in these neurons. It therefore seems likely either that other EVH1 ligands exist or that localization in growth cones is mediated by ligands that interact with other portions of the Mena molecule.

Identification of one potential Mena-binding protein was made possible by the observation that the EVH1 domain of Mena, but not of EVL or VASP, binds with high affinity to peptides containing the sequence DLPPPP in which an L is substituted for the canonical F residue (Niebuhr et al. 1997). Based on this observation, Kidd and colleagues speculated that DLPPPP motifs present in the Robo/Sax3 family of axon guidance molecules may link this receptor to the actin cytoskeleton by recruiting Mena/Ena (Kidd et al. 1998). Robo is thought to repel axons from the midline, and, in *Drosophila*, loss of Robo results in promiscuous midline crossing (Kidd et al. 1998). In contrast, the Mena phenotype appears, based on anatomic analysis, to result from failure to cross the midline, while *Ena* mutants display only a mild Robo-like phenotype (Wills et al. 1999a). Therefore, the potential interaction between Robo and Ena/Mena is likely to represent only one aspect of the function of these molecules in axon guidance.

**What Is the Function of Mena in Axon Guidance?**

Growth cone motility requires the dynamic regulation of actin polymerization at the tips of filopodia. The fact that Mena(+) is localized at the tips of filopodia and can induce the protrusive activity of actin polymerization suggests that one function of Mena(+) may be to regulate actin polymerization in filopodia. In the absence of Mena, animals were sensitive to a 2-fold reduction in the levels of Profilin I, consistent with a model in which Mena and Profilin function in a common process. Unfortunately, the severe brain defects of the *Mena*$^{\beta geo/\beta geo}$*; profilin I*$^{-/+}$ embryos prohibited analysis of axonal pathways in these animals. Nonetheless, it is tempting to speculate that Mena function in axon guidance involves interaction with Profilin. Biochemical data indicate that Profilin is a high-affinity ligand for Mena (Gertler et al. 1996) and that rapid movement of Listeria depends upon the ability of Ena/VASP proteins to recruit Profilin (Smith et al. 1996). Furthermore, Profilin itself has recently been shown to be essential for filopodial formation and neurite extension in cultured cells and for motor axon outgrowth in *Drosophila* (Suetsugu et al. 1998; Wills et al., 1999b [this issue of *Neuron*]).

It is possible that Mena influences cytoskeletal dynamics by physically concentrating Profilin in areas of the cell that require dynamic actin polymerization. In many cell types, however, Profilin is present in concentrations on the order of 100 μM and appears to be broadly distributed throughout the cell (Tseng et al. 1984), suggesting that physical concentration may not by itself be key to regulating Profilin function. While little is known about the concentration of Profilin in growth cones, similar reasoning may

apply. Alternatively, the Mena–Profilin interaction may modulate Profilin function, thereby influencing actin dynamics.

The question of how Mena and Profilin ultimately regulate actin cytoskeletal dynamics is likely to be complex. A simple model based on studies of Listeria motility would predict that Ena/VASP family members function to recruit Profilin and enhance the rate of actin polymerization and cell motility (Pollard 1995). Based on this model, one might predict that mutations in either Ena/VASP proteins or in Profilin would lead to decreased cell motility. Genetic studies indicate, however, that loss of Ena/VASP family members can actually enhance cell motility. In mice, loss of VASP increases the rate of platelet aggregation and attenuates the cyclic nucleotide-mediated inhibition of aggregation (Aszodi et al. 1999). If the rate of platelet aggregation is directly related to the rate of actin polymerization, then the simplest interpretation of these data is that VASP normally retards the rate of actin assembly and that this inhibitory function is potentiated by PKA phosphorylation. In *Drosophila*, loss of Ena leads to a highly penetrant "bypass" phenotype in which growth cones fail to stop or turn at the appropriate choice points, while mutations in Profilin lead to a "stop short" phenotype in which growth cones fail to advance beyond the choice point (Wills et al. 1999a, Wills et al. 1999b). Thus, although both Ena and Profilin appear to have important functions at choice points, their role in regulating growth cone dynamics is likely to involve more than simple changes in the rate of actin polymerization.

A recent report indicates that Mena and its homologs may be directly involved in response to the Netrin signaling pathway. Unc34, the *C. elegans* homolog of Mena, was identified in a screen for suppressors of axonal guidance defects induced by ectopic expression of the Netrin receptor Unc5 (Colavita and Culotti 1998). In vertebrates, Netrin-1 and DCC, a Netrin receptor that mediates chemoattractive responses, are required for spinal commissural axon guidance and formation of the corpus callosum and the hippocampal and anterior commissures (Serafini et al. 1996; Fazeli et al. 1997). Although the cytoplasmic targets of the Netrin receptors have not been identified, it is known that Netrin-1 signaling is modulated by cyclic nucleotide-dependent protein kinases (Ming et al. 1997). This ability of second messenger signaling to modify growth cone chemotaxis may be one way in which axons can integrate signals from multiple guidance systems. Given that fact that Mena is an in vivo substrate for PKA, as well as the phenotype of the *Mena* mutants and the genetic interaction between Unc34/Mena and the Netrin signaling pathway, it seems possible that Mena and its relatives may represent a convergence point for these signaling pathways. Experiments are underway to determine if Mena is one of the critical factors that transduce these diverse signals into the changes in cytoskeletal dynamics required for growth cone guidance.

**Acknowledgments**

We gratefully acknowledge Pieter Dikkes, William Perry, and Christine Canida for expert technical assistance and Drs. Reinhard Fässler, Anthony Koleske, David Van Vactor, and members of the Gertler lab for critical reading of the manuscript. We thank Drs. Peter L. Woodhams and Mike Webb for the gift of the Py antibody, Drs. Gretchen Snyder and Angus Nairn for the DARPP32 antibody, and Dr. Frank Solomon for gift of the 13H9 antibody. L. M. L. is supported by a fellowship from the Anna Fuller

Foundation, and M. A. G. is a Medical Foundation Research fellow with funding through the June Rockwell Levy Foundation; additional support was provided by NIH grants HD28478 and MR Center grant HD18655 (to J. D. M.), GM53236 (to D. J. K.), and HD24875 and HD25326 (to P. S.). This research was supported by grants from Merck and Co. and the Medical Foundation and by NIH grant GM58801 (to F. B. G.).

## References

Ahern-Djamali, S.M., Comer, A.R., Bachmann, C., Kastenmeier, A.S., Reddy, S.K., Beckerle, M.C., Walter, U., and Hoffmann, F.M. (1998). Mutations in Drosophila enabled and rescue by human vasodilator-stimulated phosphoprotein (VASP) indicate important functional roles for Ena/VASP homology domain 1 (EVH1) and EVH2 domains. Mol. Biol. Cell *9*, 2157-2171.

Aszodi, A., Pfeifer, A., Ahmad, M., Glauner, M., Zhou, X.-H., Ny, L., Andersson, K.-E., Kehrel, B., Offermanns, S., and Fässler, R. (1999). The vasodilator-stimulated phosphoprotein (VASP) is involved in cGMP- and cAMP-mediated inhibition of agonist-induced platelet aggregation, but is dispensable for smooth muscle function. EMBO J *18*, 37-48.

Butt, E., Abel, K., Krieger, M., Palm, D., Hoppe, V., Hoppe, J., and Walter, U. (1994). cAMP- and cGMP-dependent protein kinase phosphorylation sites of the focal adhesion vasodilator-stimulated phosphoprotein (VASP) in vitro and in intact human platelets. J. Biol. Chem *269*, 14509-14517.

Caroni, P. (1998). Driving the growth cone. Science *281*, 1465-1466.

Chen, J., Chang, S., Duncan, S.A., Okano, H.J., Fishell, G., and Aderem, A. (1996). Disruption of the MacMARCKS gene prevents cranial neural tube closure and results in anencephaly. Proc. Natl. Acad. Sci. USA *93*, 6275-6279.

Colavita, A. and Culotti, J.G. (1998). Suppressors of ectopic UNC-5 growth cone steering identify eight genes involved in axon guidance in Caenorhabditis elegans. Dev. Biol *194*, 72-85.

Copp, A.J. (1994). Genetic models of mammalian neural tube defects. Ciba Found. Symp *181*, 118-134.

Elkins, T., Zinn, K., McAllister, L., Hoffmann, F.M., and Goodman, C.S. (1990). Genetic analysis of a Drosophila neural cell adhesion molecule: interaction of fasciclin I and Abelson tyrosine kinase mutations. Cell *60*, 565-575.

Fazeli, A., Dickinson, S.L., Hermiston, M.L., Tighe, R.V., Steen, R.G., Small, C.G., Stoeckli, E.T., Keino-Masu, K., Masu, M., and Rayburn, H. *et al.* (1997). Phenotype of mice lacking functional Deleted in colorectal cancer (Dcc) gene. Nature *386*, 796-804.

Fink, R.P. and Heimer, L. (1967). Two methods for selective silver impregnation of degenerating axons and their synaptic endings in the central nervous system. Brain Res *4*, 369-374.

Flanagan, J.G. and Van Vactor, D. (1998). Through the looking glass: axon guidance at the midline choice point. Cell *92*, 429-432.

Friedrich, G. and Soriano, P. (1991). Promoter traps in embryonic stem cells: a genetic screen to identify and mutate developmental genes in mice. Genes Dev *5*, 1513-1523.

Gertler, F.B., Doctor, J.S., and Hoffmann, F.M. (1990). Genetic suppression of mutations in the Drosophila abl proto-oncogene homolog. Science *248*, 857-860.

Gertler, F.B., Hill, K.K., Clark, M.J., and Hoffmann, F.M. (1993). Dosage-sensitive modifiers of Drosophila abl tyrosine kinase function: prospero, a regulator of axonal outgrowth, and disabled, a novel tyrosine kinase substrate. Genes Dev *7*, 441-453.

Gertler, F.B., Comer, A.R., Juang, J.L., Ahern, S.M., Clark, M.J., Liebl, E.C., and Hoffmann, F.M. (1995). enabled, a dosage-sensitive suppressor of mutations in the Drosophila Abl tyrosine kinase, encodes an Abl substrate with SH3 domain-binding properties. Genes Dev *9*, 521-533.

Gertler, F.B., Niebuhr, K., Reinhard, M., Wehland, J., and Soriano, P. (1996). Mena, a relative of VASP and Drosophila Enabled, is implicated in the control of microfilament dynamics. Cell *87*, 227-239.

Gomez, T.M., Roche, F.K., and Letourneau, P.C. (1996). Chick sensory neuronal growth cones distinguish fibronectin from laminin by making substratum contacts that resemble focal contacts. J. Neurobiol *29*, 18-34.

Goslin, K., and Banker, G. (1991). Rat hippocampal neurons in low density culture. In Culturing Nerve Cells, G. Banker and K. Goslin, eds. (Cambridge, MA: MIT Press), pp. 251–282.

Goslin, K., Birgbauer, E., Banker, G., and Solomon, F. (1989). The role of cytoskeleton in organizing growth cones: a microfilament-associated growth cone component depends upon microtubules for its localization. J. Cell Biol *109*, 1621-1631.

Halbrügge, M. and Walter, U. (1989). Purification of a vasodilator-regulated phosphoprotein from human platelets. Eur. J. Biochem *185*, 41-50.

Hogan, B., Beddington, R., Costantini, F., and Lacy, E. (1994). Immunocytochemistry of whole mount embryos. In Manipulation of the Mouse Embryo. B. Hogan, R. Beddington,

F. Costantini, and E. Lacy, eds. (Plainview, NY: Cold Spring Harbor Laboratory Press), pp. 340–367.

Honig, M.G. and Hume, R.I. (1989). Dil and diO: versatile fluorescent dyes for neuronal labelling and pathway tracing [see comments]. Trends Neurosci *12*, 333-341.

Howell, B.W., Hawkes, R., Soriano, P., and Cooper, J.A. (1997). Neuronal position in the developing brain is regulated by mouse disabled-1. Nature *389*, 733-737.

Imamoto, A. and Soriano, P. (1993). Disruption of the csk gene, encoding a negative regulator of Src family tyrosine kinases, leads to neural tube defects and embryonic lethality in mice. Cell *73*, 1117-1124.

Karfunkel, P. (1971). The role of microtubules and microfilaments in neurulation in Xenopus. Dev. Biol *25*, 30-56.

Keynes, R. and Cook, G.M. (1996). Axons turn as netrins find their receptor. Neuron *17*, 1031-1034.

Kidd, T., Brose, K., Mitchell, K.J., Fetter, R.D., Tessier-Lavigne, M., Goodman, C.S., and Tear, G. (1998). Roundabout controls axon crossing of the CNS midline and defines a novel subfamily of evolutionarily conserved guidance receptors. Cell *92*, 205-215.

Koester, S.E. and O'Leary, D.D. (1994). Axons of early generated neurons in cingulate cortex pioneer the corpus callosum. J. Neurosci *14*, 6608-6620.

Koleske, A.J., Gifford, A.M., Scott, M.L., Nee, M., Bronson, R.T., Miczek, K.A., and Baltimore, D. (1998). Essential role for abl and arg tyrosine kinases in neurulation. Neuron *21*, 1259-1272.

Li, E., Bestor, T.H., and Jaenisch, R. (1992). Targeted mutation of the DNA methyltransferase gene results in embryonic lethality. Cell *69*, 915-926.

Macklis, J.D. (1993). Transplanted neocortical neurons migrate selectively into regions of neuronal degeneration produced by chromophore-targeted laser photolysis. J. Neurosci *13*, 3848-3863.

Ming, G.L., Song, H.J., Berninger, B., Holt, C.E., Tessier-Lavigne, M., and Poo, M.M. (1997). cAMP-dependent growth cone guidance by netrin-1. Neuron *19*, 1225-1235.

Mitchison, T. and Kirschner, M. (1988). Cytoskeletal dynamics and nerve growth. Neuron *1*, 761-772.

Niebuhr, K., Ebel, F., Frank, R., Reinhard, M., Domann, E., Carl, U.D., Walter, U., Gertler, F.B., Wehland, J., and Chakraborty, T. (1997). A novel proline-rich motif present in ActA of Listeria monocytogenes and cytoskeletal proteins is the ligand for the EVH1 domain, a protein module present in the Ena/VASP family. EMBO J *16*, 5433-5444.

Orioli, D., Henkemeyer, M., Lemke, G., Klein, R., and Pawson, T. (1996). Sek4 and Nuk receptors cooperate in guidance of commissural axons and in palate formation. EMBO J *15*, 6035-6049.

Ozaki, H.S. and Wahlsten, D. (1993). Cortical axon trajectories and growth cone morphologies in fetuses of acallosal mouse strains. J. Comp. Neurol *336*, 595-604.

Paglini, G., Kunda, P., Quiroga, S., Kosik, K., and Caceres, A. (1998). Suppression of radixin and moesin alters growth cone morphology, motility, and process formation in primary cultured neurons. J. Cell Biol *143*, 443-455.

Pollard, T.D. (1995). Actin cytoskeleton. Missing link for intracellular bacteria motility?. Curr. Biol *5*, 837-840.

Probst, M. (1901). Über den Bau des balkenlosen GroÉ¿hirns, sowie über Mikrogyrie und Heterotypie der grauen Substanz. Arch. Psychiatr *34*, 709-786.

Reinhard, M., Halbrugge, M., Scheer, U., Wiegand, C., Jockusch, B.M., and Walter, U. (1992). The 46/50 kDa phosphoprotein VASP purified from human platelets is a novel protein associated with actin filaments and focal contacts. EMBO J *11*, 2063-2070.

Serafini, T., Colamarino, S.A., Leonardo, E.D., Wang, H., Beddington, R., Skarnes, W.C., and Tessier-Lavigne, M. (1996). Netrin-1 is required for commissural axon guidance in the developing vertebrate nervous system. Cell *87*, 1001-1014.

Silver, J., Lorenz, S.E., Wahlsten, D., and Coughlin, J. (1982). Axonal guidance during development of the great cerebral commissures: descriptive and experimental studies, in vivo, on the role of preformed glial pathways. J. Comp. Neurol *210*, 10-29.

Smith, G.A., Theriot, J.A., and Portnoy, D.A. (1996). The tandem repeat domain in the Listeria monocytogenes ActA protein controls the rate of actin-based motility, the percentage of moving bacteria, and the localization of vasodilator-stimulated phosphoprotein and profilin. J. Cell Biol *135*, 647-660.

Smith, J.L. and Schoenwolf, G.C. (1997). Neurulation: coming to closure. Trends Neurosci *20*, 510-517.

Snyder, E.Y., Yoon, C., Flax, J., and Macklis, J.D. (1997). Multipotent neural progenitors can differentiate toward replacement of neurons undergoing targeted apoptotic degeneration in adult mouse neocortex. Proc. Natl. Acad. Sci. USA *94*, 11663-11668.

Stumpo, D.J., Bock, C.B., Tuttle, J.S., and Blackshear, P.J. (1995). MARCKS deficiency in mice leads to abnormal brain development and perinatal death. Proc. Natl. Acad. Sci. USA *92*, 944-948.

Suetsugu, S., Miki, H., and Takenawa, T. (1998). The essential role of profilin in the assembly of actin for microspike formation. EMBO J *17*, 6516-6526.

Sydor, A.M., Su, A.L., Wang, F.S., Xu, A., and Jay, D.G. (1996). Talin and vinculin play distinct roles in filopodial motility in the neuronal growth cone. J. Cell Biol *134*, 1197-1207.

Theriot, J.A. and Mitchison, T.J. (1993). The three faces of profilin. Cell *75*, 835-838.

Theriot, J.A., Rosenblatt, J., Portnoy, D.A., Goldschmidt-Clermont, P.J., and Mitchison, T.J. (1994). Involvement of profilin in the actin-based motility of L. monocytogenes in cells and in cell-free extracts. Cell *76*, 505-517.

Tseng, P.C., Runge, M.S., Cooper, J.A., Williams, R.C.Jr. , and Pollard, T.D. (1984). Physical, immunochemical, and functional properties of Acanthamoeba profilin. J. Cell Biol *98*, 214-221.

Van Etten, R.A., Jackson, P.K., Baltimore, D., Sanders, M.C., Matsudaira, P.T., and Janmey, P.A. (1994). The COOH terminus of the c-Abl tyrosine kinase contains distinct F- and G-actin binding domains with bundling activity. J. Cell Biol *124*, 325-340.
Wahlsten, D. (1982). Deficiency of corpus callosum varies with strain and supplier of the mice. Brain Res *239*, 329-347.

Wills, Z., Bateman, J., Korey, C., Comer, A., and Van Vactor, D. (1999). The receptor-like protein tyrosine phosphatase Dlar controls axon guidance decisions with the associated protein tyrosine kinase abl and the phosphoprotein substrate Enabled. Neuron *22*, 301-312.

Wills, Z., Marr, L., Zinn, K., Goodman, C.S., and Van Vactor, D. (1999). Profilin and the Abl tyrosine kinase are required for motor axon outgrowth in the *Drosophila* embryo. Neuron *22*, 291-299.

Woodhams, P.L., Webb, M., Atkinson, D.J., and Seeley, P.J. (1989). A monoclonal antibody, Py, distinguishes different classes of hippocampal neurons. J. Neurosci *9*, 2170-2181.

Wu, D.Y. and Goldberg, D.J. (1993). Regulated tyrosine phosphorylation at the tips of growth cone filopodia. J. Cell Biol *123*, 653-664.

Wu, D.Y., Wang, L.C., Mason, C.A., and Goldberg, D.J. (1996). Association of beta 1 integrin with phosphotyrosine in growth cone filopodia. J. Neurosci *16*, 1470-1478.

Zallen, J.A., Yi, B.A., and Bargmann, C.I. (1998). The conserved immunoglobulin superfamily member SAX-3/Robo directs multiple aspects of axon guidance in C. elegans. Cell *92*, 217-227.

# CHAPTER 3

## Mena and VASP are Required for Multiple Actin-Dependent Processes that Shape the Vertebrate Nervous System

A. Sheila Menzies[1], Attila Aszodi[2], Scott E. Williams[3], Alexander Pfeifer[4], Ann M. Wehman[1], Keow Lin Goh[1], Carol A. Mason[3], Reinhard Fassler[2], Frank B. Gertler[1*]

[1]Department of Biology, Massachusetts Institute of Technology Cambridge, Massachusetts 02139; [2]Department for Molecular Medicine, Max Planck Institute for Biochemistry, Martinsried, Germany 82152; [3]Departments of Pathology, Anatomy and Cell Biology Center for Neurobiology and Behavior, Columbia University College of Physicians and Surgeons, New York, New York 10032; [4]Department of Pharmacy, Ludwig-Maximilians University, Munich, Germany 81377

ASM performed the experiments presented in this manuscript with the exception of experiments in Figure 2A and 2B which were performed by AMW and Figure 7 which were performed by SEW and CAM. KLG performed experiments that were not included in the manuscript. AA, AP and RF contributed the *VASP-/-* mice. FBG generated the *Mena-/-* mice.

This chapter has been accepted for publication in Journal of Neuroscience.

**Abstract**

Ena/VASP proteins regulate the geometry of the actin cytoskeleton thereby influencing cell morphology and motility. Analysis of invertebrate mutants implicates Ena/VASP function in several actin-dependent processes such as axon and dendritic guidance, cell migration and dorsal closure. In vertebrates, genetic analysis of Ena/VASP function is hindered by the broad and overlapping expression of the three highly related family members, Mena, VASP and EVL. Mice deficient in either Mena or VASP exhibit subtle defects in forebrain commissure formation and platelet aggregation, respectively. In this study, we investigate the consequence of deleting both Mena and VASP. *Mena-/- VASP-/-* double mutants die perinatally and display defects in neurulation, craniofacial structures and the formation of several fiber tracts in the central and peripheral nervous systems.

**Introduction**

Regulation of cell morphology and motility is fundamental to nervous system development. During early embryogenesis, transformation of the neuroepithelium from a relatively flat layer into a tube-like structure involves the concerted regulation of cell motility within the neuroepithelium, cell shape changes at future hinge points and elevation and fusion of neural folds. As development proceeds, neuroepithelial cells proliferate, ultimately giving rise to differentiated neurons. Migration of neurons to their appropriate location in the developing nervous system and proper extension and pathfinding of axons and dendrites ensures the formation of appropriate synaptic

connections. All these morphogenetic processes require actin-driven changes in cell shape, such that perturbation of actin dynamics either by treatment with actin depolymerizing drugs (Morriss-Kay and Tuckett, 1985; Bentley and Toroian-Raymond, 1986; Davidson and Keller, 1999) or genetic deletion of actin-regulatory genes (Juriloff and Harris, 2000; Meyer and Feldman, 2002) results in neurulation, cell migration and axon guidance defects.

The Ena/VASP family of actin-regulatory proteins functions in a variety of cell types to regulate cell morphology and motility (Krause et al., 2003). *Drosophila* Ena was originally identified as a genetic suppressor of *abl*-dependent phenotypes (Gertler et al., 1990). The three vertebrate orthologs are Mena (Mammalian Enabled), VASP (Vasodilator-Stimulated Phosphoprotein) and EVL (Ena-VASP Like). Ena/VASP proteins localize to focal adhesions and areas requiring dynamic remodeling of the actin cytoskeleton, including lamellipodial protrusions and filopodial tips. The ability of Ena/VASP proteins to bind F-actin and protect growing filaments from being capped regulates the geometry of the actin network. Ena/VASP activity promotes the formation of long unbranched actin filaments (Bear et al., 2002). The resulting filaments are arranged into different structures depending on the cell type. In *Dictyostelium* and neurons, Ena/VASP promotes the formation of filopodial structures composed of bundled F-actin (Han et al., 2002; Lebrand et al., 2004).

Genetic analysis in *Drosophilia* and *C. elegans* demonstrates that Ena/VASP proteins are required for the guidance of cell bodies, axons and dendrites. Ena/VASP

functions downstream of Abl and the axon guidance receptors, Robo (Bashaw et al., 2000), Dlar (Wills et al., 1999), DCC (Gitai et al., 2003) and Unc-5 (Colavita and Culotti, 1998). Furthermore, these genetic interactions are supported by biochemical interactions between Ena/VASP and Abl (Gertler et al., 1996; Howe et al., 2002), Dlar (Wills et al., 1999) and Robo (Bashaw et al., 2000). Additionally, Ena functions with Abl during dorsal closure of the *Drosophilia* embryo, a process dependent upon convergent extension of epithelial cells at the dorsal midline (Grevengoed et al., 2001) and analogous to neurulation in vertebrates. Analysis of *Mena-/-* mice reveals defective formation of the corpus callosum (CC), dorsal hippocampal commissure (DHC) and ventral hippocampal commissure (VHC) in 50% of mutants (Lanier et al., 1999). Mena function in neurulation is revealed through genetic interaction with the actin monomer binding protein, Profilin I, in which half of *Mena-/-ProI+/-* mice do not close their cephalic neural tube (Lanier et al., 1999). *VASP-/-* mice do not exhibit nervous system defects but VASP deficient platelets have an increased aggregation response to known stimulants and partial resistance to cAMP and cGMP effects (Aszodi et al., 1999; Hauser et al., 1999).

Mena and VASP function interchangeably in fibroblast motility assays (Loureiro et al., 2002) and are expressed in a broad and overlapping expression pattern during development and adulthood (Aszodi et al., 1999; Lanier et al., 1999; Gambaryan et al., 2001). Given the limited and partially penetrant phenotypes of *Mena-/-* and *VASP-/-* mice, we hypothesized that mice lacking both Mena and VASP would exhibit more severe defects than single mutant animals. In the present study, we report that *Mena-/-*

*VASP-/-* (*M-/-V-/-*) mice die perinatally and display defects in neurulation, craniofacial structures and several axonal pathways in the central and peripheral nervous systems.

## Material and Methods

**Animals and Histology** Mena (Lanier et al., 1999) and VASP (Aszodi et al., 1999) mutant mice were previously generated. The MenaVASP (MV) line was initiated by crossing Mena mutants maintained on either a 129sv ($M^{129}$) or c57BL6 ($M^{c57}$) background to VASP mutants maintained on a mixed background. The resulting MV mice were intercrossed for several generations and the progeny analyzed at various stages of development. While no MV backcrossed lines were analyzed, littermate controls (*M+/- V+/-*, *M+/- V+/+* and *M+/+ V+/-*) did not exhibit phenotypes displayed by mutants. Furthermore, the callosal defects in *M-/-V+/-* mice are identical to those previously reported for *M-/-* mice which were the F1 hybrid progeny of matings between $M^{129}$ and $M^{c57}$ mice ($M^{129/c57\ F1}$-/-). In the present study, callosal development was analyzed in mutant *M-/-V+/-* and $M^{129/c57\ F1}$-/- mice and compared to control *M+/-V+/-* and $M^{129/c57\ F1}$+/ littermates, respectively. Mice heterozygeous for Mena and VASP were intercrossed to generate double null progeny at an expected frequency of 1/16. To increase the fraction of double null progeny, *M+/- V-/-* intercrosses and *M+/-V+/-* x *M+/-V-/-* matings were also performed. For timed-pregnant matings, E0 was considered the morning the vaginal plug was detected. Silver staining of adult brain sections and SEM of E9.5 embryos was performed as previously described (Lanier et al., 1999). H&E staining was performed on 5μm paraffin sections using standard technique.

**Immunohistochemistry** Mena (2197) and VASP (2010) polyclonal antibodies were purified using N-terminal Mena and GST-VASP protein affinity columns, respectively. Immunolabeling with Mena antibodies (2197, affinity purified 2197, and monoclonal H8C2G5) and VASP affinity purified 2010 antibodies was performed on 10μm frozen sections of 4% paraformaldehyde (PFA) fixed E10.5 embryos and E17 heads. Sections were blocked with 10%serum/10%BSA in PBST (PBS + 0.05% Tween-20) and incubated with primary and secondary antibodies diluted in 1% serum/1%BSA/ PBS at 4°C overnight, followed by several washes with PBST. Sections were counterstained with DAPI. Phalloidin-Alexa 594 (Molecular Probes, Eugene, OR) was used at 1:300 to label F-actin in E10.5 frozen sections. Double and triple labeling of Mena and VASP with neurofilament 2H3 (1:4, Developmental Studies Hybridoma Bank, University of Iowa, Iowa City, IA), Islet1/2 (1:10000, gift of T. Jessell, Columbia University, New York, NY) and/or GLAST (1:2000, Chemicon, Temecula, CA) in E14.5 heads was performed with minor modifications. 20μm frozen sections were blocked 60 minutes with 10% normal goat serum in PBS + 0.2% triton, then incubated with primary antibodies diluted in block overnight at 4°C. Primary antibodies were detected with Cy3, Cy5- (Jackson ImmunoResearch, West Grove, PA) or AlexaFluor 488- and Alexa 568- (Molecular Probes) conjugated secondary antibodies or goat-anti-rabbit-Biotin (Vector Laboratories, Burlingame, CA) followed by streptavidin-FITC (PharMingen, San Diego, CA).

Immunolabeling with anti-GFAP antibodies (DAKO, Carpinteria, CA) was performed on 50μm vibratome sections of heads stored in 4% PFA as previously described (Shu and Richards, 2001) with minor modifications. Briefly, sections were

treated with 1%NaB and washed with PBS. Overnight incubation with anti-COW GFAP antibody (1:1000 in 2% goat serum/ 0.2% TritonX-100/ PBS) and 2 hour incubation with goat anti-rabbit-Biotin (1:600 in 0.2% TritonX-100/PBS) and streptavidin-FITC, were performed at room temperature and followed by PBS washes. Sections were counterstained with DAPI, mounted onto slides and imaged with an epifluorescent microscope.

Anti-neurofilament labeling of E10.5 whole mount embryos was performed as previously described (Hogan, 1994). Briefly, embryos were fixed in MeOH:DMSO (4:1) overnight at 4°C, washed with MeOH:DMSO:$H_2O_2$ (4:1:1) at room temperature to block endogenous peroxidase activity and then stored in 100% MeOH at –20°C. For staining, embryos were rehydrated in successive washes of 50% MeOH, PBS and PBSMT (PBS; 2% non-fat dry milk; 0.5% TritonX-100). Embryos were incubated with primary 2H3 and secondary donkey anti-mouse-HRP antibodies at 1:500 in PBSMT/10% donkey serum overnight at 4°C, followed by several washes with PBSMT. HRP activity was detected with DAB/NiCl solution (Vector Lab). Embryos were washed with PBT (PBS/ 0.2%BSA/ 0.5% TritonX-100), post-fixed with 4% PFA and cleared with methyl salicylate before imaging with a CCD camera attached to a dissecting microscope.

**Carbocyanine Dye Labeling** Embryonic brains were fixed with 4% paraforaldehyde. DiI crystals were injected laterally along the midline to label callosal fibers. For double labeling experiments, brains were cut to expose the fimbria where DiA crystals were placed as previously described (Livy and Wahlsten, 1997). Brains were placed in 4% PFA for 4-8 weeks to allow diffusion of lipophilic dyes along axons. Subsequently,

brains were sucrose infiltrated and vibratome sectioned coronally or horizontally. Sections were counterstained with DAPI, mounted onto slides and imaged with an epifluorescent microscope.

To label RGC projections, small crystals of DiI were applied to the optic nerve head of one retina to completely label all axons exiting the eye. Labeled samples were incubated for 4-7 days at 37°C in PBS + 0.02% $NaN_3$ (Sigma). After labeling, both optic nerves were severed and the intact forebrain, containing the optic nerves, optic chiasm, and optic tract, was dissected from the skull. Brains were imaged as wholemounts, with the chiasm on the ventral surface, using an epifluorescent dissecting stereomicroscope. Guidance errors were judged blind to genotype.

## Results

### Mena and VASP proteins are broadly expressed during development.

Ena/VASP proteins are broadly expressed and two or more family members have been detected in all tissue lysates examined by Western analysis (Lanier et al., 1999). Within the nervous system, Mena and VASP expression was detectable early in development and persisted throughout embryogenesis and into adulthood. In the E10.5 embryo, Mena and VASP were highly expressed in the neuroepithelium, which gives rise to the future brain and spinal cord (Figure 1A-1D). Mena and VASP proteins were distributed throughout the stratified neuroepithelium but concentrated along the apical surface facing the lumen of the neural tube and in neuroepithelial cells residing in the medial hinge point (MHP) of the cephalic neural tube (Figure 1C, 1D). Apical constriction of these hinge point cells

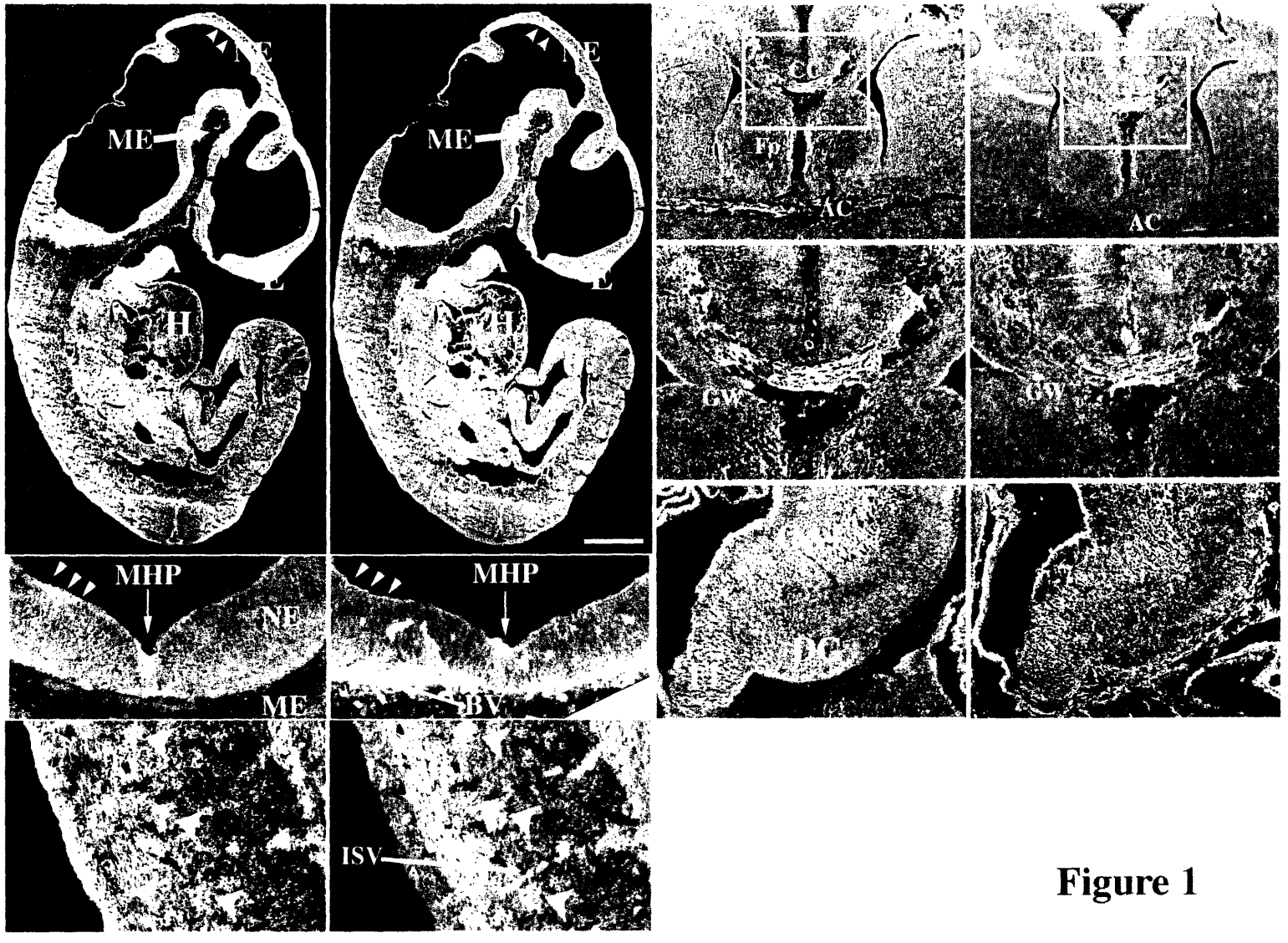


**Figure 1**

**Figure 1. Developmental Expression of Mena and VASP Protein.**

At E10.5, Mena (A, C, E) and VASP (B, D, F) proteins are broadly distributed. In sagittal embryo sections, Mena (A) and VASP (B) are detected in several structures including the neuroepithelium (NE), the underlying mesoderm (ME), overlying ectodermm (E), branchial arch (BA), and heart (H). Frontal sections through the cephalic neural tube shows that Mena (C) and VASP (D) are expressed throughout the neuroepithelium but concentrated at the apical surface (arrowheads in A-D) and cells in the medial hinge point (MHP). VASP is also detected in blood vessels (BV) within and surrounding the neural tube. VASP (F) is also highly expressed in the intersomitic vessels (ISV) running between the dorsal root ganglia which also express VASP (arrowheads in F) and Mena (arrowheads in E).

In the E17 brain, Mena (G, I, K) and VASP (H, J, L) label axons traveling in the corpus callosum (CC), fornix (Fo), and anterior commissure (AC). Mena and VASP expression in the midline region (magnification of boxed areas in G and H) are shown in I and J, respectively. Mena and VASP label the corpus callosum as well as the glial wedge (GW). Within the hippocampus, Mena (K) and VASP (L) are enriched in the CA1 region and fimbria (Fi) while Mena but not VASP is enriched in the dentate gyrus (DG).

Scale bar (in B) is 500μm for A and B, 120μm for C, D, and I-L, 100μm for E and F and 300μm for G and H.

allows bending of the neural tube, one of the early events in neural tube closure. Mena and VASP were also highly expressed by dorsal root ganglia and motor neurons within the spinal cord (Figure 1E, 1F and data not shown). Expression was not restricted to the nervous system as both Mena and VASP were abundant in the ectoderm overlying the neuroepithelium, branchial arch, and heart while lower levels were detected in the mesoderm underlying the neuroepithelium (Figure 1A, 1B). VASP, unlike Mena, was highly expressed in the vasculature system and labeled vessels within the neural tube, vessels lining the neural tube (Figure 1D) and vessels of the intersomitic artery where Mena expression was minimal (Figure 1F).

In the developing brain, Mena and VASP proteins were expressed in all regions and labeled several major commissural fiber tracts (Figure 1G-1J; Lanier et al., 1999). Mena and VASP were expresed by projection neurons within the cortex and were seen along their axons traveling within the corpus callosum. The optic chiasm, VHC and anterior commissure (AC) were also strongly labeled with Mena and to a lesser extent VASP (Figure 1G and 1H and data not shown). Mena and VASP were also detected near the lateral ventricles in the glial wedge, a structure important for the formation of the corpus callosum (Figure 1I and 1J). Within the hippocampus, Mena was detected in the fimbria, CA1 and dentate gyrus regions while VASP was expressed in the fimbria and CA1 region but not in the dentate gyrus (Figure 1K and 1L). To ensure the specificity of the Mena and VASP signal, *M*-/- and *V*-/- sections and no primary antibody controls were used (data not shown).

**Mena and VASP deficient mice die perinatally and display severe neural tube defects and facial malformations.** Mena and VASP double heterozygotes were intercrossed to generate mice deficient in both Mena and VASP. Recovery of *M-/-V-/-* adults was extremely rare (Supplemental Table 1). To increase the frequency of *M-/-V-/-* progeny, *M+/-V-/-* mice were also used for matings. From over 200 litters, only three *M-/-V-/-* adults were recovered. Matings with male *M-/-V-/-* mice revealed that these mutants were fertile. From the *M+/-V+/-* intercross, approximately forty percent fewer *M-/-V+/-* progeny were recovered than expected. To determine if *M-/-V-/-* and *M-/-V+/-* animals died *in utero*, litters were harvested at middle (E10.5) and late (E18.5) stages of embryogenesis. *M-/-V-/-* and *M-/-V+/-* embryos were recovered at nearly the expected Mendelian frequencies at both embryonic stages (Supplemental Table 2) indicating that these animals died perinatally.

External examination of embryos harvested at E10.5-E18.5 revealed that sixty-four percent of *M-/-V-/-* embryos (n= 164) displayed defective closure of their cephalic neural tube (Figure 2A). Neural tube defects were not observed in any control *M+/- V+/-* littermates (n=105). Failure of anterior neural tube closure disrupted normal brain development and resulted in exencephaly (Figure 2B). Exencephalic *M-/-V-/-* mutants exhibited severe disruption of regionalization and lamination of brain structures (data not shown). *M-/-V-/-* embryos also displayed malformations in neural crest cell derived facial structures that ranged from moderate deformities of the nose and mouth to severe facial clefts (Figure 2B). Similar neural tube defects were seen in eighteen percent of *M+/-V-/-* embryos (n= 313). Only four *M-/-V+/-* embryos (n=56) displayed neurulation

**Supplemental Table 1 Reduced Viability of *M-/- V-/-* and *M-/- V+/-* Mice**

| | *M+/+ V+/+* | *M+/+ V+/-* | *M+/+ V-/-* | *M+/- V+/+* | *M+/- V+/-* | *M+/- V-/-* | *M-/- V+/+* | *M-/- V+/-* | *M-/- V-/-* |
|---|---|---|---|---|---|---|---|---|---|
| Actual | 39 | 50 | 24 | 52 | 101 | 44 | 20 | **27*** | **1*** |
| Expected | 22 | 45 | 22 | 45 | 90 | 45 | 22 | 45 | 22 |

Litters from *M+/- V+/-* intercrosses were genotyped 8-14 days after birth. Reduced numbers of *M-/- V+/-* and *M-/- V-/-* mice were recovered at statistcially significant frequencies (*p <0.02).

**Supplemental Table 2** ***M-/- V-/-* and *M-/- V+/-* mice do not die *in utero***

| Mating Pair | Progeny Classes (actual / expected) | | | | | |
|---|---|---|---|---|---|---|
| | *M+/+ V+/-* | *M+/+ V-/-* | *M+/- V+/-* | *M+/- V-/-* | *M-/- V+/-* | *M-/- V-/-* |
| E10.5 | | | | | | |
| *M+/-V+/-* x *M+/-V-/-* | 10 / 11 | 10 / 11 | 22 / 23 | 24 / 23 | 12 / 11 | 12 / 11 |
| *M+/-V-/-* x *M+/-V-/-* | N/A | 15 / 21 | N/A | 49 / 42 | N/A | 20 / 21 |
| Total | 10 / 11 | 25 / 32 | 22 / 23 | 73 / 65 | 12 / 11 | 32 / 32 |
| E18.5 | | | | | | |
| *M+/-V+/-* x *M+/-V-/-* | 1 / 3 | 2 / 3 | 7 / 6 | 8 / 6 | 3 / 3 | 1 / 3 |
| *M+/-V-/-* x *M+/-V-/-* | N/A | 50 / 41 | N/A | 71 /82 | N/A | 43 / 41 |
| Total | 1 / 3 | 52 / 44 | 7 / 6 | 79 / 88 | 3 / 3 | 44/ 44 |

Litters from *M+/- V+/-* intercrosses and *M+/- V+/-* x *M+/- V-/-* crosses were harvested at E10.5 and E18.5. All progeny classes were recovered at the expected Mendelian frequencies.

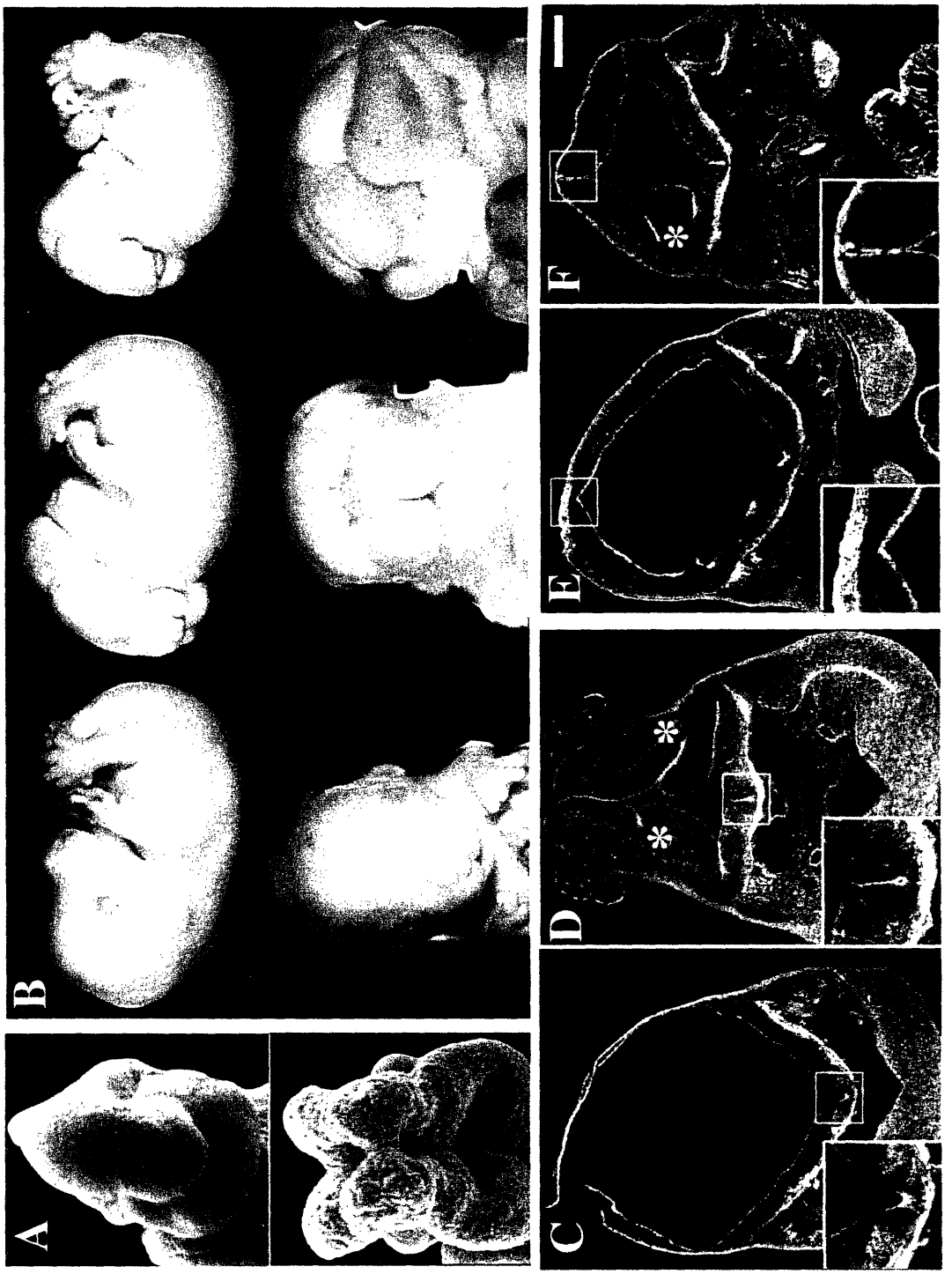


Figure 2

**Figure 2. Neurulation and Craniofacial Defects.**

(A) SEM of E9.5 cephalic neural tubes of control (top) and *M-/-V-/-* (bottom) littermates. The neural tube is closed in the control but is open in the mutant.

(B) E13.5 exencephalic mutants exhibit mild (middle) to severe (right) facial clefts as compared with control (left) littermates.

(C-F) Phalloidin stained frontal sections through the cephalic neural tube of E10.5 controls (C, E) and *M-/-V-/-* (D, F) littermates exhibiting severe (D) and mild (F) neural tube defects.

(C-D) In contrast to the control (C), the mutant neural folds are splayed apart and an accumulation of actin is found at the base of the mutant neural tube (D, boxed area enlarged in inset).

(E-F) The dorsal neural folds are not fused properly in the mutant (F, boxed area enlarged in inset) as compared with the control (E, boxed area enlarged in inset). Exencephalic (D) and non-exencephalic (F) mutant neuroepithelia contain several invaginations (asterisks) that are not observed in controls (C, E).

Scale bar in (F) is 250μm for (C-F) and 100μm for boxed insets in (C-F).

defects. The frequency of exencephaly did not completely account for the reduced viability of *M-/-V-/-* and *M-/-V+/-* animals. Further analysis of these mutants revealed additional defects in nervous system development.

Defective cephalic neural tube closure was observed as early as E9.5, a stage when control littermates had closed neural tubes (Figure 2A). Histological examination showed significant differences in neural tube defects between individual animals. In many *M-/-V-/-* mutants, the neural folds were completely splayed apart (Figure 2D). In other less severe mutants, the neuroepithelial folds bent medially but exhibited defects at the dorsal midline such as failure of neural fold fusion (Figure 2F). Invaginations of the neuroepithelial folds were frequently seen in the ventral and dorsal neural tube. Phalloidin stained sections of exencephalic mutants revealed an accumulation of filamentous actin at the base of the cephalic neural folds at E10.5 (Figure 2D). No actin accumulation was observed in control animals (Figure 2C, E) or in non-exencephalic mutants (Figure 2F).

**Sensory and motor branches of spinal nerves exhibit defects in axon projections.** Neurons whose cell bodies reside in the dorsal root ganglia (DRG) and motor column of the spinal cord extend axons that comprise the sensory and motor branches of spinal nerves, respectively. At the forelimb level, cervical 4-8 and thoracic 1 spinal nerves converge to form the branchial plexus at the base of the forelimb bud. Spinal nerve development was analyzed by anti-neurofilament whole mount staining of E10.5 embryos. While the DRG and motor column appeared normal, spinal nerve development

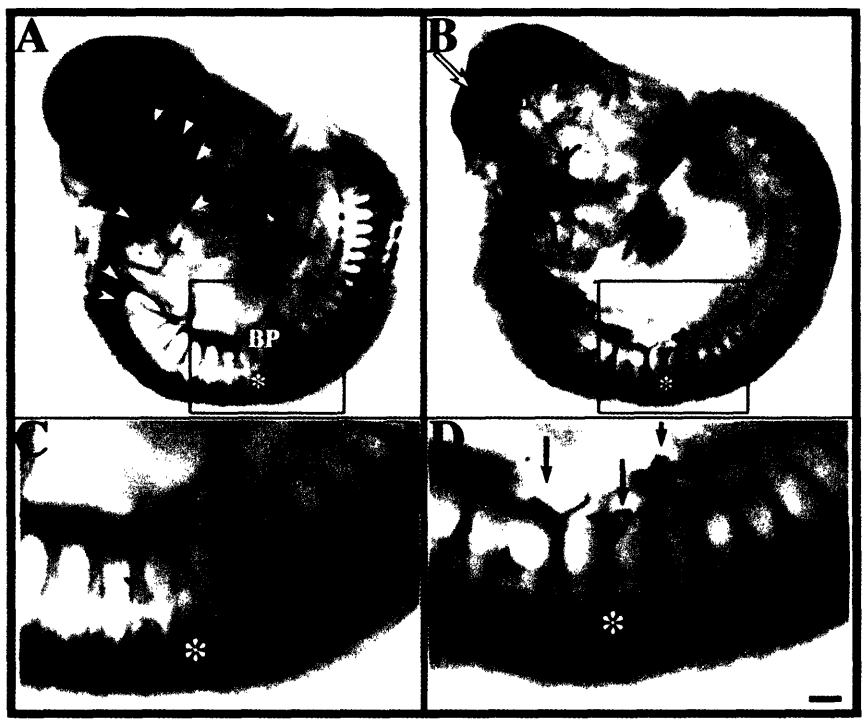


**Figure 3**

**Figure 3. Spinal Nerve Defects.**

Whole mount anti-neurofilament immunohistochemistry of E10.5 control (A, C) and *M-/-V-/-* (B, D) littermates. Boxed areas in A and B are enlarged in C and D, respectively. Spinal nerves extend and converge to form the branchial plexus (BP) in control animals (A, C). In *M-/-V-/-* mutants, spinal nerves are misrouted and/or have failed to extend (arrows in D). Cranial ganglia, cranial nerves (arrowheads) and dorsal root ganglia (asterisks indicate corresponding DRGs) appear to develop normally in both, control (A) and mutant (B) embryos. Note the open neural tube in the mutant (open arrows in B). Scale bar in (D) is 250μm for (A, B) and 100μm for (C, D).

was perturbed in twenty-five percent of *M-/-V-/-* mutants (n=16) (Figure 3). Spinal nerve defects were not observed in littermates containing at least one wildtype allele of Mena or VASP. Defects included failed extension, presence of misrouted fibers, and reduced convergence of spinal nerves forming the branchial plexus. These results indicate that Mena and VASP function are required at various steps of spinal nerve development.

Despite the neurulation defects, development of nearby cranial ganglia and cranial nerves appeared undisturbed in exencephalic *M-/-V-/-* mice (Figure 3). Histological analysis of embryonic spinal cords did not reveal defects in spinal commissure formation indicating that deletion of Mena and VASP affected select populations of neurons in the spinal cord and neighboring dorsal root ganglia.

**Formation of several forebrain commissures is dependent on Mena and VASP.** Commissures are composed of axons that cross the midline and form connections in the contralateral side of the body. There are four major forebrain commissures connecting the two brain hemispheres, the CC, DHC, VHC and AC (Figure 4A). Analysis of brains of nonexencephalic *M-/-V-/-* mutants revealed the complete absence of these four major forebrain commissures (Figure 4C). Axons of the CC, DHC, and VHC arrived at the midline but appeared bundled and did not cross, whereas AC axons did not arrive at the midline and therefore did not cross. These defects were completely penetrant in the five *M-/-V-/-* mutants examined (2 adult and 3 late stage embryo (E18.5, E17.5) brains) (Table 1). Cortical lamination appeared similar in control and mutant brains (data not shown).

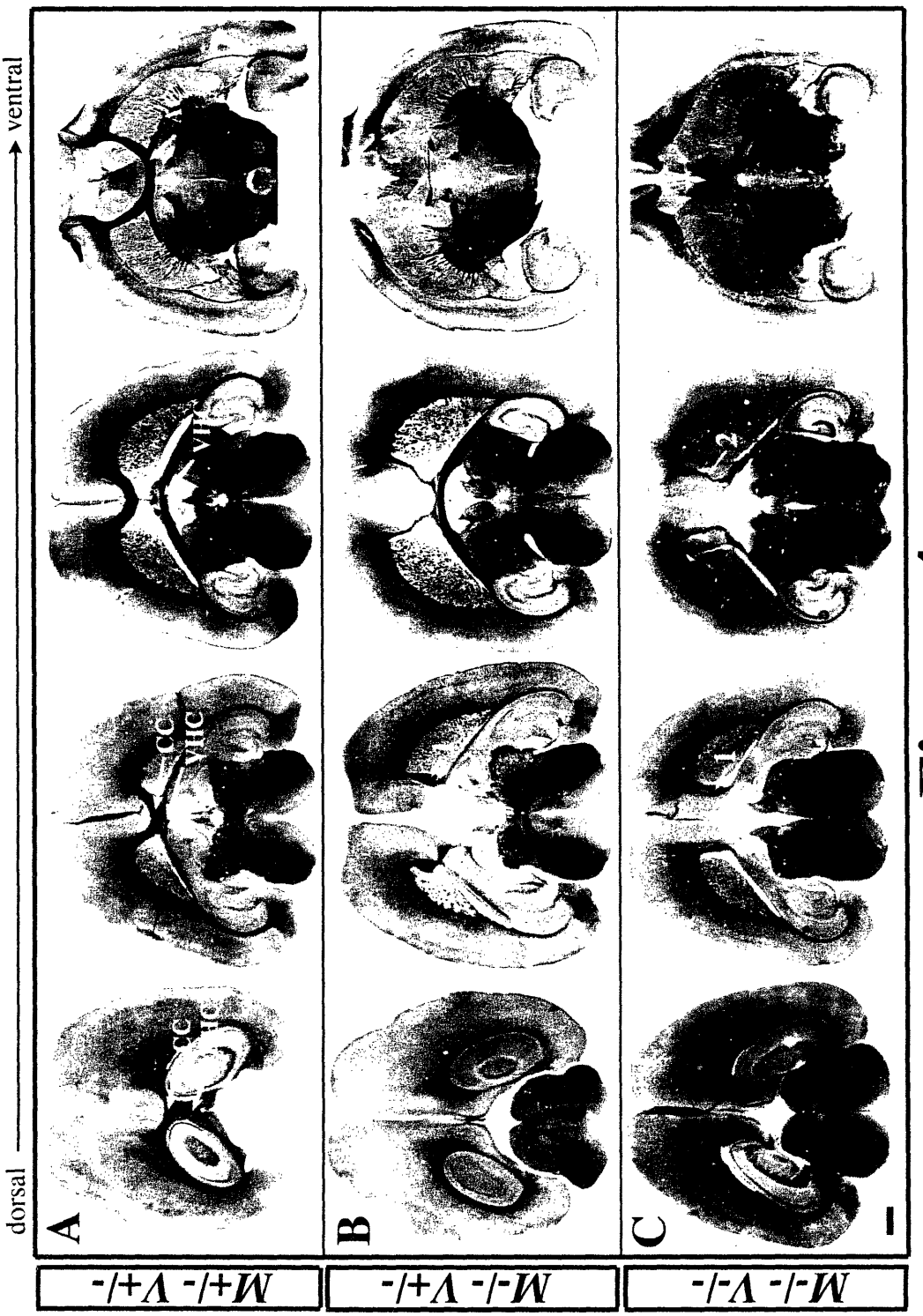


Figure 4

**Figure 4. Forebrain Commissure Defects.**

Silver stained horizontal sections of adult brains.

(A) Serial sections through control *M*+/- *V*+/- brain indicate the location of the Corpus Callosum (CC), Dorsal Hippocampal Commissure (DHC), Ventral Hippocampal Commissure (VHC) and Anterior Commissure (AC) as they appear along the dorsal-ventral (left to right) axis.

(B) Sections through the *M*-/- *V*+/- brain reveal the complete absence of the CC and DHC. In dorsal sections, misrouted callosal axons form dense Probst bundles (arrow 1) lateral to the midline. While the rostral portion of the VHC (seen in dorsal sections) bundles lateral to the midline and does not cross, the caudal portion of the VHC (seen in ventral sections) is formed and contacted by ectopically projecting callosal fibers (arrow 2). The anterior commissure is defective with only a few fibers crossing midplane (arrow 3) and severely misrouted fibers within the temporal lobe of the AC (arrow 4).

(C) Sections through the *M*-/- *V*-/- brain revealed the complete absence of all four commissures; CC, DHC, VHC and AC. In dorsal sections, misrouted callosal axons form dense Probst bundles (arrow 1), whereas further ventrally, callosal fibers ectopically contact fibers of the aberrant VHC (arrow 2).

Scale bar is 2mm.

**Table 1 Dose Dependent Defects in Forebrain Commissures**

| Genotype | DHC | CC | VHC | AC |
|---|---|---|---|---|
| *M+/- V+/-* (n= 8 ) | - | - | - | - |
| *M+/+ V-/-* (n= 6) | - | - | - | - |
| *M+/- V-/-* (n= 13) | 31% | 31% | 31% | - |
| *M-/- V+/+* (n= 22) | 55% | 55% | 55% | - |
| *M-/- V+/-* (n= 11) | 82% | 82% | 82% | 20% |
| *M-/- V-/-* (n= 5) | 100% | 100% | 100% | 100% |

Percentage of mice exhibiting defects in the corpus callosum (CC), dorsal hippocampal commissure (DHC), ventral hippocampal commissure (VHC) and anterior commissure (AC). Penetrance of forebrain commissure defects increases as the number of Mena and VASP alleles is reduced in mutant mice.

Analysis of mutants with varying numbers of Mena and VASP alleles confirmed a dose sensitive effect of these genes on forebrain commissure formation. Approximately eighty percent of *M-/- V+/-* mice exhibited CC, DHC and VHC defects while a subset of these mutants exhibited AC defects (Table 1). The CC and DHC were completely absent in *M-/- V+/-* brains, while the VHC was reduced, forming caudally but not rostrally (Figure 4B). Only a few AC axons reached the midplane and crossed. Identical CC, DHC and VHC defects occurred in fifty percent of *M-/-* brains, however the AC did form in *M-/-* mutants (Lanier et al., 1999). Alternatively, while VASP deficient mutants did not exhibit commissure defects, approximately thirty percent of *M+/-V-/-* mutants exhibited identical CC, DHC and VHC defects as *M-/-* and *M-/-V+/-* mice (Table 1). Defects in the four major forebrain commissures were most severe and completely penetrant in mutants lacking all wildtype Mena and VASP alleles. Therefore, forebrain commissure formation requires both Mena and VASP function, but is more sensitive to deletion of Mena.

Mena and VASP function in corpus callosum development was studied in more detail. Embryonic brains of control and mutant littermates were examined at stages when callosal axons normally arrive and cross the midline. Callosal fibers were labeled with DiI to determine when and where the pathfinding defects occurred. In coronal sections of E16.5 control brains, callosal fibers arrived at the midline region but had not yet crossed (Figure 5A). At this stage, mutant fibers arrived at a similar position near the midline with no indication of pathfinding problems. One day later at E17.5, many control

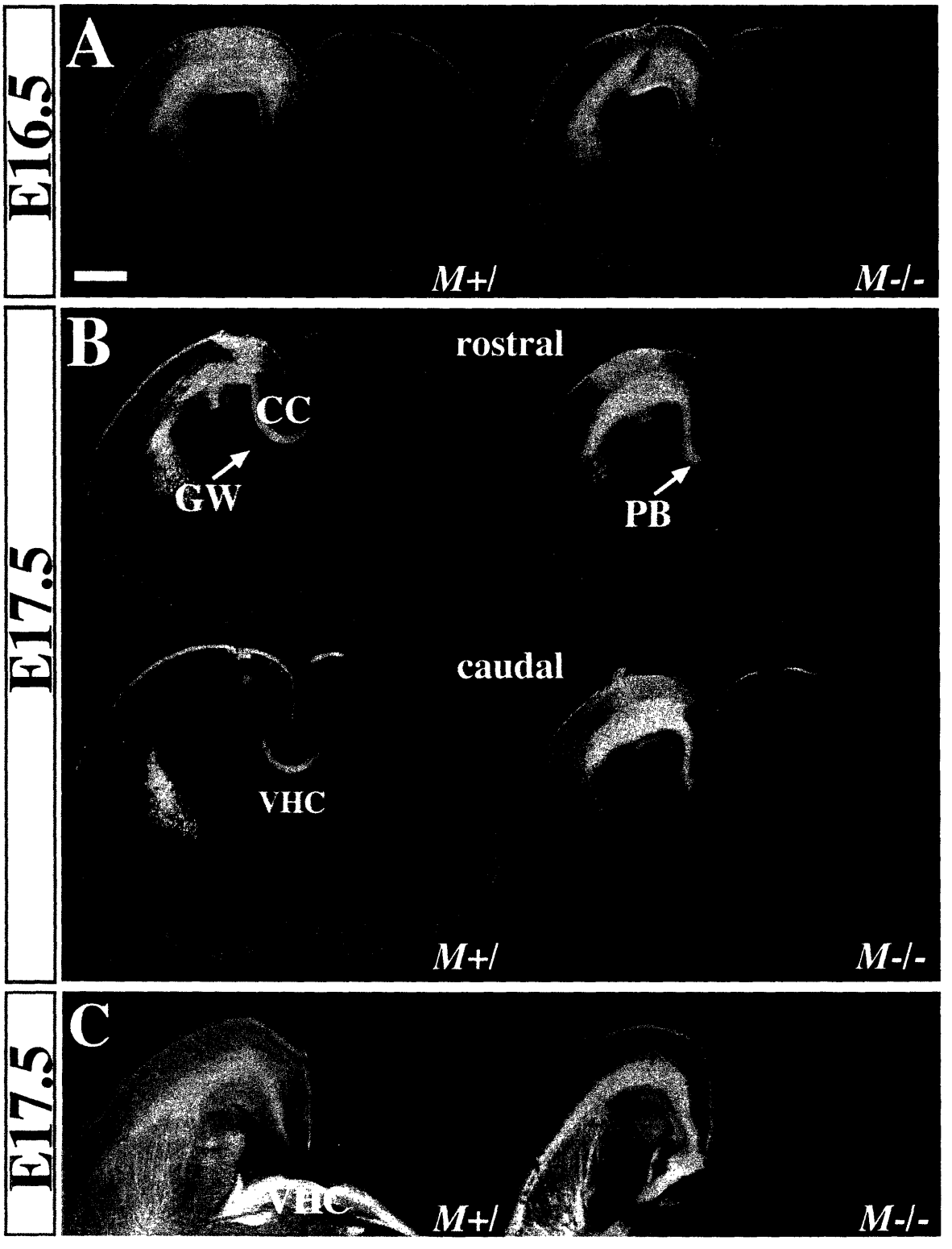


**Figure 5**

**Figure 5. Corpus Callosum Development.**

(A-B) DiI labeled callosal fibers (red) in coronal sections counterstained with DAPI (blue).

(A) At E16.5, callosal fibers in control and *M-/-* brains have arrived at similar positions near the midline region but have not yet crossed.

(B) At E17.5, callosal fibers in control brains (left panel) have crossed the midline and project into the contralateral cortex. Callosal fibers (CC) cross at a level dorsal to the glial wedge (GW), shown in rostral (top panel) and caudal (bottom panel) sections of the same brain. However, in *M-/-* brains (right panel), callosal fibers travel further ventrally, do not cross the midline and form Probst bundles (PB) adjacent to the midline. In caudal sections of the same brain, mutant callosal fibers contact the ventral hippocampal commissure (VHC).

(C) DiI labeled callosal fibers (red) and DiA labeled hippocampal commissure fibers (green) in horizontal sections of E17.5 brains. In control brains, the callosal and hippocampal commissure fibers appear as distinct tracts. In mutant brains, the callosal fibers (red) travel in a greater caudal-ventral direction to reach the VHC (green). Scale bar is 400μm.

callosal fibers crossed the midline at a level dorsal to the glial wedge (GW) (Figure 5B); however, in mutant brains, callosal fibers had not crossed. Rather, mutant callosal fibers traveled further ventrally and formed a bundle of misrouted fibers, called a Probst bundle (Probst, 1901), positioned below the GW. Normally the CC and VHC appeared as two distinct structures along the entire rostral-caudal axis. In caudal sections of mutant brains, however, labeled callosal fibers contacted the VHC ectopically. This was more obvious in horizontal sections of E17.5 brains where fibers of the CC and VHC were labeled with DiI and DiA, respectively (Figure 5C). Unlike controls, mutant callosal fibers traveled in a caudo-ventral direction to contact the VHC.

Because misrouting of callosal fibers occurred near the midline, mutant brains were examined for development of midline structures. Fusion of the cerebral hemispheres and guidance signals from the GW and indusium griseum (IG) have been shown to influence callosal guidance at the midline (Ozaki and Wahlsten, 1993; Shu and Richards, 2001). Hemisphere fusion occurs when the walls of the sulcus medianus telencephali medii (SMTM) bend medially and fuse with the pial membrane (Wahlsten, 1981) (Figure 6A). Callosal fibers travel underneath the fusion point to arrive in the contralateral hemisphere. Examination of embryonic brains revealed that hemisphere fusion is perturbed in mutant brains (Figure 6B). The walls of the SMTM appeared to bend toward and touch the pia as seen in brains of control littermates; however, in mutants the pial membrane extended further ventrally. Hemisphere fusion also appeared perturbed in the mutant diencephalon. In mutant brains, a gap existed where normally the

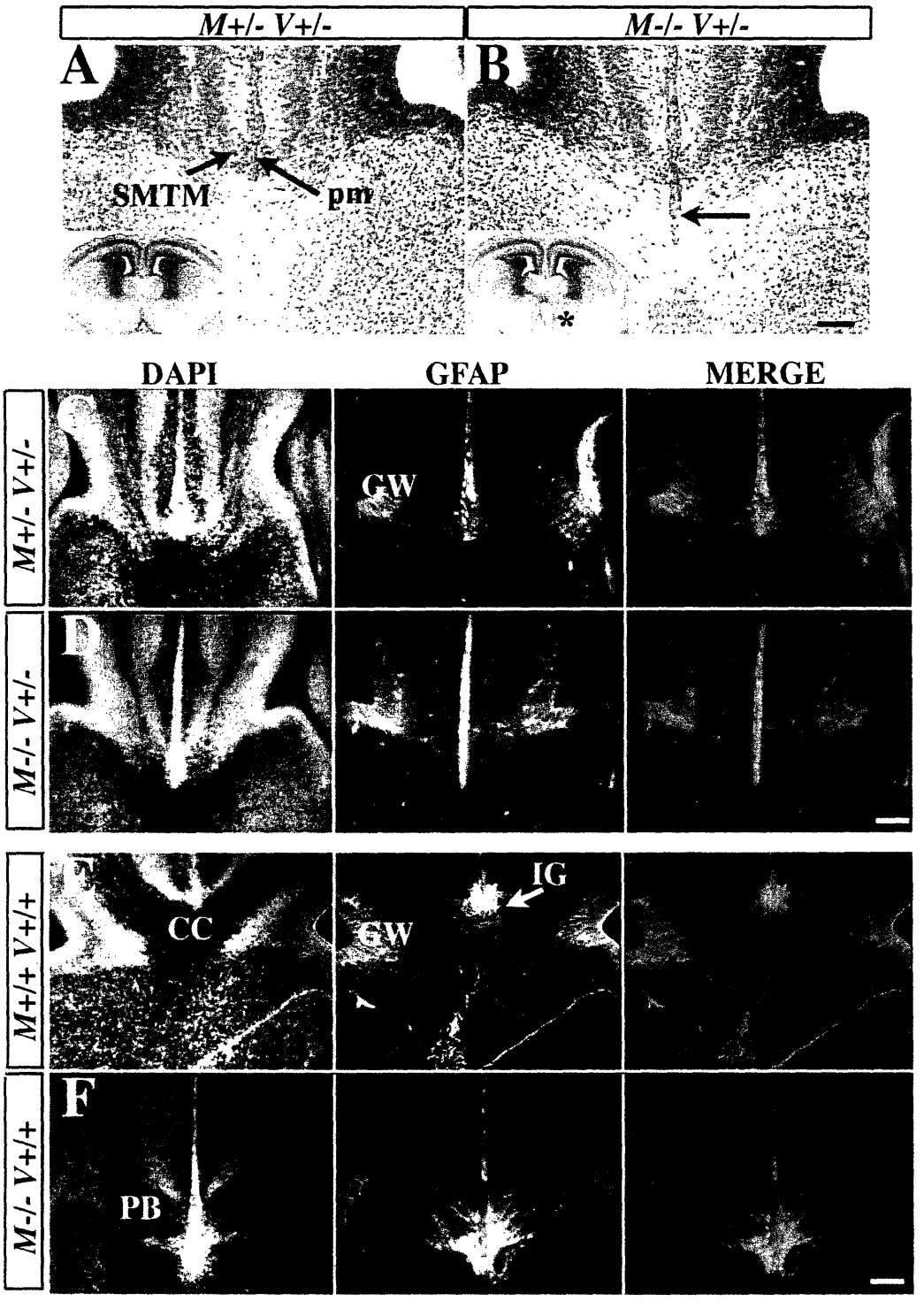


**Figure 6**

**Figure 6. Midline Development.**

(A,B) H&E stained coronal sections of E16.5 brains. Cerebral hemispheres are not fused properly in the mutant *M-/- V+/-* brain (A) as compared to the control brain (B). The walls of the sulcus medianus telencephali medii (SMTM) bend medially and fuse with the pial membrane (pm) in control brains. However, in mutant brains, the walls of the SMTM bend medially but the hemispheres do not properly fuse because of the ventrally penetrating pial membrane (arrow in B). In the mutant diencephalon, a gap is present where normally the walls of the thalamus meet forming the interthalamic adhesion (asterisk in B).

(C-F) Midline glia are examined in control and mutant brains by anti-GFAP immunohistochemistry.

(C,D) At E16.5, glial wedge (GW) development is similar in control (C) and mutant (D) brains. Glial processes of the GW extend from the lateral ventricles toward the midline.

(E, F) In the E17.5 control brains (E), the GW and indusium griseum (IG) glia are well-developed. The corpus callosum (CC) forms dorsal to the GW. In the E17.5 mutant brains (F), the GW is less pronounced. Misrouted callosal axons form Probst Bundles (PB) positioned ventral to the GW. Displaced IG glia, which are normally located at the midline where the hemispheres have fused, appear to extend GFAP positive processes into the PB.

Scale bars are 100μm, except 600μm for insets in A.

walls of the thalamus meet forming the interthalamic adhesion (inset in Figure 6B). Anterior commissure fibers cross ventral to this fusion point.

Glia of the GW and IG both express the repulsive guidance factor, Slit, and are thought to guide callosal fibers across the midline via a surround repulsion mechanism (Shu and Richards, 2001). The GW is composed of glia whose cell bodies reside in the lateral ventricles and whose processes extend out towards the midline. IG glia are positioned at the dorsal midline where the hemispheres fuse. GFAP staining revealed that at E16.5, a stage when callosal axons arrive in the midline region, GW development was similar in mutant and littermate controls (Figures 6C and 6D). In contrast, at E17.5 mutant callosal fibers were bundled into Probst bundles and the GW appeared distorted (Figures 6E and 6F). Furthermore, GFAP-positive fibers were found within the Probst bundle. These fibers are likely glial extension of IG glia that were mispositioned due to improper hemisphere fusion.

**Optic chiasm formation in Mena mutants is perturbed.** The optic chiasm is an X-shaped midline structure comprised of the axons of retinal ganglion cells (RGCs), which are the sole projection neurons from the eye. Unlike many other commissures in the brain, the optic chiasm is a partial decussation. Most retinal axons cross the midline and project into the contralateral optic tract. However, a minority of retinal fibers, originating largely from ventrotemporal retina, do not cross and instead join the optic tract on the ipsilateral side of the brain (arrow in Figures 7D, 7E,and 7F). Retinal axons reach the chiasm midline beginning at ~E12.5, but the first ipsilaterally-projecting axons do not

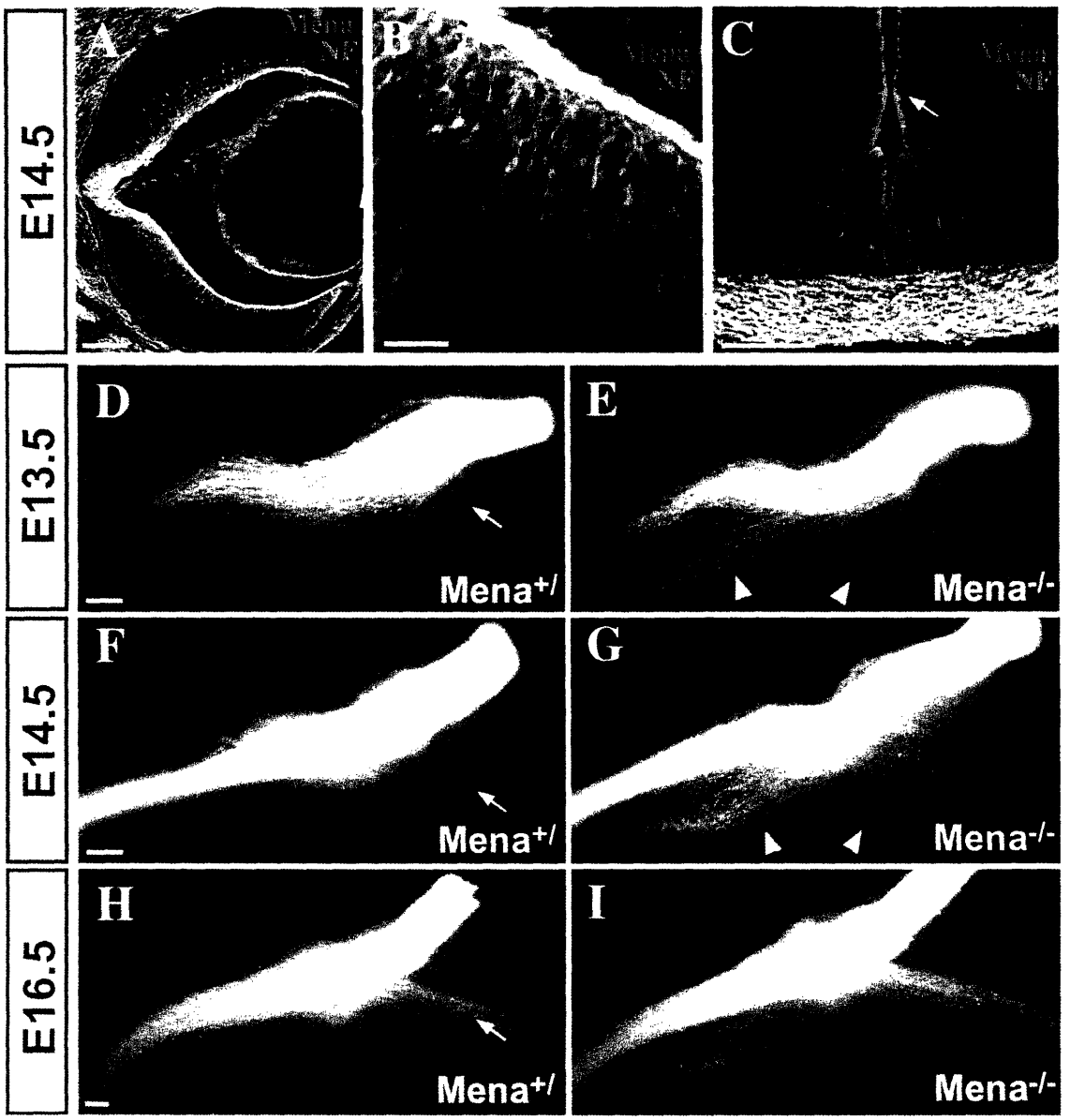


**Figure 7**

**Figure 7. Role of Mena in Optic Chiasm Development.**

(A-C) Expression of Mena protein in the E14.5 mouse visual system.

(A) Mena protein is expressed throughout the developing retina, but is most abundant in the RGC layer. Highest levels are found on RGC axons, which are positive for neurofilament (NF). (B) High magnification images of a coronal section of retina, demonstrating that Mena is mostly highly expressed in the Islet-positive (Isl1/2) RGC layer of the retina.

(C) In this mid-chiasm frontal section, NF-positive RGC axons at the chiasm midline express Mena as well. Mena is also found at lower levels throughout the ventral diencephalon, in both the neurons and GLAST-positive midline glia (arrow) of the chiasm region.

(D-I) Wholemount ventral views of the optic chiasm in control (D, F, H) and *Mena*$^{-/-}$ littermates (E, G, I) as revealed by unilateral anterograde labeling with DiI. In control embryos, the axons in the chiasm region are generally tightly fasciculated, particularly at older ages (H). The majority of axons cross the midline (asterisks in D, E) to project to the contralateral side of the brain, although a minority project ipsilaterally (arrows in D, F, H). In *Mena*$^{-/-}$ mutants, many axons become defasciculated at the midline, and stray posteriorly (arrowheads in E, G), giving the appearance of a double optic tract. This phenotype is fully penetrant, but exhibits variable expressivity, and is generally most severe at younger ages (E, G). Dorsal is up in (A-C). Anterior is up in (D-I).

Scale bars are 100 $\mu$m, except 25 $\mu$m in (B).

appear until ~E14 (Colello and Guillery, 1990; Godement et al., 1990; Sretavan, 1990). Mena protein was enriched throughout the RGC layer in E14.5 retina (Figure 7A), and was expressed on retinal axons throughout their trajectory (Figures 7A- 7C). Mena is also found throughout the ventral diencephalon (Figures 7C). Mena mRNA expression by *in situ* hybridization yielded consistent results (data not shown). VASP protein appears to be minimally expressed in RGCs and the ventral diencephalon (data not shown).

To determine whether Ena/VASP proteins are required for proper formation of the optic chiasm, we examined the retinal projections in Mena and VASP mutant embryos by unilateral anterograde labeling with DiI (Figures 7D-I; data not shown). In control animals (Figures 7D, 7F,and 7H), most crossed and uncrossed RGC fibers remained tightly bundled within the optic nerves and optic tracts, though a few axons strayed caudally from the midline. However, in *M*-/- mutants at E13.5-E14.5, many axons became defasciculated around the midline, and strayed into inappropriate regions posterior to the chiasm, ipsilateral and contralateral to the labeled optic nerve (arrowheads in Figures 7E and 7G). By E16.5, these guidance errors appeared to be largely corrected in the mutants (Figures 7I, n=6). Errors were made by both ipsilaterally- and contralaterally-projecting axons, and were observed in 100% of *M*-/- and *M*-/- *V*+/- embryos at younger ages (n=12). By contrast, such errors were never observed in control animals (*M*+/- or *M*+/+, n=12). Furthermore, this phenotype did not seem to dependent on VASP function, as *M*+/- *V*-/- (n=4) and *M*+/- *V*+/- animals (n=8) are indistinguishable from controls (data not shown). This is consistent with our observation that VASP is expressed at very low levels in the retina and chiasm region.

Since the corpus callosum defects observed in *M-/-V-/-* mutants can be attributed at least in part to a failure of the cerebral hemisphere fusion, we investigated whether midline structures of the ventral diencephalon on which the chiasm forms appear normal in *M-/-* embryos. Two groups of midline cells are implicated in RGC axon guidance at the midline – the midline glial palisade expressing the radial glial antigens RC2 and GLAST, and the early-born chiasm neurons that express SSEA-1. Both midline populations appeared normal in *M-/-* embryos compared to controls (data not shown).

## Discussion

Ena/VASP function is critical for several actin-dependent morphogenic processes. Mena and VASP are required for viability and the formation of several neural derived structures. Neural tube, craniofacial, spinal nerve and anterior commissure defects are exhibited in *M-/-V-/-* mice but not single *M-/-* and *V-/-* mutants, indicating the required function of both genes for development of these structures. While deletion of VASP enhances many Mena-dependent axon guidance phenotypes in the forebrain, the optic chiasm phenotype reveals a third category of defects which is dependent on Mena but not VASP. The variable penetrance of defects in the single mutant animals may reflect the relative abundance of Mena and VASP proteins in the affected cell types.

**Ena/VASP function in neurulation.** Neurulation is a major morphogenetic event requiring the cooperative efforts of intrinsic forces within the neuroepithelium and extrinsic forces in the surrounding tissue (Smith and Schoenwolf, 1997). Neuroepithelial

cells in future hinge point regions serve as attachment sites to the underlying tissue and become wedge-shaped by constriction of actin filaments in the apical neuroepithelium and basal expansion by interkinetic nuclear migration. Bending of the neural plate at the medial hinge point (MHP) and dorsolateral hinge points (DLHP) and elevation of the neural folds transforms the cephalic neural tube into a diamond shaped structure. Cell rearrangement within the dorsal neural tube appear to promote the apposition of neural folds (Davidson et al., 1999), which fuse subsequently at the dorsal surface.

Neurulation defects are observed in several gene targeted mutants of actin regulatory proteins, many of which directly bind actin filaments, including the nonreceptor tyrosine kinases Arg and Abl, the PKC substrates MARCKS and MacMARCKS, p190RhoGAP, Vinculin, and Shroom (Juriloff and Harris, 2000) as well as proteins involved in cell adhesion such as N-cadherin (Radice et al., 1997), NCAM (Cremer et al., 1994), integrins (De Arcangelis et al., 1999), and the bi-directional signaling molecule, ephrin-5A (Holmberg et al., 2000).

Requirement for Profilin I, an actin monomer binding protein, in neurulation is observed when Profilin I mutations are introduced into the *Mena* mutant background. Approximately fifty percent of *M-/-P+/-* mutants are exencephalic (Lanier et al., 1999). Interestingly, *V-/-P+/-* mice are recovered at nearly the Mendelian frequency and are viable and fertile (AMW and FBG, unpublished observations). Mena-Profilin interaction may facilitate actin monomer incorporation into growing filaments and promote filament elongation which produces the cell shape changes necessary for neurulation.

Cephalic neurulation is highly sensitive to perturbation of actin dynamics whereas spinal neurulation is relatively insensitive (Ybot-Gonzalez and Copp, 1999). Neurulation defects in *M-/-V-/-* mice are restricted to the cephalic neural tube resulting in exencephaly, but not spina bifida. Examination of E10.5 *M-/-V-/-* neural tubes reveals disorganized and invaginated neuroepithelia. In most mutants, neural folds are completely splayed apart and do not meet at the midline whereas in other mutants neural folds bend inward but do not fuse. Mena and VASP are expressed in both the neuroepithelium and surrounding cephalic mesenchyme and epidermis. Within the neuroepithelium, Mena and VASP are enriched at the apical surface where F-actin, catenins, cadherins and Abl/Arg are also concentrated. Mena and VASP are particularly enriched at the MHP and may be required within the neuroepithelium, principally for apical constriction of cells at future hinge points to bend the neural plate and/or ensure attachment to the underlying tissue. Failure at DLHPs could result in the severe phenotype in which the neural folds are splayed apart. The milder neurulation defects (invaginated neuroepithelium and defective fusion of dorsal neural folds) exhibited by *M-/-V-/-* mutants may result from other cellular functions such as adhesion of neural folds and rearrangement of cells within the neuroepithelium. Additionally, Mena and VASP may function in the underlying mesoderm and surface ectoderm to provide the protrusive force necessary to elevate the folds and facilitate fusion at the dorsal midline.

Genetic studies show that *Drosophila* Ena and Abl genetically interact in dorsal closure, a process analogous to vertebrate neurulation (Grevengoed et al., 2001). Mice deficient in the vertebrate Abl orthologs, Arg and Abl, exhibit similar cephalic

neurulation defects as *M-/-V-/-* mutants (Koleske et al., 1998). Ena/VASP proteins bind Abl (Gertler et al., 1996; Howe et al., 2002) and may function with Abl family members in neurulation. In *abl* mutant flies, Ena is mislocalized, suggesting that Abl regulates Ena localization (Grevengoed et al., 2001). Moreover in *abl* mutants, ectopic actin accumulations in apical microvilli are observed in areas of mislocalized Ena. Reduction in Ena levels suppresses this phenotype suggesting that Ena promotes the formation of these actin rich structures (Grevengoed et al., 2003). Alternatively, Abl may regulate Ena/VASP function by direct phosphorylation. While the combined overexpression of Abl, Mena and the Abi 1 adaptor protein results in phosphorylation of Mena at Y296 (Tani et al., 2003), this site is not conserved in the other family members. Whether endogenous Mena and VASP are physiological Abl substrates remains to be determined.

**Ena/VASP function in axon guidance.** Many of the axonal defects seen in *M-/-V-/-* mice involve midline guidance decisions, a major choice point in the developing nervous system, where axons must choose to cross to the contralateral side or remain ipsilateral. Upon encountering the midline, growth cones assume complex morphologies displaying numerous filopodia (Godement et al., 1994). Growth cone filopodia serve important exploratory roles and integrate diverse guidance signals into an overall directional response (Dickson BJ, 2002). Ena/VASP proteins localize to filopodial tips and have been shown to regulate filopodial formation. Therefore, the critical requirement for dynamic reorganization of the actin cytoskeleton at the midline and other choice points may be compromised in Ena/VASP deficient axons and result in the observed pathfinding defects. Recently, it has been shown that inhibiting the function of all Ena/VASP

proteins in cultured hippocampal neurons blocks the filopodial response to netrin-1, supporting a cell-autonomous function of Ena/VASP proteins in axon guidance (Lebrand et al., 2004). Furthermore, Ena/VASP proteins are phosphorylated at a conserved PKA site upon netrin stimulation. Attractive or repulsive response to guidance cues, such as netrin and slit, can be reversed by changes in the intracellular concentrations of cyclic nucleotides (cAMP and cGMP) (Song and Poo, 1999). PKA/PKG dependent phospho-regulation of Ena/VASP proteins, which is crucial for Ena/VASP function in fibroblast random motility and in platelets, may be one mechanism to modulate growth cone response to given guidance factors.

Callosal defects observed in *M*-/- and *M*-/-*V*+/- mutants are similar to phenotypes of mice deficient in netrin-1 (Serafini et al., 1996), DCC (Fazeli et al., 1997), and Slit2 (Bagri et al., 2002). Slit mediated repulsion and netrin mediated attraction are thought to guide callosal axons towards and across the midline. Callosal fibers pass through a region flanked by Slit expressing GW and IG glia (Shu and Richards, 2001) to arrive at the midline where netrin is expressed. When Slit2 expression is perturbed in the GW, callosal axons travel ventrally into the septum (Shu et al., 2003). The fact that *Mena* mutant axons travel more ventrally before bundling may indicate a defect in their response to Slit mediated repulsion.

The presence of hemisphere fusion defects in mutants exhibiting forebrain commissure defects raises the possibility that axonal pathway defects may be a consequence of the altered terrain. Interestingly, terminal phenotypes of several acallosal

mutants appears similar, irrespective of the presence or absence of hemisphere fusion (Stumpo et al., 1995; Brouns et al., 2000; Shen et al., 2002). Hemisphere fusion defects may result from failures in cell adhesion and/or migration. An early specification defect in the dorsal neural tube which gives rise to the midline region where forebrain commissures form may also manifest in later defects in commissure formation. Furthermore, because Mena and VASP are extensively expressed by the affected neurons as well as the midline glia, axonal pathway defects may result from the absence of Ena/VASP function in the neurons, glia or both. Additional experiments are required to dissect the cell-autonomous role of Ena/VASP proteins in callosal axon guidance.

In the visual system, high levels of Mena protein detected on retinal axons suggest that Mena may act cell autonomously in retinal axon guidance. In contrast to dorsal forming forebrain commissures, optic chiasm defects are not associated with midline defects. Both slit and robo are expressed in the ventral diencephalon, anterior and posterior to where the chiasm forms (Erskine et al., 2000). However, *Slit1/2* double mutants exhibit a phenotype that is very different than that observed in *Mena* mutants. In these embryos, axons form an anterior ectopic chiasm and make dorso-ventral guidance errors, but generally do not stray posteriorly (Plump et al., 2002). In zebrafish, robo2 is expressed in the retina, and the phenotype of the *robo2* mutant *astray* is characterized by widespread retinal guidance errors (Fricke et al., 2001). Interestingly, however, the *astray* phenotype does not mirror the mouse *Slit1/2* phenotype. Since both *Robo1* and *Robo2* are expressed in the mouse retina (Erskine et al., 2000; Niclou et al., 2000;

Ringstedt et al., 2000; Fricke et al., 2001), analysis of *Robo* mutants may clarify whether Mena acts in this pathway.

**Redundant Functions of Ena/VASP proteins.** Functional similarity between Ena/VASP proteins is demonstrated by the ability of any family member to rescue the random cell motility defects of cultured Ena/VASP deficient fibroblasts (Loureiro et al., 2002). Deletion of Mena and VASP reveals additional phenotypes not observed in either single knockout animal. It is likely that in *M-/-V-/-* animals expression of the third family member, EVL, masks the requirement for Ena/VASP function in other cell types. For example, expression of a construct that dominantly interferes with the function of all Ena/VASP family members specifically in migrating neocortical neurons results in their misplacement within the neocortex (Goh et al., 2002). In a different mouse model, overexpression of a C-terminal fragment of VASP specifically in keratinocytes results in transgenic mice with skin defects (Vasioukhin et al., 2000). Cortical lamination and skin defects are not detected in the present study. This suggests that the continued expression of EVL alone, is likely sufficient for proper development of many tissues in *M-/-V-/-* animals. Transgenic strategies that inhibit the function of all Ena/VASP proteins in a temporal and cell-type specific manner will be critical to study the cell-autonomous function of Ena/VASP in a variety of cell types and processes.

**Acknowledgements**
We thank R. Bronson for helpful discussions and expert assistance in histological examination. We also thank A. Caron for help in histology, C. Candida, K. O'Brien and

A. Dousis for mouse maintainence and genotyping, M. Barzik for providing GST-VASP protein, T. Jessell for the gift of Islet-1/2 antibodies and members of the Gertler lab for critical reading of this manuscript. A.S.M. was supported on a David Koch Graduate Fellowship. S.E.W. was supported on a National Eye Institute training grant (T32 EY 13933). Funding was provided by NIH grants to C.A.M (EY012736) and F.B.G. (GM58801).

## References

Aszodi A, Pfeifer A, Ahmad M, Glauner M, Zhou XH, Ny L, Andersson KE, Kehrel B, Offermanns S, Fassler R (1999) The vasodilator-stimulated phosphoprotein (VASP) is involved in cGMP- and cAMP-mediated inhibition of agonist-induced platelet aggregation, but is dispensable for smooth muscle function. Embo J 18:37-48.

Bagri A, Marin O, Plump AS, Mak J, Pleasure SJ, Rubenstein JL, Tessier-Lavigne M (2002) Slit proteins prevent midline crossing and determine the dorsoventral position of major axonal pathways in the mammalian forebrain. Neuron 33:233-248.

Bashaw GJ, Kidd T, Murray D, Pawson T, Goodman CS (2000) Repulsive axon guidance: Abelson and Enabled play opposing roles downstream of the roundabout receptor. Cell 101:703-715.

Bear JE, Svitkina TM, Krause M, Schafer DA, Loureiro JJ, Strasser GA, Maly IV, Chaga OY, Cooper JA, Borisy GG, Gertler FB (2002) Antagonism between Ena/VASP proteins and actin filament capping regulates fibroblast motility. Cell 109:509-521.

Bentley D, Toroian-Raymond A (1986) Disoriented pathfinding by pioneer neurone growth cones deprived of filopodia by cytochalasin treatment. Nature 323:712-715.

Brouns MR, Matheson SF, Hu KQ, Delalle I, Caviness VS, Silver J, Bronson RT, Settleman J (2000) The adhesion signaling molecule p190 RhoGAP is required for morphogenetic processes in neural development. Development 127:4891-4903.

Colavita A, Culotti JG (1998) Suppressors of ectopic UNC-5 growth cone steering identify eight genes involved in axon guidance in Caenorhabditis elegans. Dev Biol 194:72-85.

Colello RJ, Guillery RW (1990) The early development of retinal ganglion cells with uncrossed axons in the mouse: retinal position and axonal course. Development 108:515-523.

Cremer H, Lange R, Christoph A, Plomann M, Vopper G, Roes J, Brown R, Baldwin S, Kraemer P, Scheff S, Barthels D, Rajewsky K, Wille W (1994) Inactivation of the N-

CAM gene in mice results in size reduction of the olfactory bulb and deficits in spatial learning. Nature 367:455-459.

Davidson LA, Keller RE (1999) Neural tube closure in Xenopus laevis involves medial migration, directed protrusive activity, cell intercalation and convergent extension. Development 126:4547-4556.

De Arcangelis A, Mark M, Kreidberg J, Sorokin L, Georges-Labouesse E (1999) Synergistic activities of alpha3 and alpha6 integrins are required during apical ectodermal ridge formation and organogenesis in the mouse. Development 126:3957-3968.

Dickson BJ (2002) Molecular mechanisms of axon guidance. Science 298:1959-1964.

Erskine L, Williams SE, Brose K, Kidd T, Rachel RA, Goodman CS, Tessier-Lavigne M, Mason CA (2000) Retinal ganglion cell axon guidance in the mouse optic chiasm: expression and function of robos and slits. J Neurosci 20:4975-4982.

Fazeli A, Dickinson SL, Hermiston ML, Tighe RV, Steen RG, Small CG, Stoeckli ET, Keino-Masu K, Masu M, Rayburn H, Simons J, Bronson RT, Gordon JI, Tessier-Lavigne M, Weinberg RA (1997) Phenotype of mice lacking functional Deleted in colorectal cancer (Dcc) gene. Nature 386:796-804.

Fricke C, Lee JS, Geiger-Rudolph S, Bonhoeffer F, Chien CB (2001) astray, a zebrafish roundabout homolog required for retinal axon guidance. Science 292:507-510.

Gambaryan S, Hauser W, Kobsar A, Glazova M, Walter U (2001) Distribution, cellular localization, and postnatal development of VASP and Mena expression in mouse tissues. Histochem Cell Biol 116:535-543.

Gertler FB, Doctor JS, Hoffmann FM (1990) Genetic suppression of mutations in the Drosophila abl proto-oncogene homolog. Science 248:857-860.

Gertler FB, Niebuhr K, Reinhard M, Wehland J, Soriano P (1996) Mena, a relative of VASP and Drosophila Enabled, is implicated in the control of microfilament dynamics. Cell 87:227-239.

Gitai Z, Yu TW, Lundquist EA, Tessier-Lavigne M, Bargmann CI (2003) The netrin receptor UNC-40/DCC stimulates axon attraction and outgrowth through enabled and, in parallel, Rac and UNC-115/AbLIM. Neuron 37:53-65.

Godement P, Salaun J, Mason CA (1990) Retinal axon pathfinding in the optic chiasm: divergence of crossed and uncrossed fibers. Neuron 5:173-186.

Godement P, Wang LC, Mason CA (1994) Retinal axon divergence in the optic chiasm: dynamics of growth cone behavior at the midline. J Neurosci 14:7024-7039.

Goh KL, Cai L, Cepko CL, Gertler FB (2002) Ena/VASP proteins regulate cortical neuronal positioning. Curr Biol 12:565-569.

Grevengoed EE, Loureiro JJ, Jesse TL, Peifer M (2001) Abelson kinase regulates epithelial morphogenesis in Drosophila. J Cell Biol 155:1185-1198.

Grevengoed EE, Fox DT, Gates J and Peifer M (2003) Balancing different types of actin polymerization at distinct sites : roles for Abelson kinase and Enabled. J Cell Biol 163:1267-1279.

Han YH, Chung CY, Wessels D, Stephens S, Titus MA, Soll DR, Firtel RA (2002) Requirement of a vasodilator-stimulated phosphoprotein family member for cell adhesion, the formation of filopodia, and chemotaxis in dictyostelium. J Biol Chem 277:49877-49887.

Hauser W, Knobeloch KP, Eigenthaler M, Gambaryan S, Krenn V, Geiger J, Glazova M, Rohde E, Horak I, Walter U, Zimmer M (1999) Megakaryocyte hyperplasia and enhanced agonist-induced platelet activation in vasodilator-stimulated phosphoprotein knockout mice. Proc Natl Acad Sci U S A 96:8120-8125.

Hogan B, Beddington R, Constantini F, Lacy E (1994) Immunocytochemistry of whole mount embryos. In: Manipulation of the Mouse Embryo. (Hogan B, Beddington R, Constantini F, Lacy E, eds). pp340-367. Plainview, NY: Cold Spring Harbor Laboratory Press.

Holmberg J, Clarke DL, Frisen J (2000) Regulation of repulsion versus adhesion by different splice forms of an Eph receptor. Nature 408:203-206.

Howe AK, Hogan BP, Juliano RL (2002) Regulation of vasodilator-stimulated phosphoprotein phosphorylation and interaction with Abl by protein kinase A and cell adhesion. J Biol Chem 277:38121-38126.

Juriloff DM, Harris MJ (2000) Mouse models for neural tube closure defects. Hum Mol Genet 9:993-1000.

Koleske AJ, Gifford AM, Scott ML, Nee M, Bronson RT, Miczek KA, Baltimore D (1998) Essential roles for the Abl and Arg tyrosine kinases in neurulation. Neuron 21:1259-1272.

Krause M, Dent EW, Bear JE, Loureiro JJ, Gertler FB (2003) ENA/VASP PROTEINS: Regulators of the Actin Cytoskeleton and Cell Migration. Annu Rev Cell Dev Biol 19:541-564.

Lanier LM, Gates MA, Witke W, Menzies AS, Wehman AM, Macklis JD, Kwiatkowski D, Soriano P, Gertler FB (1999) Mena is required for neurulation and commissure formation. Neuron 22:313-325.

Lebrand C, Dent EW, Strasser GA, Lanier LM, Krause M, Svitkina TM, Borisy GG, Gertler FB (2004) Critical role of Ena/VASP proteins for filopodia formation in neurons and in function downstream of netrin-1. Neuron 42:37-49.

Livy DJ, Wahlsten D (1997) Retarded formation of the hippocampal commissure in embryos from mouse strains lacking a corpus callosum. Hippocampus 7:2-14.

Loureiro JJ, Rubinson DA, Bear JE, Baltus GA, Kwiatkowski AV, Gertler FB (2002) Critical roles of phosphorylation and actin binding motifs, but not the central proline-rich region, for Ena/vasodilator-stimulated phosphoprotein (VASP) function during cell migration. Mol Biol Cell 13:2533-2546.

Meyer G, Feldman EL (2002) Signaling mechanisms that regulate actin-based motility processes in the nervous system. J Neurochem 83:490-503.

Morriss-Kay G, Tuckett F (1985) The role of microfilaments in cranial neurulation in rat embryos: effects of short-term exposure to cytochalasin D. J Embryol Exp Morphol 88:333-348.

Niclou SP, Jia L, Raper JA (2000) Slit2 is a repellent for retinal ganglion cell axons. J Neurosci 20:4962-4974.

Ozaki HS, Wahlsten D (1993) Cortical axon trajectories and growth cone morphologies in fetuses of acallosal mouse strains. J Comp Neurol 336:595-604.

Plump AS, Erskine L, Sabatier C, Brose K, Epstein CJ, Goodman CS, Mason CA, Tessier-Lavigne M (2002) Slit1 and Slit2 cooperate to prevent premature midline crossing of retinal axons in the mouse visual system. Neuron 33:219-232.

Probst M (1901) Uber den Bau des balkenlosen Grobhirns, sowie uber Mikrogyrie und Heterotypie der grauen. Substanz Arch Psychiatr:709–786.

Radice GL, Rayburn H, Matsunami H, Knudsen KA, Takeichi M, Hynes RO (1997) Developmental defects in mouse embryos lacking N-cadherin. Dev Biol 181:64-78.

Ringstedt T, Braisted JE, Brose K, Kidd T, Goodman C, Tessier-Lavigne M, O'Leary DD (2000) Slit inhibition of retinal axon growth and its role in retinal axon pathfinding and innervation patterns in the diencephalon. J Neurosci 20:4983-4991.

Serafini T, Colamarino SA, Leonardo ED, Wang H, Beddington R, Skarnes WC, Tessier-Lavigne M (1996) Netrin-1 is required for commissural axon guidance in the developing vertebrate nervous system. Cell 87:1001-1014.

Shen Y, Mani S, Donovan SL, Schwob JE, Meiri KF (2002) Growth-associated protein-43 is required for commissural axon guidance in the developing vertebrate nervous system. J Neurosci 22:239-247.

Shu T, Richards LJ (2001) Cortical axon guidance by the glial wedge during the development of the corpus callosum. J Neurosci 21:2749-2758.

Shu T, Sundaresan V, McCarthy MM, Richards LJ (2003) Slit2 guides both precrossing and postcrossing callosal axons at the midline in vivo. J Neurosci 23:8176-8184.

Smith JL, Schoenwolf GC (1997) Neurulation: coming to closure. Trends Neurosci 20:510-517.

Song HJ, Poo MM (1999) Signal transduction underlying growth cone guidance by diffusible factors. Curr Opin Neurobiol 9:355-363.

Sretavan DW (1990) Specific routing of retinal ganglion cell axons at the mammalian optic chiasm during embryonic development. J Neurosci 10:1995-2007.

Stumpo DJ, Bock CB, Tuttle JS, Blackshear PJ (1995) MARCKS deficiency in mice leads to abnormal brain development and perinatal death. Proc Natl Acad Sci U S A 92:944-948.

Tani K, Sato S, Sukezane T, Kojima H, Hirose H, Hanafusa H, Shishido T (2003) Abl interactor 1 promotes tyrosine 296 phosphorylation of mammalian enabled (Mena) by c-Abl kinase. J Biol Chem 278:21685-21692.

Vasioukhin V, Bauer C, Yin M, Fuchs E (2000) Directed actin polymerization is the driving force for epithelial cell-cell adhesion. Cell 100:209-219.

Wahlsten D (1981) Prenatal Schedule of Appearance of Mouse Brain Commissures. Brain Research 227:461-473.

Wills Z, Bateman J, Korey CA, Comer A, Van Vactor D (1999) The tyrosine kinase Abl and its substrate enabled collaborate with the receptor phosphatase Dlar to control motor axon guidance. Neuron 22:301-312.

Ybot-Gonzalez P, Copp AJ (1999) Bending of the neural plate during mouse spinal neurulation is independent of actin microfilaments. Dev Dyn 215:273-283.

# CHAPTER 4

## Conclusions and Future Directions

Regulation of cell morphology and motility is fundamental to morphogenesis of the nervous system. The Ena/VASP family of actin regulatory proteins is important for the formation of protrusive structures in a variety of cell types (Krause e al., 2003). Analysis of invertebrate Ena/VASP mutants indicates Ena/VASP proteins are important for axon guidance, cell migration and dorsal closure, a process analogous to vertebrate neurulation. My work has focused on the *in vivo* significance of the vertebrate Ena/VASP proteins. I have analyzed the phenotypes of *Mena* and *MenaVASP* mutant mice in order to identify structures and cell types especially sensitive to loss of these genes. This analysis revealed that Mena and VASP are required for several actin-driven process important for proper nervous system development, including formation of the neural tube, spinal nerves and several brain commissures.

Expression studies showed that the highly related Mena and VASP proteins share a broad and overlapping expression pattern during development. Consistent with these results, mutants lacking both Mena and VASP exhibited more severe phenotypes than single mutants. However, every tissue expressing both Mena and VASP did not exhibit defects. The skin and heart express Mena and VASP but appeared to develop normally in mutants deficient for both Mena and VASP. This suggested that these genes may not be essential for development of these tissues. Alternatively, functional compensation by EVL, the third family member, may be sufficient for proper development in the absence of Mena and VASP function. The spatial distribution of EVL remains to be determined.

Identification of neurulation defects and axon fiber tract defects in *MenaVASP* mutants indicated that Mena and VASP are required for the development of the neural tube and specific axonal pathways. However, the cell autonomous function of Ena/VASP proteins in the affected cell types has not been demonstrated. For instance, neurulation defects can arise due to defects within the neural plate, such as defective apical constriction of neuroepithelial cells, convergent extension movements within the neuroepithelium and fusion of the neural folds (Keller, 2002). Additionally, neurulation defects can result from abnormalities in surrounding mesodermal tissue. Failure of mesodermal cells to generate force required to elevate the neural folds or bend the neural plate around hinge points also result in neurulation defects. Mena and VASP are highly expressed in the neural plate and are expressed at lower levels in the mesoderm. Targeted disruption of Ena/VAP function in either the neuroepithelium or underlying mesoderm in a cell type specific manner would further elucidate the role(s) Ena/VASP proteins play in neurulation.

Additional experiments are also required to determine the cell autonomous function of Ena/VASP proteins in axon guidance. Axon fiber tract defects can result because of intrinsic defects in the neuron such that it fails to respond to appropriate guidance signals and/or because of extrinsic defects in the environment. My analysis of the corpus callosum defects in Ena/VASP mutant mice revealed defects in the trajectory of callosal fibers and defects in the midline structure. Consequently, agenesis of the corpus callosum may have resulted from a combination of intrinsic defects in the mutant callosal axons and extrinsic defects resulting from absence of hemisphere fusion. The

origin of the hemisphere fusion defect has not been investigated. The interhemispheric region evolves from the dorsal neural tube. Given the range of neurulation defects exhibited by Ena/VASP mutant mice, subtle and localized disturbance in the dorsal neural tube may have allowed brain development to continue but resulted in localized malformation of dorsal derived brain structures. Further characterization of the dorsal neural tube at early developmental stages (i.e.: E9-E12) may provide insight on the initial disturbance that subsequently resulted in abnormal hemisphere fusion.

Recently, Ena/VASP proteins were shown to regulate filopodial formation and elongation in cultured vertebrate neurons (Lebrand et al., 2004). Furthermore, inhibition of Ena/VASP activity blocked the filopodial response of neurons to netrin-1 treatment. Filopodia have been proposed to be critical for the ability of growth cones to explore the environment and respond to guidance cues (Dent and Gertler, 2003). The midline choice point is a region thought to be rich in guidance signals. Visualization of growth cones at the midline choice point in the developing brain has shown that growth cones assume complex morphologies; extending numerous filopodial and lamellipodial protrusions (Godement et al., 1994; Halloran and Kalil, 1994). Growth cones lacking filopodia may be compromised in their ability to find and respond to guidance cues and consequently exhibit pathfinding errors. Given that Ena/VASP proteins are required for filopodial formation and to mediate the filopodial response to netrin-1, the axonal fiber tract defects exhibited by Ena/VASP mutant mice may have in part resulted from the intrinsic inability of neurons to respond to appropriate guidance cues. Further experiments are necessary to demonstrate the cell autonomous function of Ena/VASP proteins in axon guidance.

**References**

Dent EW and Gertler FB (2003) Cytoskeletal dynamics and transport in growth cone motility and axon guidance. Neuron 40: 209-227.

Godemont P, Wang LC and Mason CA (1994) Retinal axon divergence in the optic chiasm: dynamics of growth cone behavior at the midline. J Neurosci 14: 7024-7039.

Halloran MC and Kalil K (1994) Dynamic behavior of growth cones extending in the corpus callosum of living cortical brain slices observed with video microscopy. J. Neurosci 14: 2161-2177.

Keller R (2002) Shaping the vertebrate body plan by polarized embryonic cell movements. Science 298: 1950-1954.

Krause M, Dent EW, Bear JE, Loureiro JJ and Gertler FB (2003) Ena/VASP proteins: regulators of the actin cytoskeleton and cell migration. Ann Rev Cell Dev Biol 19: 541-564.

Lebrand C, Dent EW, Strasser GA, Lanier LM, Krause M, Svitkina TM, Borisy GG and Gertler FB (2004) Critical role of Ena/VASP proteins for filopodial formation in neurons and in function downstream of netrin-1. Neuron 42:37-49.

# APPENDIX 1

## Ena/VASP Proteins Regulate Cerebellar Granule Cell Migration

**Abstract**

Cell migration is an actin-dependent process. The Ena/VASP family of actin regulatory proteins are implicated in the motility of a variety of cell types. I have initiated a project to investigate the role of Ena/VASP proteins in the migration of cerebellar granule cells (GCs), an extensively studied model of neuronal cell migration. GCs express all three vertebrate Ena/VASP proteins. Using a cell biological approach, I show that GCs expressing an Ena/VASP inhibitory construct exhibit altered migration in GC aggregate cultures. This is the first demonstration that Ena/VASP proteins regulate cerebellar GC migration. A mechanistic understanding of Ena/VASP function in GC migration requires further investigation.

**Introduction**

Ena/VASP proteins comprise a family of actin regulatory proteins that remodel the actin cytoskeleton in response to extracellular signals (Krause et al., 2003). Analysis of vertebrate and invertebrate Ena/VASP mutants implicates Ena/VASP proteins in several actin-dependent processes including cell migration, axon guidance, neurulation, and platelet aggregation. Vertebrates possess three highly related family members, Mena, VASP and EVL, which are able to function interchangeably in a variety of assays. Ena/VASP proteins localize to the tips of lamellipodia and filopodia and are important for the formation of actin-based protrusions in a variety of cell types.

Ena/VASP function in cell migration has been investigated using *in vitro* and *in vivo* systems. Studies using cultured fibroblasts showed that inhibiting Ena/VASP

function perturbed the geometry of the actin cytoskeleton underlying the leading edge and resulted in faster net translocation in random motility assays (Bear et al., 2000; Bear et al., 2002). Subsequently, *in vivo* studies indicated a role for Ena/VASP proteins in neuronal cell migration in the developing cortex (Goh et al., 2002). During embryogenesis, cortical neurons generated in a deep layer of the cortex, migrate along radial glia from their place of origin to populate superficial layers in the developing cortex (Gupta et al., 2002). Neurons migrate in sequential waves depending on the order in which they were generated. Later generated neurons migrate past the earlier generated neurons to occupy more superficial layers, ultimately giving rise to the mature six-layered cortex. Inhibition of Ena/VASP function resulted in aberrant positioning of cortical neurons to more superficial layers, consistent with the interpretation that these cells migrated too far. It has recently been shown that radial glia and the cortical neurons that migrate along them are derived from the same precursor cell (Malatesta et al., 2003). Because Ena/VASP function was inhibited in these precursor cells and their neuronal and radial glial descendents, this experimental approach did not definitively demonstrate that inhibition of Ena/VASP in the neurons was responsible for the observed phenotype (Goh et al., 2002). Alternatively, inhibition of Ena/VASP function in the radial glia may have caused glial defects and secondarily neuronal defects.

I have employed the cerebellar granule cell (GC) migration model system to investigate the cell autonomous function of Ena/VASP proteins in neuronal cell migration. GC migration in the postnatal cerebellum is a well-characterized model to study neuronal cell migration (Komuro and Rakic, 1998, 2001). During the first three

weeks after birth, the cerebellum is dramatically transformed, primarily due to the proliferation, differentiate and migration of GCs. GC precursors proliferate at the surface of the cerebellum in the outer external granule cell layer (EGLo) (Figure 1). Subsequently, GCs begin to differentiate by extending bipolar processes; a thick leading process and a thin trailing process. GCs migrate tangentially within the inner EGL in a saltatory fashion, using the leading process to guide the direction of cell migration. Tangentially migrating cells are thought to migrate along neuritic processes extended by other GCs. GCs switch to the radial phase of migration, in which GCs migrate along radial glial, termed Bergman glia, to travel to deeper layers of the cerebellum. Radial migration is initiated when tangentially migrating GCs pause and protrude a third process from the cell body that extends in a direction perpendicular to the cerebellar surface. The GC nucleus enters the newly formed process leaving behind the original bipolar processes, giving GCs their characteristic T-shaped morphology. GCs migrate radially in a saltatory manner past the purkinje cell layer (PCL), ultimately reaching their destination in the inner granule cell layer (IGL). Tangential and radially migrating GCs dynamically extend and retract its leading process, which exhibits a growth-cone like structure at the distal tip. The leading process searches the environment and determines the direction of cell migration. However process extension/retraction is not consistently coupled to movement of the cell body (Lambert de Rouvroit and Goffinet, 2001).

Because GCs exhibit an intrinsic migratory program *in vitro* (Kawaji et al., 2004),

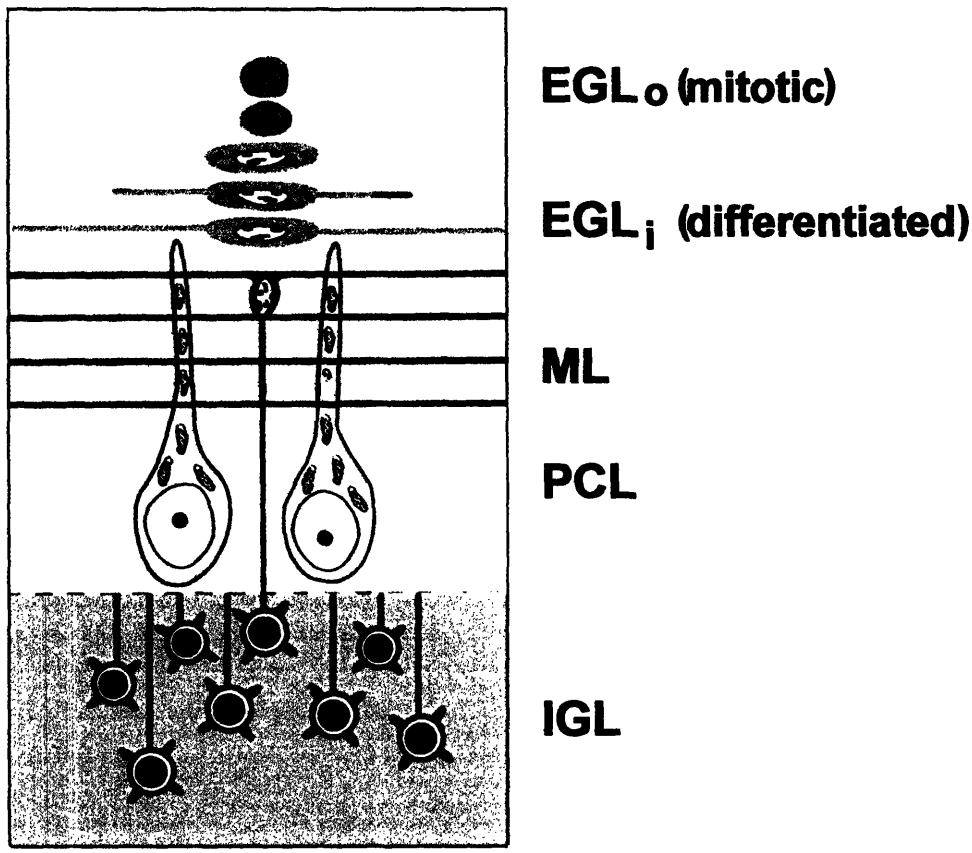


**Figure 1**

Figure 1. Schematic of granule cell development in the postnatal cerebellum. Granule cell (GC) precursors reside in the outer external granule cell layer (EGLo) and proliferate giving rise to numerous GCs. Differentiating GCs in the inner granule cell layer (EGLi) extend bipolar processes and tangentially migrate within the EGLi (not depicted). GCs migrate radially by extension of a third process that penetrates deeper into the cerebellum. The GC leaves behind the original bipolar processes, which will develop into the GC axons, in the EGL and translocates its soma past the Molecular Layer (ML) and Purkinje Cell Layer (PCL) until it reaches its destination in the IGL. This figure has been modified from Development of the Cerebellar System by Altman and Bayer (1997).

GC migration has been studied in GC aggregate cultures, a system that is readily accessible for imaging and manipulation of environmental factors. During the initial culture period, GCs within the aggregate extend neuritic process which radiate out from the aggregate center. GCs migrate out of the aggregate towards the periphery along these neuritic processes, which is similar to tangentially migrating GCs *in vivo*. GCs migrate in a general outward direction, but sometimes wander laterally, switching between different neuritic processes as they migrate away from the aggregate center. After a few days in culture, GC switch to a radial mode of migration and move their cell body in a direction perpendicular to their initial trajectory. I have employed this assay to study the role of Ena/VASP proteins in GC migration.

In this chapter, I will describe my initial progress towards understanding the function of Ena/VASP proteins in cerebellar GC migration. I have begun by determining the expression profile of Ena/VASP proteins in the cerebellum. Next, I have initiated functional studies to determine the consequences of inhibiting Ena/VASP function for GCs migration.

## Material and Methods

**Western Blot Analysis.** Protein extracts from postnatal and adult cerebella from wildtype Swiss Webster mice were prepared in ice-cold RIPA buffer [25mM Tris, pH7.5/ 150mM NaCl/ 1% NP40/ 0.5% Sodium Deoxycholate/ 0.1% SDS] + Proteinase Inhibitor Tablet (Pierce). Protein concentrations were determined using the BCA assay (Pierce). SDS-PAGE electrophoresis and Western blotting were done using standard techniques.

Antibodies included polyclonal anti-Mena (2197), anti-VASP (2010) and anti-EVL(1404).

**Immunohistochemistry.** P8 cerebellar sections were labeled with affinity purified anti-Mena (polyclonal 2197), affinity purified anti-VASP (polyclonal 2010), anti-EVL (polyclonal 1404) and anti-Calbindin (monoclonal CB-955; Sigma) antibodies. Labeling was performed on 10μm frozen sections of 4% paraformaldehyde fixed tissue. Sections were blocked with 10% BSA, 10% Normal serum in PBST [PBS + 0.05% Tween-20] and incubated overnight at 4°C with primary antibodies diluted in 1% blocking solution. Polyclonal antibodies were detected with goat-anti-rabbit-Biotin (1:200) (VectorLabs) followed by Strep-FITC (PharMingen). Monoclonal antibodies were detected with donkey anti-mouse-Alexa 488 (Molecular Probes). Mena knock-out and VASP knock-out cerebellar tissue served as controls for Mena and VASP antibodies. No primary antibody served as control for EVL antibodies.

**GC Aggregate Cultures and Transfection.** Purified GCs were prepared from P6-7 cerebella from wildtype Swiss Webster mice using the protocol by Hatten ME and colleagues (Hatten, ME, et. Al. 1991), with the exception that the pre-plating on poly-D-lysine step was omitted. For transfection, purified GCs were resuspended in the Amaxa Neuro Kit buffer (1 million cells/100μl buffer). One microgram of plasmid DNA (pCAX-EGPF-FP4-mito or control pCAX-EGFP-APPPP-mito) was added and the sample electroporated using Amaxa protocol H-13. Immediately after electroporation, the sample was washed with pre-warmed GC+serum media, spun and resuspended in

fresh media before placing in 37°C/ 5% $CO_2$ incubator. Cells were allowed to form aggregates for 2 days before plating aggregates on 35mm tissue cultures dishes coated with poly-D-lysine/laminin (20μg/ml) and grown in GC serum-free media. Aggregates were fixed 24hrs after plating and the distance between the transfected cell (judged by EGFP fluorescence) and the aggregate perimeter was measured using OpenLabs software. Migration experiments were repeated 4 times.

## Results

**Ena/VASP proteins are expressed in the developing and adult cerebellum.** To determine whether Ena/VASP proteins play a role in cerebellar GC development, expression analysis was performed to determine the temporal and spatial expression pattern of Ena/VASP proteins in the cerebellum. Granule cell migration from the outer EGL to their destination in the IGL begins shortly after birth and is complete by the third postnatal week. Protein levels of Mena, VASP and EVL in the cerebellum at several postnatal stages and at adulthood were examined (Figure 2). Western blot analysis showed that all three proteins were expressed at all stages examined. Expression levels were higher in the postnatal cerebellum compared to the adult cerebellum. These data showed that high Ena/VASP expression levels corresponded to the postnatal period of active GC migration and declined thereafter.

To determine the spatial distribution of Ena/VASP proteins within the developing cerebellum, immunolocalization of Ena/VASP proteins in postnatal cerebellar sections

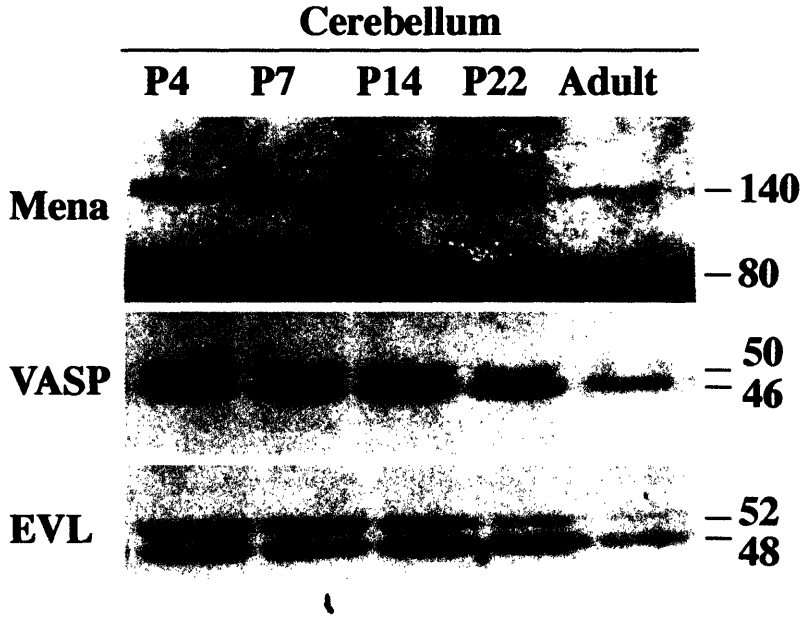


Figure 2

Figure 2. Temporal Expression Pattern of Ena/VASP Proteins in the Developing and Adult Cerebellum. Western blot analysis of Mena, VASP and EVL protein levels in cerebellar lysates at postnatal day (P) 4, P7, P14, P22 and adult. All three family members are highly expressed in the postnatal cerebellum at each stage examined but are expressed at low levels in the adult. The two bands in the Mena blot represent the alternatively spliced isoforms of 80kDa Mena and140kDa neuronal specific Mena(+). The two bands in the EVL blot represent the alternatively spliced isoforms of 46kDa EVL and 50kDa EVL-I. The upper band in the VASP blot is the Ser157 phosphorylated form of VASP.

was performed. Mena VASP and EVL exhibited similar expression patterns and were highly enriched in the inner EGL, which corresponds to the region containing migratory GCs (Figure 3). Lower expression levels of Mena, VASP and EVL were found in the outer EGL where granule precursor cells actively proliferation and within the IGL, the destination layer of migrating GCs. VASP, EVL and to a lesser extent Mena were also highly expressed by Purkinje cells, which were co-labeled with calbindin immuno-staining (Figure 3). Immunolocalization studies in P8 sections correlated high Ena/VASP expression to region of actively migrating GCs.

The subcellular localization of Ena/VASP proteins in GCs was also examined. GCs either in aggregate cultures or in dissociated cultures were immunolabeled for Mena. Mena was enriched in the growth cone like structure at the tip of the leading process and asymmetrically within the cell body at the leading pole where the leading process extends (Figure 4A,B). Within the growth cone like process, Mena was enriched at the distal tips of filopodia and lamellipodia, which is similar to its localization within growth cones of other neuronal subtypes previously examined (Figure 4C).

**Ena/VASP proteins regulate GC migration.** Expression studies correlated high Ena/VASP expression to the time and place of GC migration in the postnatal cerebellum. Because Ena/VASP family members are highly related and function interchangeably in a variety of assays, inhibition of all family members may be necessary to uncover a cellular phenotype in GCs. Indeed, the cerebellum develops normally in the rare adult *Mena-/-*

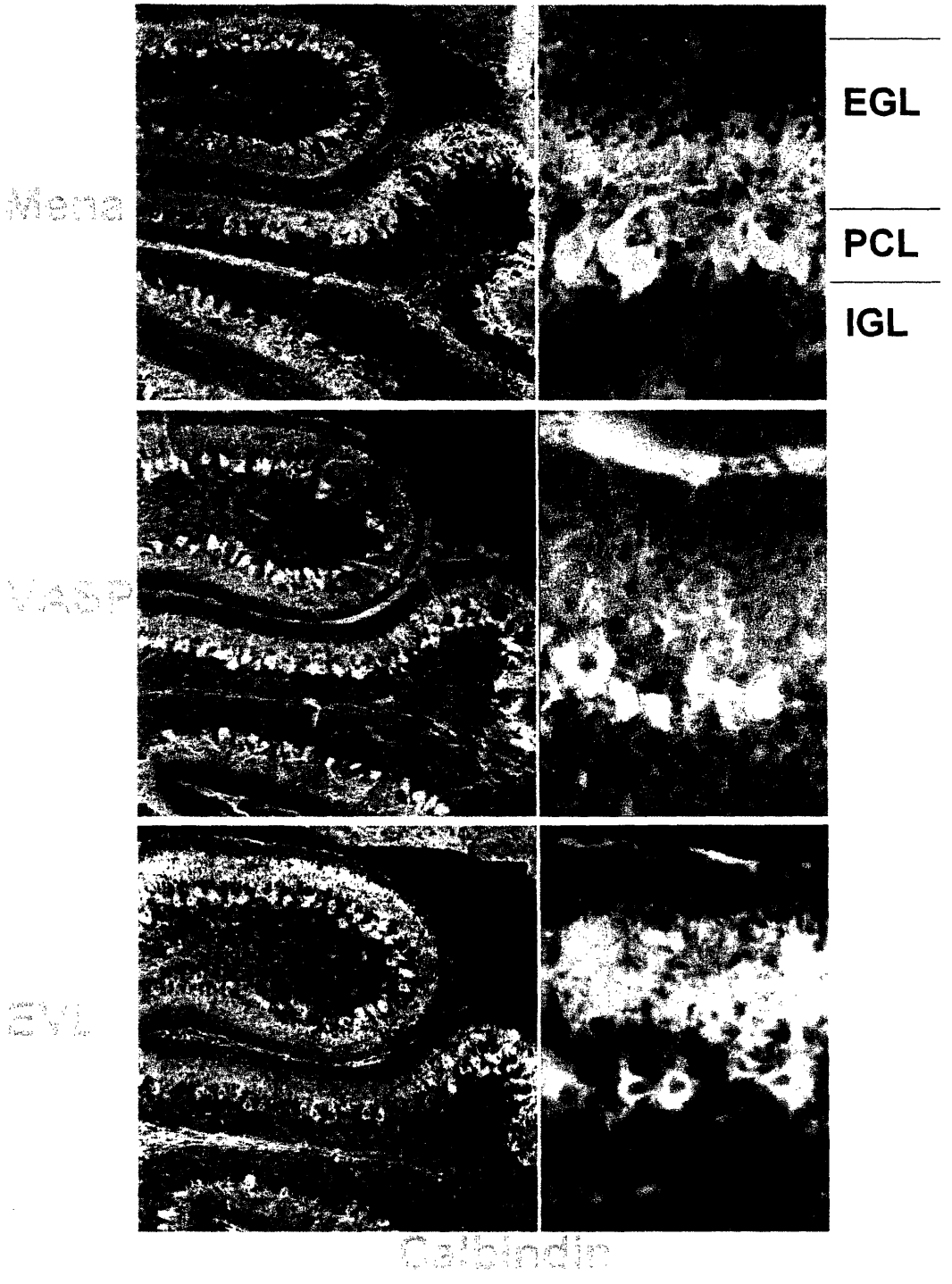


**Figure 3**

Figure 3. Spatial Distribution of Ena/VASP Proteins in the Developing Cerebellum. Immunoflorescence of Ena/VASP proteins (green) and calbindin (red) in a frozen section of P8 cerebellum. Mena, VASP and EVL are enriched in the EGLi, where differentiated and migrating GCs reside. VASP and EVL and to a lesser extent Mena are expressed by Purkinje cells which are labeled with antibodies to calbindin.

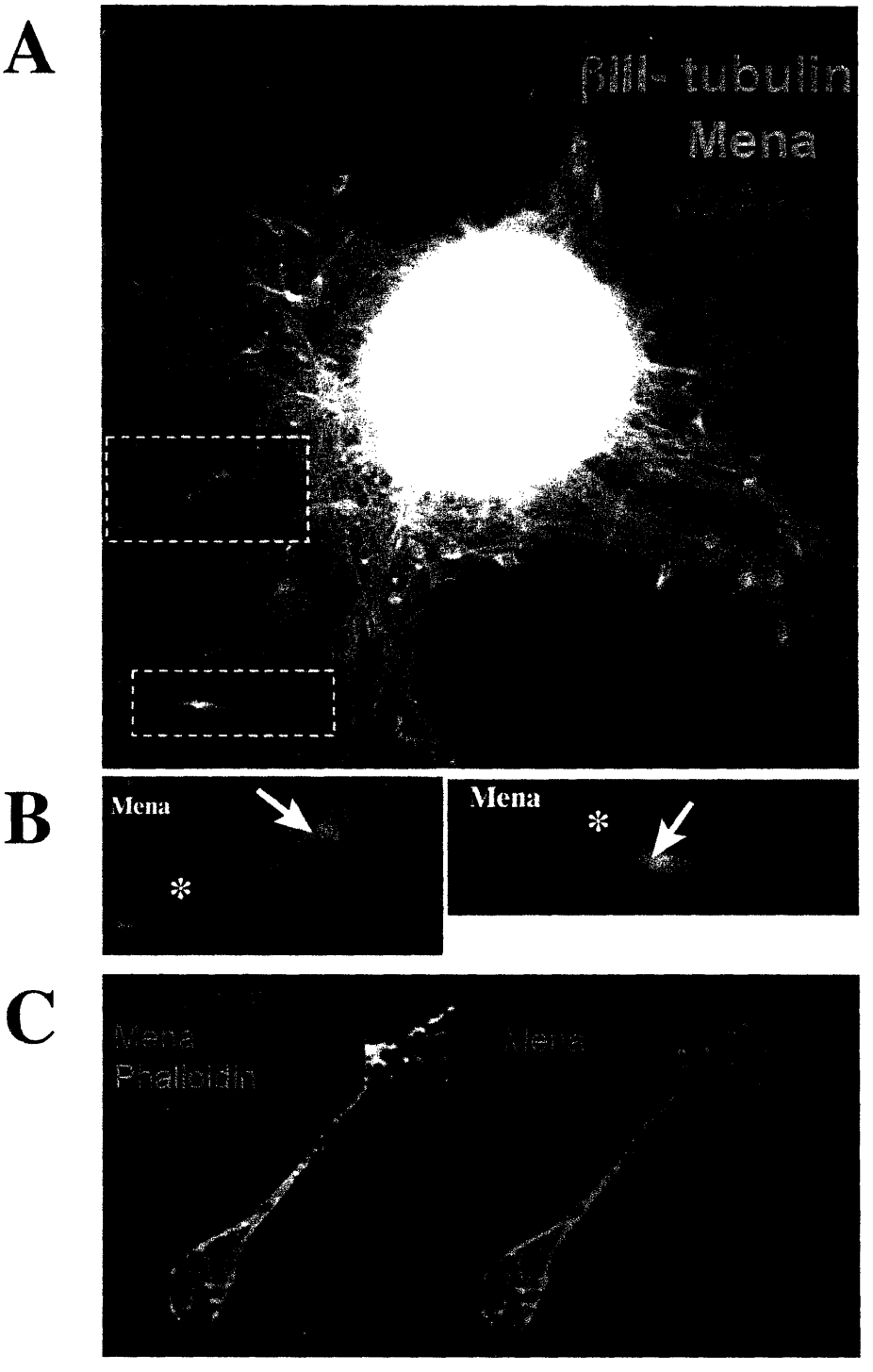


**Figure 4**

Figure 4. Subcellular Localization of Mena in Granule Cells (A, B) Granule cell aggregate culture immunolabeled for Mena (red) and neuronal specific βIII tubulin (green). Nuclei are labeled with DAPI (blue). Granule cells residing within the aggregate extend neuritic processes that radiate out of the aggregate. Individual granule cells have migrated out of the aggregate along these processes. (B) Magnification of two granule cells showing the localization of Mena. Mena is enriched at the growth-cone-like distal tip of the leading process (asterisk) and in the leading pole (arrow) where the leading process extends from the cell body. (C) Higher resolution localization of Mena (green) and neuronal specific βIII tubulin (blue) in granule cell at the unipolar stage in dissociated culture. F-actin is labeled with Phalloidin (red). Mena is enriched at the filopodial and lamellipodial tips of the growth-cone-like structure and in the leading pole (arrow) where the leading process extends from the cell body.

*VASP-/-* survivors despite exhibiting defects in brain commissure formation. This suggested that deletion of the remaining family member, EVL, may be necessary to reveal an *in vivo* requirement for Ena/VASP proteins in cerebellar development. To determine if Ena/VASP proteins regulate GC migration, I utilized a dominant interfering strategy previously employed in other cell types to inhibit the function of all Ena/VASP proteins (Bear et al., 2000; Goh et al., 2002; Lebrand et al., 2004). This strategy was based on the rationale that proper subcellular localization of Ena/VASP proteins was important for cellular function. A construct was designed to express a fusion protein containing four repeats of the consensus FPPPP motif that binds with high affinity to the EVH1 domain of all Ena/VASP proteins, fused to Enhanced Green Florescent Protein (EGFP) and a mitochondrial membrane targeting domain (mito). In fibroblasts expressing this construct, Ena/VASP proteins are bound by the EGFP-FPPPP-mito fusion protein and mislocalized to the mitochondrial membrane, essentially hijacked from their normal sites of action (Bear et al., 2000). Furthermore, these Ena/VASP inhibited cells mimic the phenotype of Ena/VASP deficient cells. A construct encoding a mutated version of the binding motif (APPPP) that was unable to bind Ena/VASP proteins, served as a control.

To determine Ena/VASP function in GC migration, purified GCs were transfected with either the EGFP-FPPPP-mito or control constructs and allowed to form aggregates in culture. Twenty-four hours after aggregates were plated many GCs had migrated out of the aggregate. The EGFP-FPPPP-mito expressing cells that had migrated out of the aggregate exhibited bipolar morphologies similar to controls and were seen to be

associated with transfected and nontransfected neuritic processes (Figure 5). The distance EGFP-FPPPP-mito expressing GC cell bodies were displaced from the perimeter of the aggregate was measured and compared to controls (Figure 6A). Cells expressing the EGFP-FPPPP-mito construct traveled an average distance of 95μm (n=1486) whereas control cells expressing the EGFP-APPPP-mito construct traveled an average distance of 69μm (n=919). Therefore, in the absence of Ena/VASP function cells traveled a greater distance on average than control cells (Figure 6B). These results provide initial evidence indicating a role for Ena/VASP function in the migration of GCs. The mechanism by which Ena/VASP regulates GC migration requires further investigation.

**Discussion**

Ena/VASP proteins are implicated in the motility of a variety of cell types. Here I show that Ena/VASP proteins are expressed by GCs and regulate cerebellar GC migration. Inhibiting Ena/VASP function by mislocalization to the mitochondria results in GCs migrating further than controls in the GC aggregate assay. There are several explanations by which inhibition of Ena/VASP proteins in GCs could promote outward migration in the aggregate system. Inhibition of Ena/VASP proteins may increase the velocity of migration. Alternatively, Ena/VASP ptoteins may regulate the tempo of migration such that cells spend less time pausing and more time migrating resulting in greater distance traveled in a defined period of time. Lastly, Ena/VASP proteins may regulate the trajectory of migrating GCs. Inhibiting Ena/VASP function may cause GCs take a more direct path, rather than switching between processes and wandering laterally en route to the periphery.

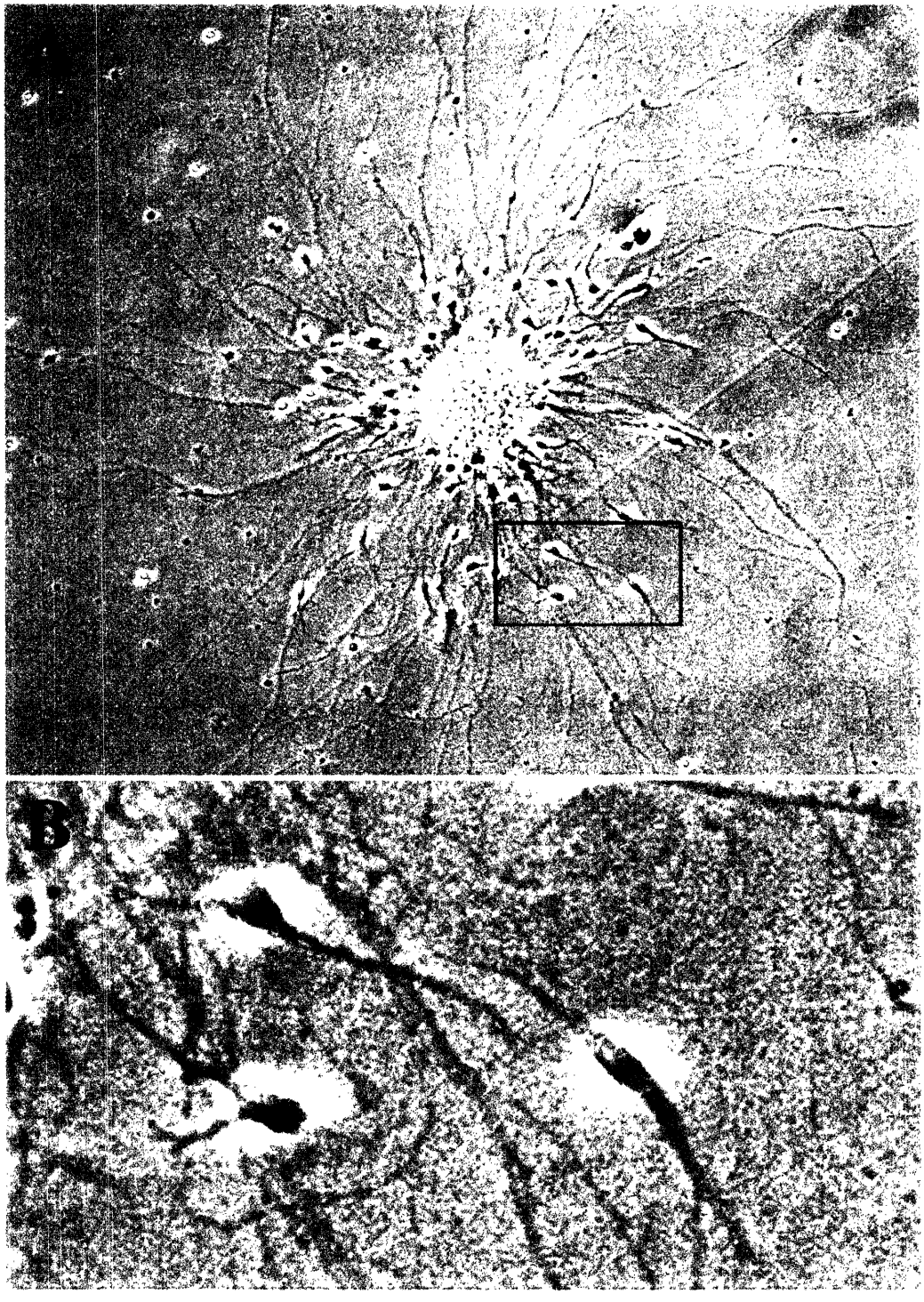

**Figure 5**

Figure 5 (A) GC aggregate composed of untransfected GCs and GCs transfected with the Ena/VASP inhibitory expression construct, EGFP-FPPP-mito, (green).

(B) High magnification view of boxed area in (A) showing three GCs that had migrated out of the aggregate. Two of these GCs are expressing the EGFP-FPPP-mito (green) construct and appears to exhibit a normal bipolar morphology.

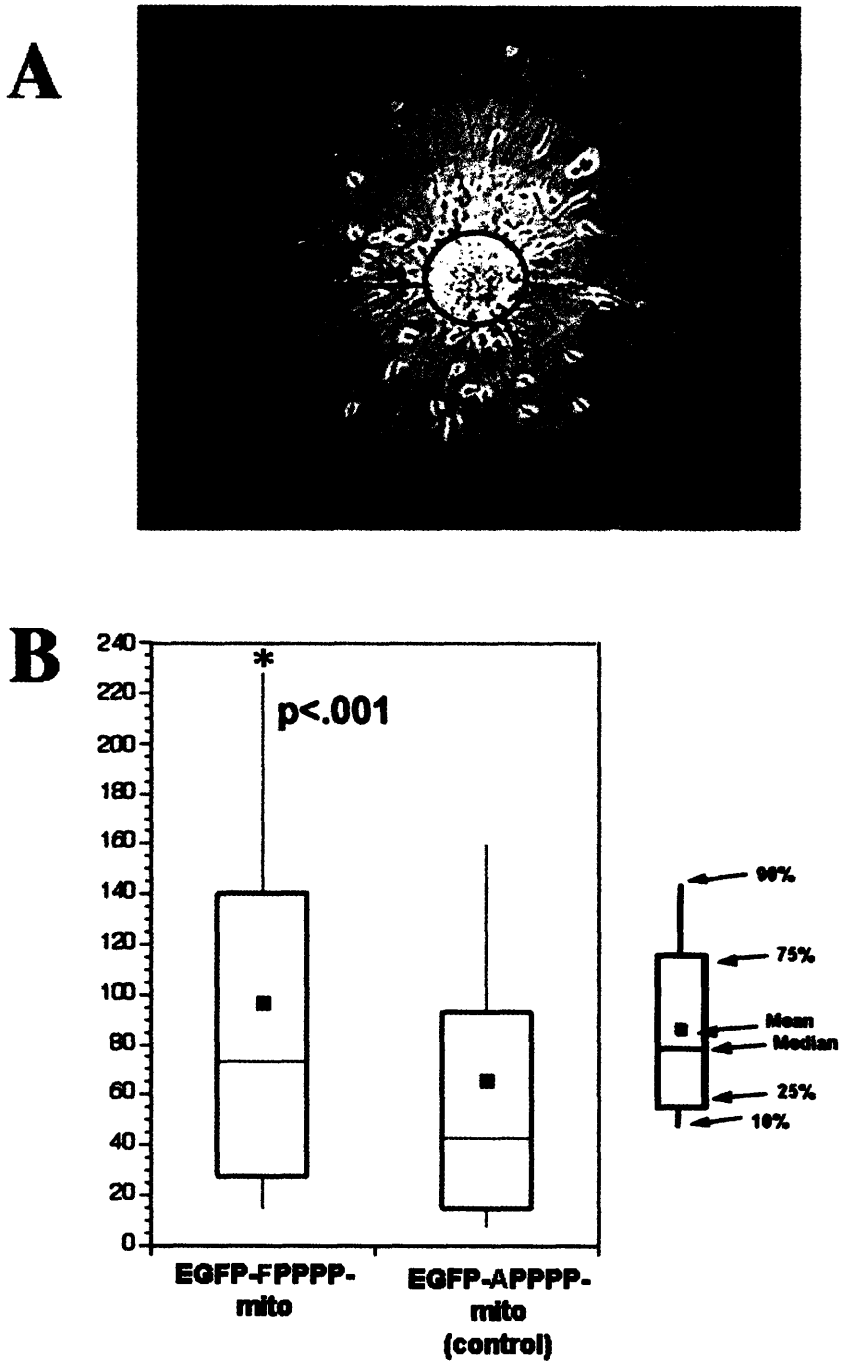
A
B
240
220
200
180
160
140
120
100
80
60
40
20
0
*
p<.001
EGFP-FPPPP-mito
EGFP-APPPP-mito (control)
90%
75%
Mean
Median
25%
10%

**Figure 6**

Figure 6 (A) Distance traveled by EGFP-FPPPP-mito and control EGFP-APPPP-mito expressing GCs was measured from the perimeter of the aggregate (black circle) to the base of the GC cell body. (B) Box and whisker plot show the distances traveled by EGFP-FPPPP-mito and control EGFP-APPPP-mito expressing GCs. GCs expressing the Ena/VASP inhibitory construct traveled further than controls in the GC aggregate.

Many of these outstanding questions can be addressed by monitoring GCs migration using time-lapse video microscopy. Movies can be quantified to determine the velocity and trajectory of migration as well as the time spent moving verses pausing. Additionally GC behavior can be monitored to detect morphological differences accompanying migration between control and Ena/VASP inhibited cells. Ena/VASP function has been shown to be critical for the formation of filopodia in cultured hippocampal neurons and other cell types. The morphological consequences of inhibiting Ena/VASP function in GCs has not be carefully examined and may readily account for the altered migration of GCs in the aggregate system. Time-lapse video microscopy will also be essential to investigate the cell autonomous function of Ena/VASP proteins in migrating GCs. Migration of Ena/VASP inhibited GCs traveling along control processes can be identified and compared to control cells migrating on processes extended by Ena/VASP inhibited cells. This analysis will provide data to differentiate a primary defect arising from inhibition of Ena/VASP function in the migrating neuron verses in the substrate supporting migration.

I have presented data showing that Ena/VASP proteins are expressed in migrating GCs and have demonstrated a functional consequence of inhibiting Ena/VASP proteins in GC migration. Additional work is required to characterize the precise role Ena/VASP proteins play in migrating GCs.

**References**


Altman J. and Bayer S. A. (1997) Development of the Cerebellar System. CRC Press, Boca Tatton, Fl.

Bear, J. E., Loureiro, J. J., Libova, I., Fassler, R., Wehland, J., and Gertler, F. B. (2000). Negative regulation of fibroblast motility by Ena/VASP proteins. Cell *101*, 717-728.

Bear, J. E., Svitkina, T. M., Krause, M., Schafer, D. A., Loureiro, J. J., Strasser, G. A., Maly, I. V., Chaga, O. Y., Cooper, J. A., Borisy, G. G., and Gertler, F. B. (2002). Antagonism between Ena/VASP proteins and actin filament capping regulates fibroblast motility. Cell *109*, 509-521.

Goh, K. L., Cai, L., Cepko, C. L., and Gertler, F. B. (2002). Ena/VASP proteins regulate cortical neuronal positioning. Curr Biol *12*, 565-569.

Gupta, A., Tsai, L. H., and Wynshaw-Boris, A. (2002). Life is a journey: a genetic look at neocortical development. Nat Rev Genet *3*, 342-355.

Hatten M. E., Gao, W, Morrison, M. E., Mason, C. A. (1991) The Cerebellum: Purification and Coculture of Identified Cell Populations. In Culturing Nerve Cells, G. Banker and K. Goslin, eds. MIT Press, Cambridge, MA.

Kawaji, K., Umeshima, H., Eiraku, M., Hirano, T., and Kengaku, M. (2004). Dual phases of migration of cerebellar granule cells guided by axonal and dendritic leading processes. Mol Cell Neurosci *25*, 228-240.

Komuro, H., and Rakic, P. (1998). Distinct modes of neuronal migration in different domains of developing cerebellar cortex. J Neurosci *18*, 1478-1490.

Komuro, H., Yacubova, E., and Rakic, P. (2001). Mode and tempo of tangential cell migration in the cerebellar external granular layer. J Neurosci *21*, 527-540.

Krause, M., Dent, E. W., Bear, J. E., Loureiro, J. J., and Gertler, F. B. (2003). Ena/VASP proteins: regulators of the actin cytoskeleton and cell migration. Annu Rev Cell Dev Biol *19*, 541-564.

Lambert de Rouvroit, C., and Goffinet, A. M. (2001). Neuronal migration. Mech Dev *105*, 47-56.

Lebrand, C., Dent, E. W., Strasser, G. A., Lanier, L. M., Krause, M., Svitkina, T. M., Borisy, G. G., and Gertler, F. B. (2004). Critical role of Ena/VASP proteins for filopodia formation in neurons and in function downstream of netrin-1. Neuron *42*, 37-49.

Malatesta, P., Hack, M. A., Hartfuss, E., Kettenmann, H., Klinkert, W., Kirchhoff, F., and Gotz, M. (2003). Neuronal or glial progeny: regional differences in radial glia fate. Neuron *37*, 751-764.

# APPENDIX 2

## Targeted Disruption of the Murine *zyxin* Gene

Laura M. Hoffman,1 David A. Nix,1 Beverly Benson,1 Ray Boot-Hanford,2 Erika Gustafsson,2 Colin Jamora,3 A. Sheila Menzies,4 Keow Lin Goh,4 Christopher C. Jensen,1 Frank B. Gertler,4 Elaine Fuchs,3 Reinhard Fässler,2,1 and Mary C. Beckerle1

Huntsman Cancer Institute and Department of Biology, University of Utah, Salt Lake City, Utah 84112,1 Department of Experimental Pathology, Lund University, 221 85 Lund, Sweden,2 Department of Molecular Genetics and Cell Biology and Howard Hughes Medical Institute, University of Chicago, Chicago, Illinois 60637,3 Department of Biology, Massachusetts Institute of Technology, Cambridge, Massachusetts 021394

ASM phenotypically characterized *zyxin*-/- brains and generated the data reported in Figure 5.

Appendix 2 was published in Molecular and Cellular Biology 23(1):70-9 (2003).

**Abstract**

Zyxin is an evolutionarily conserved protein that is concentrated at sites of cell adhesion, where it associates with members of the Enabled (Ena)/vasodilator-stimulated phosphoprotein (VASP) family of cytoskeletal regulators and is postulated to play a role in cytoskeletal dynamics and signaling. Zyxin transcripts are detected throughout murine embryonic development, and the protein is widely expressed in adults. Here we used a reverse genetic approach to examine the consequences of loss of zyxin function in the mouse. Mice that lack zyxin function are viable and fertile and display no obvious histological abnormalities in any of the organs examined. Because zyxin contributes to the localization of Ena/VASP family members at certain subcellular locations, we carefully examined the *zyxin*-/- mice for evidence of defects that have been observed when Ena/VASP proteins are compromised in the mouse. Specifically, we evaluated blood platelet function, nervous system development, and skin architecture but did not detect any defects in these systems. Zyxin is the founding member of a family of proteins that also includes the lipoma preferred partner (LPP) and thyroid receptor-interacting protein 6 (TRIP6). These zyxin family members display patterns of expression that significantly overlap that of zyxin. Western blot analysis indicates that there is no detectable upregulation of either LPP or TRIP6 expression in tissues derived from *zyxin*-null mice. Because zyxin family members may have overlapping functions, a comprehensive understanding of the role of these proteins in the mouse will require the generation of compound mutations in which multiple zyxin family members are simultaneously compromised.

## Introduction

Zyxin is a LIM domain protein that is present at sites of cell-substratum and cell-cell adhesion, where it is proposed to dock proteins involved in cytoskeletal organization and dynamics (7, 8, 11, 16). Biochemical studies have identified -actinin, members of the Enabled (Ena)/vasodilator-stimulated phosphoprotein (VASP) family, Vav, members of the cysteine-rich protein family, the LATS1 tumor suppressor, and members of the p130cas family as binding partners for zyxin (12, 19, 23, 24, 42, 43, 47, 56). The molecular architecture of zyxin is compatible with the protein's postulated role as a scaffold for the assembly of multimeric protein complexes. Zyxin displays three tandemly arrayed LIM domains, double zinc finger structures that support specific protein interactions (37, 47). In addition, zyxin exhibits at least one nuclear export signal that regulates its excursions between the nucleus and the cytoplasm (35, 36).

Zyxin also displays four proline-rich ActA repeats that can interact directly with members of the Ena/VASP family (14, 19, 34). Members of the Ena/VASP family are concentrated at focal adhesions, the leading edge of lamellipodia, and filopodial tips (19, 42). Ena/VASP proteins are involved in modulation of actin assembly and organization (4, 6, 30, 41, 48) and are required for normal fibroblast and neuron migration (5, 20). Recent work has illustrated that the proper subcellular targeting of Ena/VASP family members is essential for them to fulfill their normal roles *in vivo* (1, 5, 6).

The Ena/VASP binding capacity of zyxin has been studied in detail, and several lines of evidence suggest that zyxin plays an important role in localizing members of this

family to sites of cell-substratum adhesion. For example, microinjection of peptides that cause displacement of zyxin from focal adhesions also results in loss of Ena/VASP family members from these sites (15). In complementary experiments, targeting of zyxin to membranes or mitochondria leads to recruitment of Ena/VASP proteins (14, 18). Moreover, microinjection of peptide inhibitors that interfere with the binding of Ena/VASP proteins to partners with ActA repeats, such as zyxin, disturbs the subcellular distribution of Ena/VASP proteins and affects cell spreading and cell-cell adhesion (14, 52). Collectively, these studies suggest that failure of Ena/VASP proteins to localize properly results in defects in actin-based cell functions and implicate zyxin as an important contributor to the proper localization of Ena/VASP proteins.

The physiological consequences of disturbing Ena/VASP function have been characterized in vertebrates by analysis of mice in which Mena (mammalian Ena) or VASP functions have been compromised by gene disruption or expression of mutant constructs. Although mice that lack either Mena or VASP are viable and fertile, compromising the functions of murine Ena/VASP family members results in disturbed platelet function, nervous system development, and epithelial sheet formation (3, 21, 29, 52). Here we pursued a reverse genetic strategy to probe the role of zyxin in the mouse. We generated mice that lack zyxin function and analyzed the importance of zyxin for embryonic development and adult functions, with particular attention to processes that are known to depend on members of the Ena/VASP family. Mice that lack zyxin are both viable and fertile and do not display defects in processes that are compromised when

either VASP or Mena functions are eliminated. The existence of multiple zyxin family members may obscure our ability to detect the contribution of zyxin to these processes.

## Material and Methods

**Northern blot analysis.** *zyxin* transcript levels were analyzed by probing mouse embryo and adult multiple tissue Northern blots containing 2 $\mu$g of polyadenylated RNA per lane (Clontech Laboratories, Palo Alto, Calif.). Both a zyxin LIM domain DNA probe and a *zyxin* 3' untranslated region DNA were labeled by nick translation with [32P]dCTP and used to probe the Northern blots by standard methods (2). Glyceraldehyde-3-phosphate dehydrogenase transcript levels were monitored as a control.

***zxyin* targeting construct and generation of *zyxin*-null mice.** All mice were maintained in a specific-pathogen-free barrier facility and cared for, handled, and euthanized following guidelines approved by the Institutional Animal Care and Use Committee of the University of Utah. The neomycin resistance selection cassette pKT3lox(A) and the pTK1-pTK2-C targeting vector were provided by Kirk Thomas (University of Utah Transgenic Core Facility). The 19-kb mouse genomic DNA construct was isolated by screening a LambdaFix mouse 129 phage library with a murine *zyxin* cDNA probe (31).

To generate the targeting construct, a 4.5-kb genomic region that encompasses the translation initiation codon was replaced with a neomycin resistance cassette (*neo*) for positive selection. Deletion of the 4.5-kb DNA would remove a 5' noncoding exon and the first four coding exons for zyxin. Two thymidine kinase-negative selection cassettes

flanked the targeting construct. To assist in cloning and screening, the *Spe*I site was deleted from the 5' end of the neomycin resistance coding sequence, and a new *Spe*I site was added to the 3' end of the neomycin resistance cassette in the targeting construct. The linearized *zyxin* gene targeting construct was electroporated into the 129SVJ GS stem cell line (Genome Systems Inc., St. Louis, Mo.), and recombinant clones were selected.

Positive embryonic stem (ES) cell lines were screened for correct homologous recombination by Southern DNA analysis. Cells from two independently derived ES cell lines (86 and 185) were introduced separately into recipient morulae to generate chimeric mice. The resulting chimeric mice were mated with C57BL/6 mice (Jackson Laboratory, Bar Harbor, Maine). Tail DNAs from agouti mice in the resulting litters were analyzed by Southern blot to identify mice in which the targeted allele was transmitted via the germ line. These heterozygous mice served as the founders for two independent *zyxin*-/- mouse lines (Zyxin-86 and Zyxin-185). The mouse genome database provided information on the intron-exon boundaries and locations within the *zyxin* gene and the chromosome locations for *zyxin* gene family members (ncbi.nlm.nih.gov/genome/guide/mouse).

**Characterization of ES cell lines and mice.** Genomic DNA was prepared from mouse tails by 55°C incubation with 10 mg of proteinase K per ml in 0.5% sodium dodecyl sulfate (SDS), 50 mM Tris (pH 8), and 100 mM EDTA (25). For Southern DNA analysis, the DNA was digested with *Spe*I and then electrophoresed through a 0.8% agarose gel, depurinated (0.25 M HCl for 10 min), followed by capillary transfer (0.4 M NaOH) to nylon filters for 18 h. The DNA was neutralized (20 min in 0.5 M Tris-HCl [pH 7.5], 1.5 M NaCl), washed in 2x SSPE (20 min), dried, and UV cross-linked. The 3' *Eco*RI-

*Hin*dIII DNA fragment was labeled with [32P]dCTP (Ready To Go DNA labeling beads; Amersham Pharmacia, Piscataway, N.J.), and used to probe the DNA filters (1 h at 65°C). After washing at 42°C (0.1% SDS with sequential steps of 2x SSPE, 1x SSPE, and 0.1x SSPE), the blot was developed by autoradiography (wild-type zyxin, 11.8 kb; null mutant, 6.2 kb).

For PCR analysis, the genomic DNA was incubated with three primers, WTFzyx (5'-TAC AAG GGC GAA GTC AGG GCG AGT G-3'), WTRzyx (5'-TGG ACG AAG TTT CCG TGT GTT G-3'), and NEOFzyx (5'-GAC CGC TTC CTC GTG CTT TAC-3') and a 30-cycle PCR regimen of 95°C for 60 s, 58°C for 30 s, and 72°C for 50 s, followed by 95°C for 1 min and 72°C for 3 min. The PCR products (wild-type *zyxin*, 327 bp; null mutant, 473 bp) were electrophoresed on a 1.8% agarose gel and visualized with ethidium bromide.

For analysis of proteins, tissues were dissected from mice (euthanized by Halothane inhalation followed by cervical dislocation), weighed, homogenized in 5 parts H2O with protease and phosphatase inhibitors (100 mM phenylmethylsulfonyl fluoride, 100 mM benzamidine HCl, 1 mg of pepstatin A per ml, 1 mg of phenanthroline per ml, 0.1 M NaF, 0.2 mM sodium orthovanadate), and diluted with an equal amount of Laemmli sample buffer (28). The tissue homogenates were boiled for 5 min, and the DNA was sheared with a 26-gauge needle. Protein extracts (10 $\mu$l) were electrophoresed through denaturing 10% polyacrylamide gels and either Coomassie stained or transferred to nitrocellulose by standard methods (51). Western immunoblot analysis was performed by enhanced chemiluminescence (Amersham Pharmacia, Piscataway, N.J.) for detection.

**Antibodies.** Polyclonal rabbit antizyxin serum B71 was generated by immunizing a rabbit with keyhole limpet hemocyanin coupled to peptide CSPGAPGPLTLKEVEELEQLT (human zyxin amino acids 344 to 363, encompassing the nuclear export sequence). Polyclonal rabbit antizyxin serum B72 was generated by immunizing a rabbit with keyhole limpet hemocyanin coupled to peptide CDFPLPPPPLAGDGDDAEGAL (human zyxin amino acids 70 to 89, encompassing the first ActA repeat). Rabbit immunizations and serum collection (serum samples B71 and B72) were performed at Harlan Bioproducts for Science (Madison, Wis.). Polyclonal rabbit serum B38 (31) is now known to recognize both zyxin and lipoma preferred partner (LPP) and is therefore referred to as a panzyxin antibody. Zyxin antisera were diluted 1:10,000 for Western blot analysis.

Mouse monoclonal antizyxin antibody 1D1 was generated by immunizing mice with bacterially expressed glutathione *S*-transferase (GST)-human zyxin; the epitope maps to VVAPKPKVNPFRPGDSEPPP (human zyxin amino acids 28 to 48). Mouse monoclonal antibody 12A12 recognizes LIM3 of both zyxin and TRIP6. Mouse monoclonal antibody 164D4 against human zyxin was supplied by Matthias Krause and Jürgen Wehland (45). Polyclonal rabbit serum MP2 against LPP was supplied by Marleen Petit and Wim Van de Ven (38). Polyclonal rabbit serum B65 (supplied by Susanne Kloeker) is directed against mouse TRIP6 peptide KQPEPSRLPQGRSLPR and was affinity purified for these studies. Antibodies directed against laminin (Sigma-Aldrich, St. Louis, Mo.), keratin 1, keratin 5, loricrin (BabCo, Berkeley, Calif.), and fillagrin (BabCo, Berkeley, Calif.) were used as described previously (40).

**Platelets.** Platelet-rich plasma was prepared from blood collected from wild-type and *zyxin-/-* mice by established procedures (3). Platelets were exposed to collagen, and the timing of the resulting shape change and aggregation response was measured with a lumiaggregometer (Aggrecorder II PA-3220; Kyoto Kaiichi Kagaku, Kyoto, Japan) as described previously (3, 57). Both collagen and ADP were used as agonists.

Platelet-rich plasma was prepared for Western blot analysis as follows. After anesthetization and cardiac puncture of three wild-type and three *zyxin-/-* mice, blood was collected into 1.5-ml microcentrifuge tubes containing 20 $\mu$l of anticoagulant citrate dextrose (110 mM sodium citrate [pH 7.4], 2.45% dextrose) plus 250 $\mu$l of blood per tube. Phosphate-buffered saline containing 4.4 mM EDTA and 0.5% bovine serum albumin was added to the blood-anticoagulant citrate dextrose mixture (400 $\mu$l per tube). Centrifugation at 1,000 rpm (Eppendorf microcentrifuge) for 10 min sedimented the red and white blood cells. The supernatant was recentrifuged at 2,700 rpm for 4 min and aspirated. Next, 300 $\mu$l of ammonium chloride solution (150 mM ammonium chloride, 1 mM potassium bicarbonate, 0.1 mM EDTA, pH 7.4) was added to each pellet and mixed, followed by the addition of 400 $\mu$l of phosphate-buffered saline-EDTA-bovine serum albumin and centrifugation at 2,700 rpm for 4 min. After the platelet pellets were washed twice in phosphate-buffered saline-EDTA-bovine serum albumin and evaluated by microscopic inspection, they were resuspended in SDS sample buffer, electrophoresed (approximately 400,000 platelets per lane), transferred, and probed as described above.

**Histology and immunocytochemistry.** For general histological analysis to compare wild-type and *zyxin-/-* mice, tissues were dissected, fixed, embedded, and stained as

described previously (9). For examination of brain morphology, silver staining was performed on five adult brains sectioned along the horizontal plane to evaluate possible commissure defects (29). Immunocytochemical analysis of tail skin from newborn mice was performed as described previously (40, 52).

**Flow cytometry.** Blood samples (0.5 ml) from mice of various *zyxin* genotypes were incubated with labeled antibodies specific for mouse blood cell markers. The labeled blood cells were then sorted into populations of B cells, T cells (CD4+ and CD8+), granulocytes, and monocytes by flow cytometry (University of Utah Flow Cytometry Core Facility). The blood cell populations were analyzed for standard error means and paired *t* tests with Prism software (Graph Pad, San Diego, Calif.).

## Results

Knowledge of zyxin's binding partner repertoire as well as its molecular architecture suggests that the protein serves as a scaffold for the docking of multiple protein partners (Fig. 1A) (12, 19, 23, 24, 42, 43, 46, 47, 56). One of zyxin's notable features is the presence of four proline-rich motifs called ActA repeats. These repeats were first identified in the ActA protein of *Listeria monocytogenes*, where they make a contribution to the intracellular motility of this pathogenic bacterium (30, 34). ActA repeats serve as docking sites for members of the Ena/VASP family (34, 44). Ena/VASP

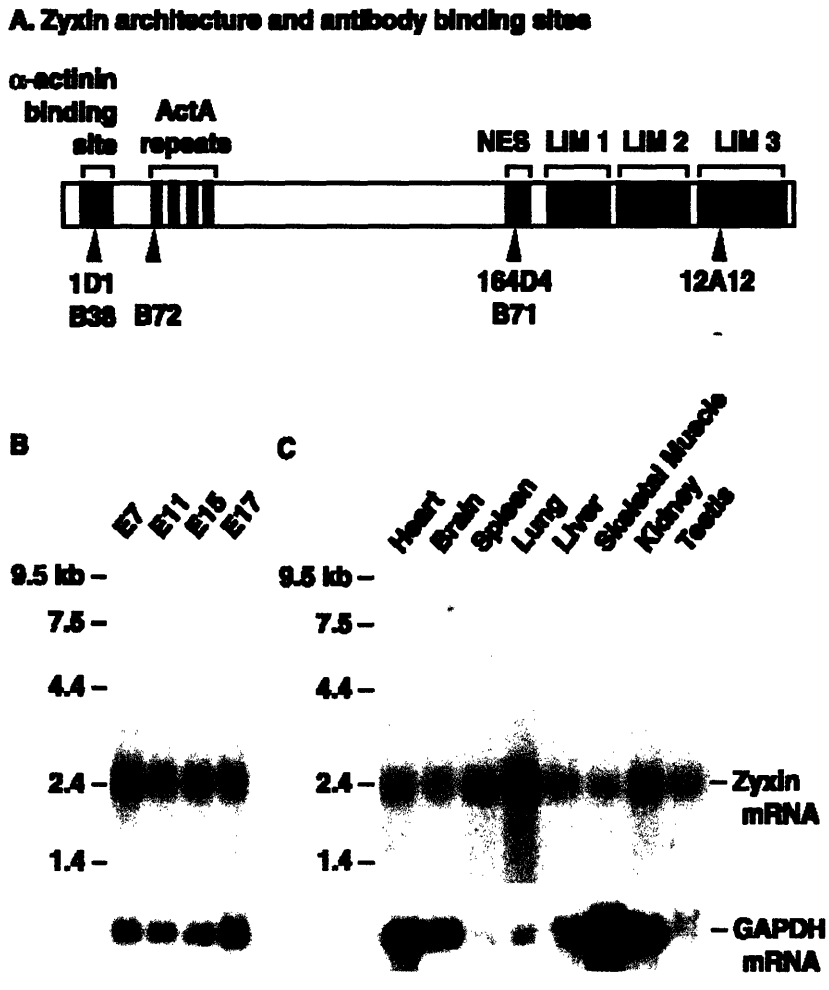
A. Zyxin architecture and antibody binding sites
α-actinin binding site
ActA repeats
NES
LIM 1
LIM 2
LIM 3
1D1
B38
B72
164D4
B71
12A12
B
E7
E11
E15
E17
9.5 kb
7.5
4.4
2.4
1.4
C
Heart
Brain
Spleen
Lung
Liver
Skeletal Muscle
Kidney
Testis
9.5 kb
7.5
4.4
2.4
1.4
Zyxin mRNA
GAPDH mRNA

# Figure 1

**Figure. 1. Zyxin structure and expression.**

(A) Zyxin architectural features including the -actinin binding site, four proline-rich ActA repeats for binding to Mena and VASP, the leucine-rich nuclear export sequence (NES), and three double zinc finger LIM domains. Epitopes recognized by several antizyxin antibodies used in our analysis are marked with arrowheads; mouse monoclonal antibodies (1D1, 164D4, and 12A12) are above the rabbit polyclonal antibodies (B38, B72, and B71).

(B) Northern blot of 2 $\mu$g of polyadenylated RNA isolated from mouse embryos (day 7, day 11, day 15, and day 17 of gestation) reveals that zyxin transcripts are present throughout embryogenesis.

(C) Northern blot of 2 $\mu$g of polyadenylated RNA isolated from adult mouse tissues illustrates widespread expression of zyxin transcripts in the adult mouse. The Northern blots shown were probed with a *zyxin* cDNA that encodes the C-terminal LIM domains. To ensure that no transcripts encoding irrelevant LIM proteins were contributing to the signal, the blots were stripped and reprobed with a *zyxin*-specific 3' untranslated region probe; identical signals were obtained (data not shown). As an additional control, the blots were stripped and reprobed to detect glyceraldehyde-3-phosphate dehydrogenase (GAPDH) transcripts, which are present at variable levels depending on the tissue type.

proteins contribute to the control of actin assembly and organization (4, 44) and have been shown to play important roles in platelets, neurons, and keratinocytes in the mouse (3, 29, 42, 52). Because zyxin plays a central role in localizing Ena/VASP proteins to certain subcellular locations (15), we postulated that elimination of zyxin function may perturb processes that depend on Ena/VASP proteins.

In order to test this hypothesis and to learn more about the physiological role of zyxin in vivo, we examined zyxin function in a mouse model system. By Northern analysis, we determined that murine zyxin is encoded by a single transcript of 2.4 kb that is expressed throughout embryonic development (Fig. 1B). Evaluation of *zyxin* RNA expression in adult mouse tissues indicated that *zyxin* is ubiquitously expressed (Fig. 1C).

**Targeted disruption of *zyxin* gene.** In order to study the role of zyxin in the mouse, we generated a deletion allele by standard methods for engineering gene disruptions by homologous recombination (Fig. 2A) (10, 32). To abolish zyxin function, approximately 4.5 kb of *zyxin* gene sequence, including coding sequence for the translational initiation codon, was replaced with a neomycin resistance selection cassette. Inspection of the available mouse genome sequence confirmed that a 5' noncoding exon plus four exons encoding amino acids 1 to 333 would be deleted by this strategy. Properly targeted ES cells were identified by Southern blot analysis (Fig. 2B) and were incorporated into recipient morulae. The resulting chimeric animals were bred to C57BL/6 mice to generate heterozygous mice, which were subsequently interbred. The progeny of *zyxin*+/- intercrosses were genotyped by either Southern blot (Fig. 2C) or PCR (Fig. 2D) analysis.

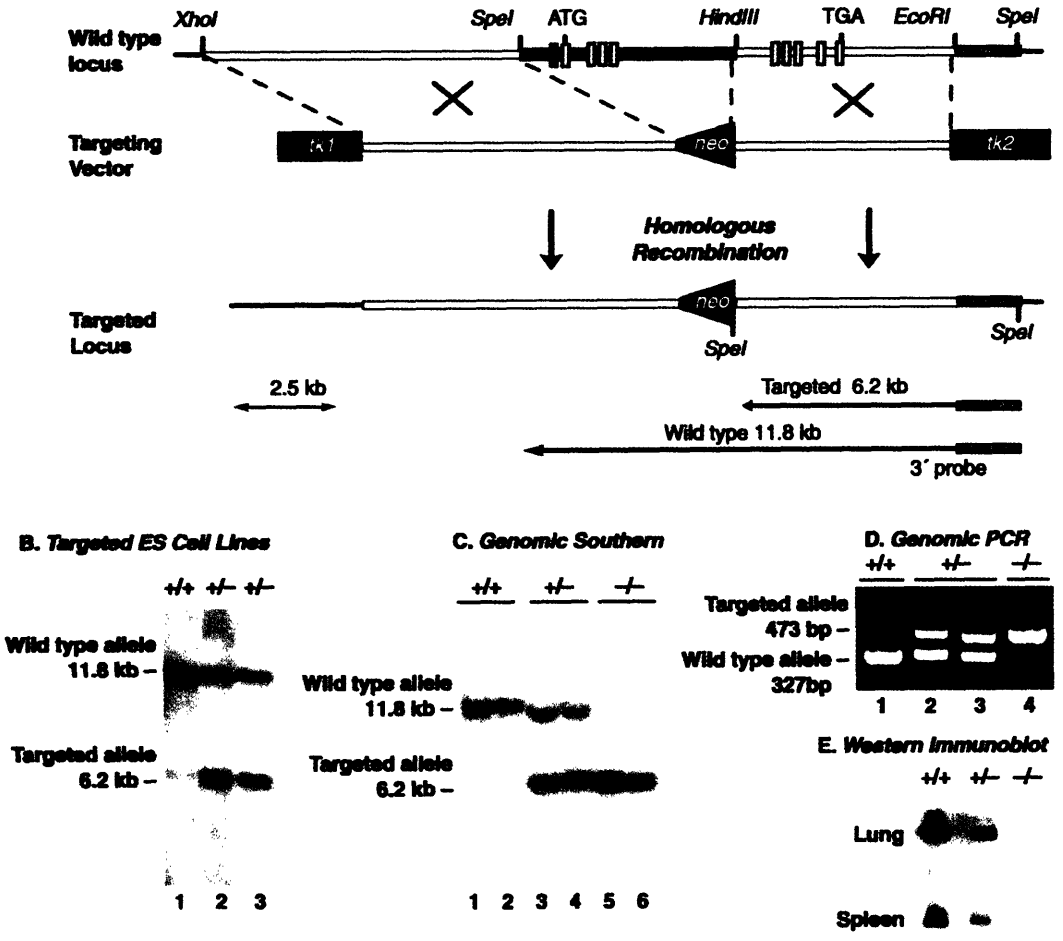
Wild type locus
XhoI
SpeI
ATG
HindIII
TGA
EcoRI
SpeI
Targeting Vector
tk1
neo
tk2
Homologous Recombination
Targeted Locus
neo
SpeI
SpeI
2.5 kb
Targeted 6.2 kb
Wild type 11.8 kb
3′ probe
B. Targeted ES Cell Lines
+/+ +/− +/−
Wild type allele 11.8 kb –
Targeted allele 6.2 kb –
1 2 3
C. Genomic Southern
+/+ +/− −/−
Wild type allele 11.8 kb –
Targeted allele 6.2 kb –
1 2 3 4 5 6
D. Genomic PCR
+/+ +/− −/−
Targeted allele 473 bp –
Wild type allele – 327bp
1 2 3 4
E. Western Immunoblot
+/+ +/− −/−
Lung
Spleen

# Figure 2

**Figure. 2. Disruption of murine *zyxin* gene.**

(A) Partial restriction map of the *zyxin* genomic region used for generation of the targeting construct. Restriction enzyme sites on the wild-type *zyxin* gene, the targeting vector, and the correctly targeted DNA following homologous recombination are shown. This approach deleted 4.5 kb of *zyxin* genomic sequence, which includes a 5' noncoding exon (small shaded box) and the first four coding exons (small white boxes) for amino acids 1 to 333. The ATG methionine start codon in the first coding exon and the TGA stop codon in the final coding exon are shown. (B) Southern blot of *Spe*I-digested genomic DNA from two neomycin-resistant embryonic stem (ES) cell lines probed with the 3' 1.2-kb *Eco*RI-*Hin*dIII DNA identified correctly targeted DNA (wild type, 11.8 kb; targeted mutant, 6.2 kb).

(C) Southern blot of *Spe*I-digested genomic DNA from mouse tail samples distinguishes wild-type (+/+), heterozygous (+/-), and homozygous-null (-/-) genotypes.

(D) Genomic PCR with *zyxin*- and *neo*-specific primers with mouse tail genomic DNA confirms the wild-type (+/+), heterozygous (+/-), and homozygous-null (-/-) genotypes (wild type, 327 bp; *zyxin*-null, 473 bp). (E) Western blot analysis of lung and spleen tissue extracts from zyxin wild-type (+/+), heterozygous (+/-), and homozygous-null (-/-) mice with antizyxin antibody 164D4. No zyxin protein was detected in samples derived from the *zyxin*-null mouse with any of the antibodies specific for epitopes located throughout the zyxin protein.

To evaluate the consequences of loss of zyxin function, *zyxin*+/- mice were intercrossed. The resulting progeny displayed a normal Mendelian ratio of *zyxin*+/+, *zyxin*+/-, and *zyxin*-/- animals (Table 1), indicating that zyxin is not absolutely essential for development. To demonstrate that zyxin protein is indeed missing from the *zyxin*-null mice, tissue extracts from wild-type, heterozygous, and *zyxin*-null mice were analyzed by Western blot. Analysis of two tissues, lung and spleen, that displayed relatively high levels of *zyxin* mRNA is shown in Fig. 2E.

Tissues isolated from *zyxin*+/- mice displayed reduced zyxin levels, and no zyxin was detected in tissues from *zyxin*-/- animals. The absence of zyxin protein expression was confirmed with multiple antizyxin antibodies whose epitopes mapped to the N-terminal, central, and C-terminal regions of the protein (Fig. 1A and data not shown). Since the mouse genome sequence suggests that our targeting strategy would leave five coding exons for the C-terminal half of zyxin, it is important that our Western blot analysis confirmed that there is no detectable expression of these partial zyxin products.

***zyxin*-/- animals can mate and produce offspring, indicating that zyxin expression is not essential for either male or female fertility.** Histological examination of the tissues evaluated by Northern analysis in Fig. 1C revealed that the *zyxin*-null mice displayed no obvious abnormalities in tissue architecture (data not shown). Since zyxin is highly expressed in blood cells (31), we examined the white blood cell population of four sets of littermates with assorted zyxin genotypes (+/+, +/-, and -/-). Flow cytometric analysis

**TABLE 1. Genotypes of progeny resulting from heterozygous (*zyxin*+/-) intercrosses**

| Genotype | No. of mice generated (% of total) | No. predicted by Mendelian genetics (% of total) |
|---|---|---|
| *zyxin*+/+ | 72 (23) | 78 (25) |
| *zyxin*+/- | 162 (52) | 155 (50) |
| *zyxin*-/- | 77 (25) | 78 (25) |

indicated that loss of zyxin did not significantly affect resting populations of B cells, T cells (CD4+ or CD8+), granulocytes, or monocytes (Table 2).

**Expression of zyxin family members is not upregulated in *zyxin*-/- animals.** Recently, two proteins that show a high degree of structural similarity to zyxin have been identified (Fig. 3A). LPP is the closest zyxin relative, with conserved proline-rich ActA repeats, LIM domains, and almost identical mobility in SDS-PAGE (38). Zyxin and LPP exhibit overlapping tissue expression and a similar subcellular distribution, and they also share some binding partners (31, 38, 39). Thyroid receptor-interacting protein 6 (TRIP6), also called zyxin-related protein (ZRP-1), has significant amino acid identity with human zyxin, particularly in the three C-terminal LIM domains (33, 53, 55). Zyxin, LPP, and TRIP6 have all been shown to localize at sites of cell adhesion (11, 38, 53). The shared architectural features and subcellular localizations of these proteins suggest that they may have common functions *in vivo*.

We examined whether the expression of either LPP or TRIP6 is elevated in the *zyxin*-null mice because upregulation of these proteins could theoretically compensate for elimination of zyxin expression. Total protein isolated from the lung, spleen, bladder, kidney, heart, and liver samples derived from *zyxin*+/+, *zyxin*+/-, and *zyxin*-/- animals were probed with antibodies that specifically recognize zyxin, LPP, and TRIP6. Western blot analysis of lung, a tissue that expresses particularly high levels of zyxin (Fig. 1C), is shown in Fig. 3B and C. Zyxin levels were reduced by approximately one half in the heterozygote, and, as expected, no zyxin protein was observed in the sample derived from

**TABLE 2. Flow cytometry analysis of blood cell populations from wild-type (*zyxin*+/+) heterozygous (*zyxin*+/-) and homozygous-null (*zyxin*-/-) littermates[a]**

| Genotype | Mean % of total ± SEM | | | | |
|---|---|---|---|---|---|
| | B cells Macrophages | T cells (CD4+) | T cells (CD8+) | Granulocytes | |
| Wild type | 43.4 ± 4.8 | 26.9 ± 3.2 | 14.3 ± 1.1 | 15.5 ± 2.0 | 7.1 ± 1.5 |
| Heterozygous | 49.2 ± 4.8 | 24.2 ± 1.3 | 18.1 ± 2.9 | 20.8 ± 2.7 | 7.4 ± 0.9 |
| Null | 36.7 ± 4.3 | 29.5 ± 4.0 | 15.8 ± 1.2 | 14.0 ± 1.8 | 5.5 ± 0.6 |

[a] Four mice per genotype were tested. The standard error of the mean was calculated with the Graph Pad Prism statistical analysis software.

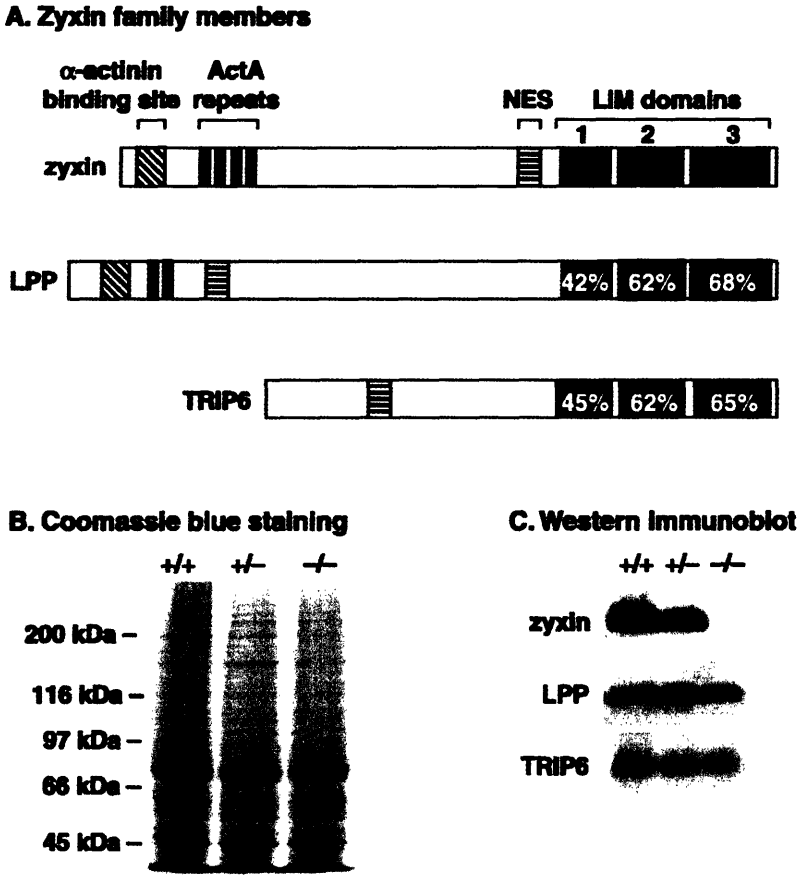
A. Zyxin family members
α-actinin binding site
ActA repeats
NES
LIM domains
1
2
3
zyxin
LPP
42%
62%
68%
TRIP6
45%
62%
65%
B. Coomassie blue staining
+/+
+/−
−/−
200 kDa –
116 kDa –
97 kDa –
66 kDa –
45 kDa –
C. Western immunoblot
+/+
+/−
−/−
zyxin
LPP
TRIP6

# Figure 3

**Figure 3. Zyxin family member structure and protein expression.**

(A) Alignment of human zyxin family members. Certain sequence motifs present in zyxin, including an -actinin binding site (diagonal bars), proline-rich ActA repeats (shaded), nuclear export sequence (NES) (horizontal bars), and three C-terminal LIM domains (solid), are also observed in zyxin's closest relative, LPP. Another zyxin family member, TRIP6, displays a nuclear export signal and three C-terminal LIM domains. Accession numbers are X94991 (human zyxin) (31), NM_005578 (human LPP) (39), and AJ001902 (human TRIP6) (55). The mouse genome sequence database identifies the *zyxin* gene on mouse chromosome 6, the *LPP* gene on mouse chromosome 16, and the *TRIP6* gene on mouse chromosome 5.

(B and C). Expression of zyxin family members in mice. In panel B, a Coomassie blue-stained gel of total lung protein from *zyxin*+/+, *zyxin*+/-, and *zyxin*-/- mice is shown to illustrate comparable protein loading. As can be seen in the Western immunoblots shown in panel C, zyxin (B71 antiserum), LPP (MP2 antiserum), and TRIP6 (affinity-purified B65 antibody) are all expressed in wild-type lung tissue. Zyxin protein is reduced in samples from *zyxin*+/- animals and is absent in *zyxin*-/- animals. LPP and TRIP6 levels are unaffected when zyxin expression is eliminated.

from the *zyxin*-/- lung. No change in either LPP or TRIP6 protein levels was detected when zyxin function was compromised by mutation (Fig. 3C). Results similar to these shown with lung tissue were also found for bladder, spleen, kidney, heart, and liver (data not shown). These results illustrate that upregulated expression of zyxin family members does not occur in response to mutation of the *zyxin* gene. Interestingly, we found that all of the wild-type tissues examined displayed expression of at least two zyxin family members (data not shown). Therefore, although no compensatory upregulated expression of zyxin family members was observed, it remains possible that the presence of multiple family members contributes to the survival of the mice.

As discussed above, one of the best-characterized biochemical activities of zyxin is its ability to bind members of the Ena/VASP family and contribute to the proper subcellular localization of these proteins to sites of cell adhesion. Like *zyxin*-null animals, mice that lack either VASP or Mena are viable and fertile. However, higher-resolution analysis revealed contributions of Ena/VASP proteins to platelet function (21), axon guidance (29), and epithelial sheet formation (52). Therefore, we examined the consequences of eliminating zyxin function for these three systems in which zyxin is postulated to contribute via its capacity to dock Ena/VASP proteins.

**Analysis of zyxin-deficient platelet function.** Two groups have generated mice that lack VASP function (3, 21). These mice are viable and fertile but display an altered platelet activation response. Resting platelets are discoid, nonadhesive cells. When exposed to an agonist such as collagen, thrombin, or ADP, they become activated; they rapidly change their shape and begin to aggregate with each other. The precise timing and extent of these

two responses to agonist can be monitored by the use of an aggregometer, which detects these two stages as changes in light transmission (57). Although the patterns of expression of Mena and VASP often overlap, platelets provide an example of a cell that expresses primarily VASP (3), enhancing the likelihood of being able to detect a VASP loss-of-function phenotype. Indeed, as can be seen in Fig. 4A, platelets that lacked VASP function underwent shape change precociously but ultimately aggregated to the same extent as their wild-type counterparts (3). In contrast, the activation profiles of wild-type and *zyxin-/-* platelets were completely coincident, and the platelets achieved comparable aggregation maxima (Fig. 4B), illustrating that zyxin is not required for normal platelet response.

To determine if multiple zyxin family members are expressed in platelets and to determine if their levels are altered in the absence of zyxin, a Western blot analysis was performed (Fig. 4C). Zyxin was readily detected in wild-type platelets but not in *zyxin-/-* platelets. In equivalently loaded samples, small amounts of TRIP6 were observed but no LPP was detected. Thus, as in other tissues, multiple zyxin family members are expressed in platelets.

**Analysis of nervous system development.** Mice that lack Mena expression are also viable and fertile, but particular deficiencies in brain development were noted in approximately half of the mutant animals examined (29). Specifically, in *Mena-/-* brains, the corpus callosum and dorsal hippocampal commissure are absent, while the ventral hippocampal commissure is present but reduced in thickness. To evaluate these structures

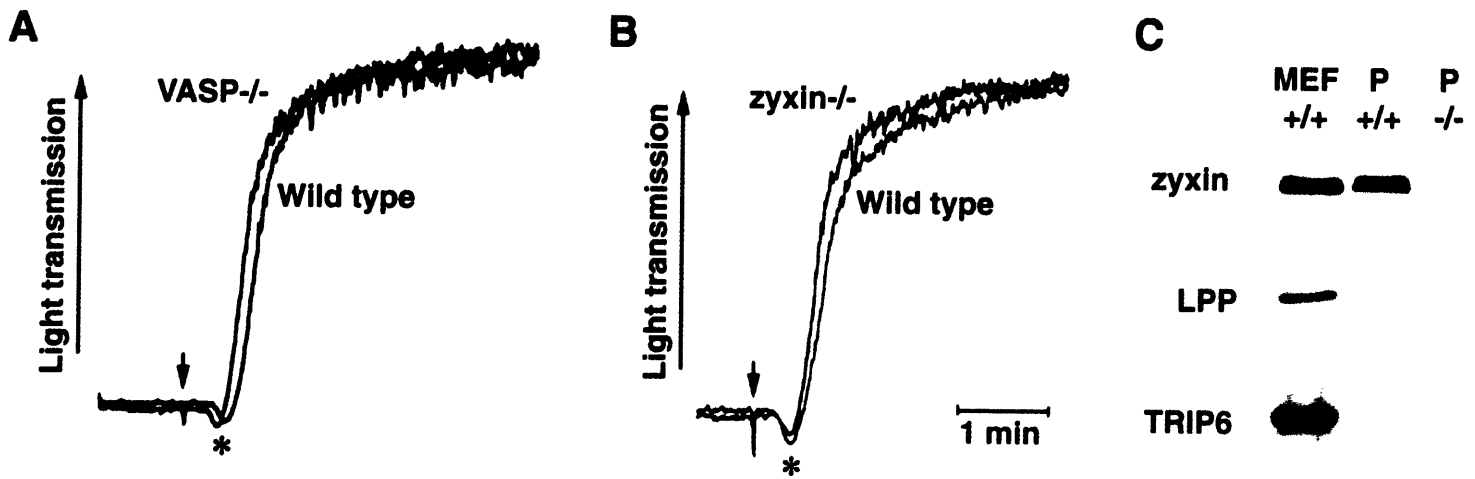
A
VASP-/-
Wild type
Light transmission
*
B
zyxin-/-
Wild type
Light transmission
1 min
*
C
MEF
+/+
P
+/+
P
-/-
zyxin
LPP
TRIP6

**Figure 4**

**Figure 4. Platelet activation response is not altered by elimination of zyxin function.** Platelets isolated from wild-type, *VASP*-/-, and *zyxin*-/- animals were stimulated with collagen (arrow) in the presence of calcium, and the platelet activation and aggregation responses were monitored by measuring light transmission.

(A) As has been reported previously (3), *VASP*-/- platelets display a precocious shape change response (*) but then proceed to aggregate to the same extent as wild-type platelets.

(B) In contrast, the timing of the platelet shape change of *zyxin*-/- platelets is similar to what is observed for wild-type platelets. The slight leftward shift of the aggregation trace shown for the *zyxin*-/- platelets relative to wild-type platelets was not a consistent finding.

(C) Expression of zyxin family members in platelets. Approximately 10 $\mu$g of wild-type mouse embryo fibroblast (MEF) protein and comparable amounts of protein from wild-type platelets (P +/+) and *zyxin*-null platelets (P -/-) were electrophoresed through SDS-10% polyacrylamide gels, transferred to nitrocellulose, and probed for zyxin family member expression. Zyxin protein (B71 antiserum) is detectable in mouse embryo fibroblasts and wild-type platelets but not in *zyxin*-null platelets. LPP (MP2 antiserum) is detectable in mouse embryo fibroblasts but is not detectable under these conditions in wild-type or *zyxin*-null platelets. TRIP6 (affinity-purified B65 antibody) is detectable in mouse embryo fibroblasts and is seen at low levels in both wild-type and *zyxin*-null platelets. A faint immunoreactive band that migrates at 66 kDa is detected with antizyxin (B71) antibody in both *zyxin*+/+ and *zyxin*-/- platelets. This band was not observed in any other murine tissue that we analyzed and may reflect a platelet-expressed protein that has some similarity to zyxin. As expected for platelets, these platelet extracts were positive

for VASP expression and negative for Mena expression by Western blot analysis (data not shown).

in *zyxin*-null mice, we compared silver-stained sections of wild-type, *zyxin*-/-, and *Mena*-/- brains (Fig. 5). *zyxin*-null brains did not exhibit defects in any commissure in the brain (ventral or dorsal hippocampal commissures, anterior or posterior commissures, commissures of the superior and inferior colliculi, habenular commissure, or decussation of the superior cerebellar peduncle). Other major fiber tracts such as the internal and external capsules also appeared to be unaffected in *zyxin*-null brains. Note that the ectopic callosal fibers seen contacting the ventral portion of the ventral hippocampal commissure in *Mena*-/- brain (arrow) were not seen in the *zyxin*-/- brain. We did not detect any deficits in axon guidance associated with elimination of zyxin function.

**Analysis of epidermis.** Transgenic mice expressing a fragment of VASP thought to perturb function in their keratinocytes develop skin blisters that appear to result from perturbation of cell-cell junctions (52). Expression of this mutant VASP disturbs the subcellular distribution of endogenous, full-length Ena/VASP family members (52). Because zyxin plays an important role in the proper subcellular localization of Ena/VASP proteins, it was interesting to consider the possibility that elimination of zyxin might likewise lead to disturbances in the skin by compromising the normal subcellular localization of Ena/VASP family members.

The first step toward evaluating the possibility that zyxin plays a role in cellular adhesions in the skin was to examine the subcellular distribution of zyxin in the skin. As can be seen in Fig. 6A, zyxin was concentrated at the borders of wild-type epidermal keratinocytes. The basement membrane, which is demarcated by laminin, serves to

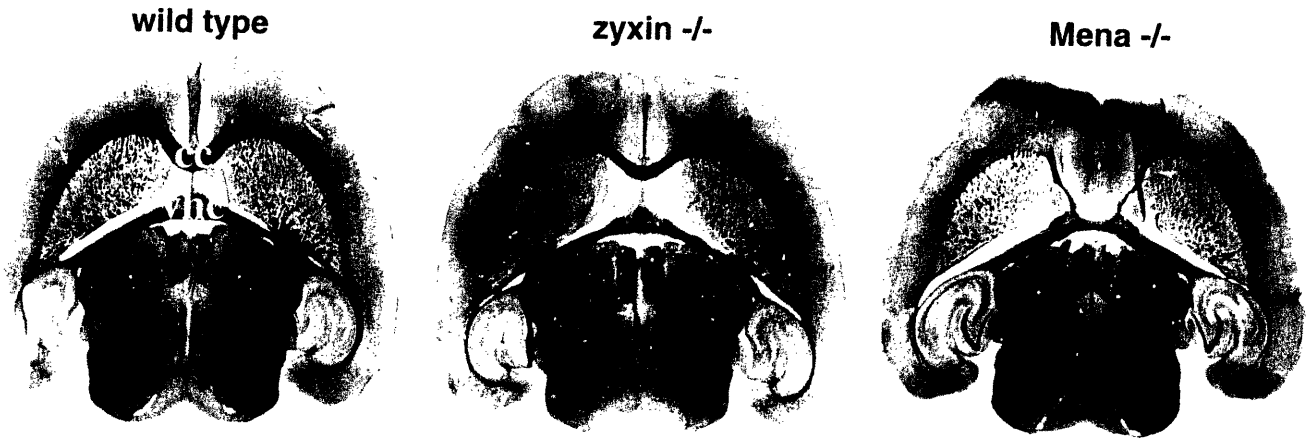


**Figure 5**

**Figure 5. Loss of zyxin function does not affect brain development.**

Horizontal sections from wild-type, *zyxin*-/-, and *Mena*-/- adult brains were analyzed by silver staining. The major commissures evident at this plane of section are the corpus callosum (cc) and the ventral hippocampal commissure (vhc). Brain structures, including those affected by loss of Mena function (29), such as the corpus callosum and ventral hippocampal commissure, form normally in the *zyxin*-/- mice.

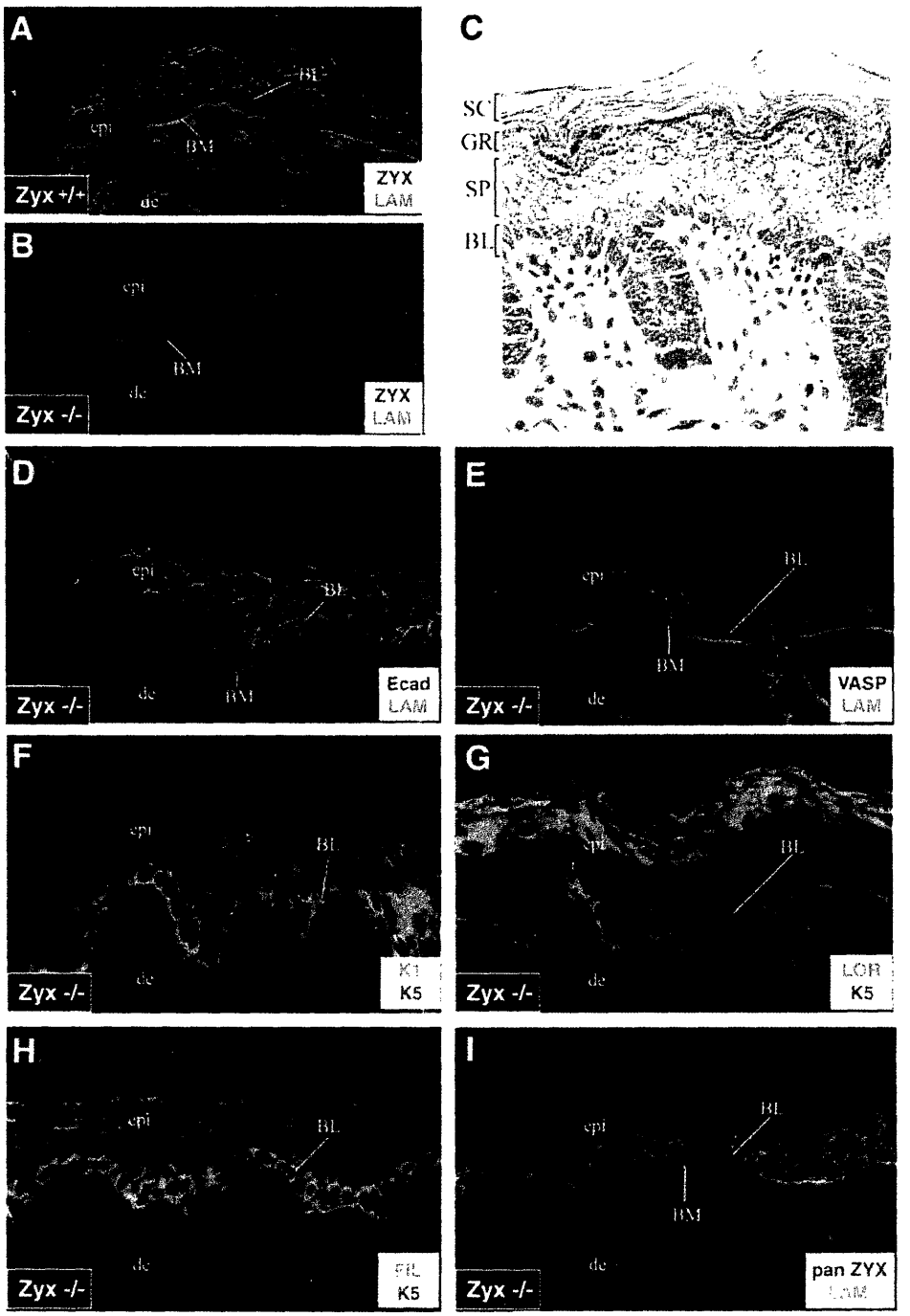
A
BL
epi
BM
Zyx +/+
de
ZYX
LAM
B
epi
BM
de
Zyx -/-
ZYX
LAM
C
SC
GR
SP
BL
D
epi
BL
Zyx -/-
de
BM
Ecad
LAM
E
epi
BL
BM
Zyx -/-
de
VASP
LAM
F
epi
BL
Zyx -/-
de
K1
K5
G
epi
BL
Zyx -/-
de
LOR
K5
H
epi
BL
de
Zyx -/-
FIL
K5
I
BL
epi
BM
de
Zyx -/-
pan ZYX
LAM

# Figure 6

**Figure 6. Differentiation and architecture of the skin are normal in *zyxin*-/- animals.** Skins from wild-type (+/+) (A) and *zyxin*-null (-/-) (B to I) newborn mice were prepared for analysis.

(A) Wild-type mouse skin stained for laminin (LAM) and zyxin (ZYX) exhibits normal basement membrane (BM) (laminin stain) and epidermal zyxin localization (B71 antizyxin polyclonal rabbit serum).

(B) *zyxin*-null mouse skin stained for laminin and zyxin.

(C) *zyxin*-null mouse skin stained with hematoxylin and eosin. BL, basal layer; SC, stratum corneum; GR, granular layer; SP, spinous layer.

(D to I) *zyxin*-null mouse skin stained for E-cadherin and laminin (D), VASP and laminin (E), keratin 1 (K1) and keratin 5 (K5) (F), loricrin (LOR) and keratin 5 (G), filaggrin (FIL) and keratin 5 (H), and panzyxin (pan ZYX) (B38 antibody that detects both zyxin and LPP) and laminin (I). epi, epidermis; de, dermis.

separate the epidermis from the underlying dermis. The intensity of antizyxin labeling was more prominent at the cell borders of suprabasal layers, consistent with the enhancement of intercellular junctions in these layers. As expected, the *zyxin*-null mice showed no detectable zyxin protein anywhere in the epidermis (Fig. 6B). No visible abnormalities were noted in the skin or hair of the *zyxin*-null animals, and the skin of these mice also appeared normal at the histological level (Fig. 6C). The epidermis consisted of the standard morphologically distinct layers, and the hair follicles appeared normal.

To determine whether adhesion and VASP localization might be perturbed when zyxin is absent, we assessed the status of E-cadherin and VASP in *zyxin*-null mouse skin. Interference with VASP function in transgenic mice caused blistering and loss of cell-cell contacts which manifested at the cellular level as double lines of E-cadherin between cells (52). In contrast, the *zyxin*-null mice exhibited normal E-cadherin and VASP localization (Fig. 6D and 6E, respectively).

To test whether the biochemical program of differentiation was normal in *zyxin*-null epidermis, we used specific markers for the distinct layers of the stratified epithelium. The protein keratin 5, which is a marker for the basal layer of the epidermis, was unaltered in the *zyxin*-null skin (Fig. 6F). Likewise, the spinous layers exhibited the normal differentiation program, as keratin 1, an early marker of differentiation, was expressed immediately adjacent to the basal layer. Terminal differentiation markers of

epidermal differentiation such as loricrin (Fig. 6G) and filaggrin (Fig. 6H), which are hallmarks of the granular layer, also showed normal expression patterns.

Altogether, these data suggest that both the adhesive and differentiation programs of the epidermis are unaffected by the lack of zyxin. One possible explanation may be that the absence of phenotypic abnormalities is due to the presence of other zyxin family members which mask the consequences of loss of zyxin function. Indeed, we determined that both an LPP-specific antibody (38) and a panzyxin antibody that recognizes both zyxin and LPP (Fig. 6I) labeled the cell borders of *zyxin*-null mouse skin, demonstrating the presence of LPP in the epidermal cell junctions.

## Discussion

Zyxin is an evolutionarily conserved protein that has been implicated in cell adhesion, cell motility, and signaling. A number of zyxin binding partners have been identified by in vitro biochemical approaches. The roles of many of these partners have been elucidated by gene ablation studies in the mouse. For example, targeted disruption of the genes encoding p130Cas and Lats-1 results in significant lethality (26, 49). Disturbance of either Mena or VASP function does not lead to inviability but does affect particular cell functions (3, 21, 29). In this study, we generated mice in which the *zyxin* gene was disrupted. Here we explored the possibility that elimination of the *zyxin* gene will have consequences similar to what occurs when Mena or VASP coding sequences are ablated.

Among zyxin's binding partners, the interaction with Ena/VASP family members is the best characterized. As discussed above, numerous studies have illustrated that zyxin serves as a docking site for Ena/VASP family members and is important for the proper subcellular targeting of these proteins to particular subcellular locations, most notably focal adhesions (1, 14, 15, 19, 34, 42). Therefore, it was anticipated that elimination of zyxin might disturb Ena/VASP function by ablating a key Ena/VASP docking site within cells. Based on that perspective, one might anticipate that elimination of zyxin would have similar consequences as elimination of Mena or VASP.

As was observed of individual targeted *VASP* and *Mena* gene disruptions in the mouse, mice that lack zyxin function are viable and fertile. However, mutations in either Mena or VASP or expression of a VASP deletion construct revealed deficiencies in platelet activation, neuronal pathfinding, and epithelial cell-cell adhesion (3, 21, 29, 52). Here we examined the consequences of *zyxin* gene disruption for each of these processes. Despite the established contribution of zyxin to the docking of Mena/VASP proteins at cell adhesion sites (14), *VASP-/-* and *Mena-/-* phenotypes are not recapitulated in the *zyxin-/-* animals. Ena/VASP family members are complex, multidomain proteins. One possible explanation for the observation that *zyxin-/-* animals do not display the deficiencies observed in *VASP-/-* and *Mena-/-* mice is that phenotypes resulting from loss of Mena and VASP functions are independent of zyxin. For example, it is established that the localization, and therefore presumably the function, of Ena/VASP family members at the distal tips of lamellipodial extensions and at sites of T-cell receptor clustering are independent of zyxin (27, 45).

Alternatively, the consequences of losing zyxin could be masked by the expression of related proteins. Indeed, since initiating our efforts to target the *zyxin* gene, two proteins that are closely related to zyxin, LPP and TRIP6, were identified (33, 38, 53, 55). We detected no upregulated expression of these proteins in the *zyxin*-/- mice, so it does not appear that the lack of dramatic phenotype can be attributed to compensatory changes in LPP or TRIP6 expression. However, zyxin family members display similar functional domains and subcellular distributions, and the three zyxin family members exhibit similar tissue distribution patterns (11, 13, 31, 38, 39, 54, 55). Importantly, in the cases of blood platelets, brain, and skin, three tissues which we examined closely for a *zyxin*-null phenotype, we and others have detected expression of multiple zyxin family members (Fig. 4C and 6I) (13, 31, 39).

This is the first report describing the ablation of a gene in the zyxin family. Although no basal phenotype has yet been observed in the *zyxin*-/- mice, consequences of eliminating the *zyxin* gene may emerge if these animals are challenged by physiological stress. In order to assess further the role of the zyxin family in vivo, it will be of interest to disrupt the genes that encode other zyxin family members and to generate compound mutations. There now exist many examples in which deletion of a single member of a gene family has minimal consequences but simultaneous elimination of multiple members has a severe impact on development or adult physiology (17, 22, 50). The availability of a genetic model for studying zyxin function is a critical first step toward elucidating the role of zyxin.

**Acknowledgements**

We are grateful to Kirk Thomas (University of Utah Transgenic Core) for targeting vector constructs, the genomic phage library, and substantial technical advice. We thank Marleen Petit and Wim Van de Ven for anti-LPP serum (MP-2), Susanne Kloeker for anti-TRIP6 serum (B65), and Matthias Krause and Jürgen Wehland for antizyxin monoclonal antibody (164D4). We appreciate the contributions of Bob Schackmann (University of Utah DNA and Peptide Core Facility; NCI CA42014), Wayne Green (University of Utah Health Sciences Center Flow Cytometry Core Facility), and the University of Utah Animal Resource Center. Diana Lim provided invaluable assistance with graphic design.

This work was supported by funds provided by the National Institutes of Health to M.C.B. (GM50877) and to F.B.G. (GM58801), the Huntsman Cancer Foundation to M.C.B., a postdoctoral fellowship award by the Cancer Research Institute (New York) to B.B., a predoctoral training grant by the National Institutes of Health to D.N. (T32-CA09602), and the Fonds der Chemischen Industrie to R.F.

**References**

Ahern-Djamali, S. M., A. R. Comer, C. Bachmann, A. S. Kastenmeier, S. K. Reddy, M. C.Beckerle, U. Walter, and F. M. Hoffmann. 1998. Mutations in *Drosphila* Enabled and rescue by human vasodilator-stimulated phosphoprotein (VASP) indicate important functional roles for Ena/VASP homology domain 1 (EVH1) and EVH2 domains. Mol. Biol. Cell 9:2157-2171.

Alwine, J. C., D. J. Kemp, and G. R. Stark. 1977. Method for detection of specific RNAs in agarose gels by transfer to diazobenzyloxymethyl-paper and hybridization with DNA probes. Proc. Natl. Acad. Sci. USA 74:5350-5354.

Aszódi, A., A. Pfeifer, M. Ahmad, M. Glauner, X.-H. Zhou, L. Ny, K.-E. Andersson, B. Kehrel, S. Offermanns, and R. Fässler. 1999. The vasodilator-stimulated phosphoprotein (VASP) is involved in cGMP- and cAMP-mediated inhibition of agonist-induced platelet aggregation, but is dispensable for smooth muscle function. EMBO J. 18:37-48.

Bear, J. E., M. Krause, and F. B. Gertler. 2001. Regulating cellular actin assembly. Curr. Opin. Cell Biol. 13:158-166.

Bear, J. E., J. J. Loureiro, I. Libova, R. Fassler, J. Wehland, and F. B. Gertler. 2000. Negative regulation of fibroblast motility by Ena/VASP proteins. Cell 101:717-728.

Bear, J. E., T. M. Svitkina, M. Krause, D. A. Schafer, J. J. Loureiro, G. A. Strasser, I. V. Maly, O. Y. Chaga, J. A. Cooper, G. G. Borisy, and F. B. Gertler. 2002. Antagonism

between Ena/VASP proteins and actin filament capping regulates fibroblast motility. Cell 109:509-521.

Beckerle, M. 1998. Spatial control of actin filament assembly: lessons from *Listeria*. Cell 95:741-748.

Beckerle, M. C. 1997. Zyxin: zinc fingers at sites of cell adhesion. Bioessays 19:949-957.

Brakebusch, C., R. Grose, F. Quondamatteo, A. Ramirez, J. L. Jorcano, A. Pirro, M. Svensson, R. Herken, T. Sasaki, R. Timpl, S. Werner, and R. Fässler. 2000. Skin and hair follicle integrity is crucially dependent on Beta-1 integrin expression on keratinocytes. EMBO J. 19:3990-4003.

Capecchi, M. R. 1989. Altering the genome by homologous recombination. Science 244:1288-1292.

Crawford, A. W., and M. C. Beckerle. 1991. Purification and characterization of zyxin, an 82,000-dalton component of adherens junctions. J. Biol. Chem. 266:5847-5853.

Crawford, A. W., J. W. Michelsen, and M. C. Beckerle. 1992. An interaction between zyxin and alpha-actinin. J. Cell Biol. 116:1381-1393.

Cuppen, E., M. van Ham, D. G. Wansink, A. de Leeuw, B. Wieringa, and W. Hendricks. 2000. The zyxin-related protein TRIP6 interacts with PDZ motifs in the adaptor protein RIL and the protein tyrosine phosphatase PTP-BL European J. Cell Biol. 79:283-293.

Drees, B., E. Friederich, J. Fradelizi, D. Louvard, M. C. Beckerle, and R. M. Golsteyn. 2000. Characterization of the interaction between zyxin and members of the Ena/vasodilator-stimulated phosphoprotein family of proteins. J. Biol. Chem. 275:22503-22511.

Drees, B. E., K. M. Andrews, and M. C. Beckerle. 1999. Molecular dissection of zyxin function reveals its involvement in cell motility. J. Cell Biol. 147:1549-1560.

Drees, B. E., and M. C. Beckerle. 1999. Zyxin, p. 95-98. *In* T. Kreis and R. Vale (ed.), Guidebook to the extracellular matrix, anchor, and adhesion proteins, 2nd ed. Oxford University Press, Oxford, UK.

Esteban, L. M., C. Vicario-Abejón, P. Fernández-Salguero, A. Fernández-Medarde, N. Swaminathan, K. Yienger, E. Lopez, M. Malumbres, R. McKay, J. M. Ward, A. Pellicer, and E. Santos. 2001. Targeted genomic disruption of H-*ras* and N-*ras*, individually or in combination, reveals the dispensability of both loci for mouse growth and development. Mol. Cell. Biol. 21:1444-1452.

Fradelizi, J., V. Noireaux, J. Plastino, B. Menichi, D. Louvard, C. Sykes, R. M. Golsteyn, and E. Friederich. 2001. ActA and human zyxin harbour Arp2/3-independent actin polymerization activity. Nat. Cell Biol. 3:699-707.

Gertler, F. B., K. Niebuhr, M. Reinhard, J. Wehland, and P. Soriano. 1996. Mena, a relative of VASP and *Drosophila* Enabled, is implicated in the control of microfilament dynamics. Cell 87:227-239.

Goh, K. L., L. Cai, C. L. Cepko, and F. B. Gertler. 2002. Ena/VASP proteins regulate cortical neuronal positioning. Curr. Biol. 12:565-569.

Hauser, W., K.-P. Knobeloch, M. Eigenthaler, S. Gambaryan, V. Krenn, J. Geiger, M. Glazova, E. Rohde, I. Horak, U. Walter, and M. Zimmer. 1999. Megakaryocyte hyperplasia and enhanced agonist-induced platelet activation in vasodilator-stimulated phosphoprotein knockout mice. Proc. Natl. Acad. Sci. USA 96:8120-8125.

Heber, S., J. Herms, V. Gajic, J. Hainfellner, A. Aguzzi, T. Rülicke, H. Kretzschmar, C. v. Kock, S. Sisodia, P. Tremml, H.-P. Lipp, D. P. Wolfer, and U. Müller. 2000. Mice with combined gene knock-outs reveal essential and partially redundant functions of amyloid precursor protein family members J. Neurosci. 20:7951-7963.

Hirota, T., T. Morisaki, Y. Nishiyama, T. Marumoto, K. Tada, T. Hara, N. Masuko, M. Inagaki, K. Hatakeyama, and H. Saya. 2000. Zyxin, a regulator of actin filament assembly, targets the mitotic apparatus by interacting with h-warts/LATS1 tumor suppressor. J. Cell Biol. 149:1073-1086.

Hobert, O., J. W. Schilling, M. C. Beckerle, A. Ullrich, and B. Jallal. 1996. SH3 domain-dependent interaction of the proto-oncogene product Vav with the focal contact protein zyxin. Oncogene 12:1577-1581.

Hogan, B., R. Beddington, F. Costantini, and E. Lacy. 1994. Manipulating the mouse embryo, 2nd ed. Cold Spring Harbor Laboratory Press, Plainview, N.Y.

Honda, H., H. Oda, T. Nakamoto, Z. Honda, R. Sakai, T. Suzuki, T. Saito, K. Nakamura, K. Nakao, T. Ishikawa, M. Katsuki, Y. Yazaki, and H. Hirai. 1998. Cardiovascular anomaly, impaired actin bundling and resistance to Src-induced transformation in mice lacking p130Cas. Nat. Genet. 19:361-365.

Krause, M., A. S. Sechi, M. Konradt, D. Monner, F. B. Gertler, and J. Wehland. 2000. Fyn-binding protein (Fyb)/SLP-76-associated protein (SLAP), Ena/vasodilator-stimulated phosphoprotein (VASP) proteins and the Arp2/3 complex link T cell receptor (TCR) signaling to the actin cytoskeleton. J. Cell Biol. 149:181-194.

Laemmli, U. K. 1970. Cleavage of structural proteins during the assembly of the head of bacteriophage T4. Nature 227:680-685.

Lanier, L., M. Gates, W. Witke, A. S. Menzies, A. Wehman, J. Macklis, D. Kwiatkowski, P. Soriano, and F. Gertler. 1999. Mena is required for neurulation and commissure formation. Neuron 22:313-325.

Laurent, V., T. P. Loisel, B. Harbeck, A. Wehman, L. Gröbe, B. M. Jockusch, J. Wehland, F. B. Gertler, and M.-F. Carlier. 1999. Role of proteins of the Ena/VASP family in actin-based motility of *Listeria monocytogenes*. J. Cell Biol. 144:1245-1258.

Macalma, T., J. Otte, M. E. Hensler, S. M. Bockholt, H. A. Louis, M. Kalff-Suske, K.-H. Grzeschik, D. von der Ahe, and M. C. Beckerle. 1996. Molecular characterization of human zyxin. J. Biol. Chem. 271:31470-31478.

Mansour, S. L., K. R. Thomas, C. Deng, and M. R. Capecchi. 1990. Introduction of a *lacZ* reporter gene into the mouse *int-2* locus by homologous recombination. Proc. Natl. Acad. Sci. USA 87:7688-7692.

Murthy, K. K., K. Clark, Y. Fortin, S.-H. Shen, and D. Banville. 1999. ZRP-1, a zyxin-related protein, interacts with the second PDZ domain of the cytosolic protein tyrosine phosphatase hPTP1E. J. Biol. Chem. 274:20679-20687.

Niebuhr, K., F. Ebel, R. Frank, M. Reinhard, E. Domann, U. D. Carl, U. Walter, F. B. Gertler, J. Wehland, and T. Chakraborty. 1997. A novel proline-rich motif present in ActA of *Listeria monocytogenes* and cytoskeletal proteins is the ligand for the EVH1 domain, a protein module present in the Ena/VASP family. EMBO J. 16:5433-5444.

Nix, D. A., and M. C. Beckerle. 1997. Nuclear-cytoplasmic shuttling of the focal contact protein, zyxin: a potential mechanism for communication between sites of cell adhesion and the nucleus. J. Cell Biol. 138:1139-1147.

Nix, D. A., J. Fradelizi, S. Bockholt, B. Menichi, D. Louvard, E. Friederich, and M. C. Beckerle. 2001. Targeting of zyxin to sites of actin membrane interaction and to the nucleus. J. Biol. Chem. 276:34759-34767.

Pérez-Alvarado, G. C., C. Miles, J. W. Michelsen, H. A. Louis, D. R. Winge, M. C. Beckerle, and M. F. Summers. 1994. Structure of the carboxy-terminal LIM domain from the cysteine rich protein CRP. Nat. Struct. Biol. 1:388-398.

Petit, M. M. R., J. Fradelizi, R. M. Golsteyn, T. A. Y. Ayoubi, B. Menichi, D. Louvard, W. J. M. Van De Ven, and E. Friederich. 2000. LPP, an actin cytoskeleton protein related to Zyxin, harbors a nuclear export signal and transcriptional activation capacity. Mol. Biol. Cell 11:117-129.

Petit, M. M. R., R. Mols, E. F. P. M. Schoenmakers, N. Mandahl, and W. J. M. Van de Ven. 1996. LPP, the preferred fusion partner gene of HMGIC in lipomas, is a novel member of the LIM protein gene family. Genomics 36:118-129.

Raghavan, S., C. Bauer, G. Mundschau, Q. Li, and E. Fuchs. 2000. Conditional ablation of beta-1 integrin in skin: severe defects in epidermal proliferation, basement membrane formation, and hair follicle invagination. J. Cell Biol. 150:1149-1160.

Reinhard, M., K. Giehl, K. Abel, C. Haffner, T. Jarchau, V. Hoppe, B. M. Jockusch, and U. Walter. 1995. The proline-rich focal adhesion and microfilament protein VASP is a ligand for profilins. EMBO J. 14:1583-1589.

Reinhard, M., K. Jouvenal, D. Tripier, and U. Walter. 1995. Identification, purification, and characterization of a zyxin-related protein that binds the focal adhesion and microfilament protein VASP (vasodilator-stimulated phosphoprotein). Proc. Natl. Acad. Sci. USA 92:7956-7960.

Reinhard, M., J. Zumbrunn, D. Jaquemar, M. Kuhn, U. Walter, and B. Trueb. 1999. An alpha-actinin binding site of zyxin is essential for subcellular zyxin localization and alpha-actinin recruitment. J. Biol. Chem. 274:13410-13418.

Renfranz, P. J., and M. C. Beckerle. 2002. Doing (F/L)PPPPs: EVH1 domains and their proline-rich partners in cell polarity and migration. Curr. Opin. Cell Biol. 14:88-103.

Rottner, K., M. Krause, M. Gimona, J. V. Small, and J. Wehland. 2001. Zyxin is not colocalized with vasodilator-stimulated phosphoprotein (VASP) at lamellipodial tips and exhibits different dynamics to vinculin, paxillin, and VASP in focal adhesions. Mol. Biol. Cell 12:3103-3113.

Schmeichel, K. L., and M. Beckerle. 1998. LIM domains of cysteine-rich protein 1 (CRP1) are essential for its zyxin-binding function. Biochem. J. 331:885-892.

Schmeichel, K. L., and M. C. Beckerle. 1994. The LIM domain is a modular protein-binding interface. Cell 79:211-219.

Skoble, J., V. Auerbuch, E. D. Goley, M. D. Welch, and D. A. Portnoy. 2001. Pivotal role of VASP in Arp2/3 complex-mediated actin nucleation, actin branch-formation, and *Listeria monocytogenes* motility. J. Cell Biol. 155:89-100.

St. John, M., W. Tao, X. Fei, R. Fukumoto, M. L. Carcangiu, D. G. Brownstein, A. F. Parlow, J. McGrath, and T. Xu. 1999. Mice deficient of *Lats1* develop soft-tissue sarcomas, ovarian tumours and pituitary dysfunction. Nat. Genet. 21:182-186.

Stein, P. L., H. Vogel, and P. Soriano. 1994. Combined deficiencies of Src, Fyn, and Yes tyrosine kinases in mutant mice. Genes Dev. 8:1999-2007.

Towbin, H., T. Staehelin, and J. Gordon. 1979. Electrophoretic transfer of proteins from polyacrylamide gels to nitrocellulose sheets: procedure and some applications. Proc. Natl. Acad. Sci. USA 76:4350-4354.

Vasioukhin, V., C. Bauer, M. Yin, and E. Fuchs. 2000. Directed actin polymerization is the driving force for epithelial cell-cell adhesion. Cell 100:209-219.

Wang, Y., J. E. Dooher, M. Koedood Zhao, and T. D. Gilmore. 1999. Characterization of mouse TRIP6: a putative intracellular signaling protein. Gene 234:403-409.

Wang, Y., and T. D. Gilmore. 2001. LIM domain protein Trip6 has a conserved nuclear export signal, nuclear targeting sequences, and multiple transactivation domains Biochim. Biophys. Acta 1538:260-272.

Yi, J., and M. C. Beckerle. 1998. The human TRIP6 gene encodes a LIM domain protein and maps to chromosome 7q22, a region associated with tumorigenesis. Genomics 49:314-316.

Yi, J., S. Kloeker, C. C. Jensen, S. Bockholt, H. Honda, H. Hirai, and M. C. Beckerle. 2002. Members of the zyxin family of LIM proteins interact with members of the p130cas family of signal transducers. J. Biol. Chem. 277:9580-9589.

Zucker, M. B. 1989. Platelet aggregation measured by photometric method. Methods Enzymol. 169:117-133